TECHNISCHE UNIVERSITÄT MÜNCHEN

Department Chemie

Lehrstuhl für Biotechnologie

Regulatory Implications of Non-Trivial Splicing of Human Proteins

Patricia Schöppner

Vollständiger Abdruck der von der Fakultät für Chemie der Technischen Universität München zur Erlangung des akademischen Grades eines Doktors der Naturwissenschaften genehmigten Dissertation.

Vorsitzender:	Univ.-Prof. Dr. Aymelt Itzen
Prüfer der Dissertation:	1. Univ.-Prof. Dr. Johannes Buchner
	2. Univ.-Prof. Dr. Michael Sattler

Die Dissertation wurde am 29.03.2016 bei der Technischen Universität München eingereicht und durch die Fakultät für Chemie am 19.05.2016 angenommen.

Summary

Alternative splicing often affects structured and highly conserved regions of proteins, generating so called non-trivial splicing variants of unknown structure and cellular function. Already Birzele *et al.* claimed that the tolerance of proteins to structural deletions, insertions and replacements appeared to be higher than previously expected (Birzele et al, 2008a). Nevertheless, the common assumption remained that most alternative transcripts and especially non-trivial ones are prone to nonsense mediated decay (Lareau & Brenner, 2015) or protein degradation immediately after their translation. Thereby, the generated isoforms are thought to represent artifacts of the transcriptional machinery, which are unable to fold into stable proteins and do not contribute to the functional proteome.

In this context it was the central goal of this thesis to analyze if non-trivial splice variants can form structured and functional proteins. Accordingly, the major consequences of non-trivial alternative splicing on the conformation and function of three different human proteins (nt-svSHMT, nt-svArgianse-1 and nt-svRab1A) from two different non-trivial splicing categories (conserved α-helices, internally conserved α/β-motifs) were studied. Besides, the structural and functional properties especially the seemingly regulatory role of nt-svRab1A in the cell was investigated in more detail.

The human small G-protein Rab1A is involved in the regulation of the vesicle transfer from the ER to Golgi. The conserved non-trivial splice variant lacks nearly 40 % of the sequence of the native Rab1A, including most of the regulatory interaction sites. In this thesis it was shown that this variant of Rab1A represents a stable and folded protein, which is still able to bind nucleotides, but lost its specificity for GXP nucleotides. However, it should be mentioned that compared to other wild-type RabGTPases the measured nucleotide binding affinities in the variant studied are dramatically reduced. Furthermore, this spliced isoform displays a constantly enhanced GTP-hydrolysis activity and is no longer controlled by guanine nucleotide exchange factors or GTPase activating proteins.

Thus, the non-trivial splicing event altered the major role of this RabGTPase by completely changing its activation and inactivation mechanism. However, by co-localization experiments it was possible to demonstrate that the main localization site of the Rab1A GTPase, ER to Golgi transport vesicles, was not changed for nt-svRab1A. This could be also underlined by the observation of membrane attachment that was in contrast to the wtRab1A protein independent from prenylation.

Furthermore, nt-svRab1A was either stabilized by the formation of a homo-dimer or indirectly by the generation of hetero-oligomers with wild-type Rab1A, as well as Rab1B. Additionally, the presented results clearly indicate that the presence of nt-svRab1A in the cell temporarily enhances the vesicular transport.
Overall, the findings described in this thesis indicated a new regulatory mechanism for the Rab1A function in vesicular transport via alternative non-trivial splicing.

The comparative structural investigations of all three non-trivial spliced isoforms seem to support the view that alternative splicing preferentially results in slight rearrangements and a basically conservation and adaption of the wild-type structure.
Both members of the internally conserved α/β-category (nt-svArginase, nt-svRab1A) exhibit novel functional characteristics. The results for nt-svSHMT, belonging to the α-conserved category, further highlighted the potential of non-trivial splicing as regulatory tool in terms of a dramatic reduction of the catalytic activity in comparison to the wild-type protein.
In summary the findings of this thesis explicitly disproved the assumption that alternative transcripts are prone to nonsense mediated decay (Jaillon et al, 2008; Lareau & Brenner, 2015).
Alternative splicing executes a more prominent role in protein structure evolution and creation of functional diversity than previously expected.
Nevertheless, future studies elucidating the exact conditions under which these isoforms are present *in vivo* are necessary to allow a detailed understanding of the regulatory and mechanistically implications of non-trivial alternative splicing.

Contents

1 Introduction

1.1 Non-trivial alternative splicing

Alternative splicing is a major source for functional diversity in higher eukaryotes, as a human genome analysis has revealed a basic disparity between the number of 24.000 protein-coding genes and the 100.000 different proteins that are postulated to be synthesized (Keren et al, 2010). Despite the overall extensive species specificity of alternative splicing, many of the identified alternative splicing events are conserved and subject to cell-, tissue-, or developmental-regulation (Raj & Blencowe, 2015). In addition to generating vast repertoires of RNAs and proteins, splicing has also a profound impact on other gene regulatory layers, including mRNA transcription, turnover, and translation (Braunschweig et al, 2013). Further, alternative splicing plays an important role in the development of various protein products, being involved in diverse cellular processes, like cell growth, cell differentiation and apoptosis (Black, 2003; Schwerk & Schulze-Osthoff, 2005). It is estimated that up to 15% of all point mutations causing human genetic diseases, are caused by an mRNA splicing defect (Krawczak et al, 1992). For example, defective splicing of exon 18 in the *BRAC1* gene, potentially leads to breast and ovarian cancer (Liu et al, 2001a).

The basis of splicing is the recognition of introns and exons by the splicing machinery, via splice-site identification (Keren et al, 2010). Thereby the spliceosome, a protein complex, consisting of five small nuclear ribonucleic proteins (snRNPs) U1, U2, U4/U6 and U5, is responsible for removing the vast majority of pre-mRNA introns, followed by the ligation of the exons to form a mature mRNA (Kim et al, 2007; Nieto Moreno et al, 2015). Each snRNP consists of a small nuclear ribonucleic acid (snRNA) (or two in case of U4/U6) and a variable number of complex-specific proteins (Wahl et al, 2009). The identification of the proper exon and intron boundaries is achieved by exon- and intron-definition, in which multiple signals, originating from interactions across exons and/or introns, are recognized by the splicing machinery (Berget, 1995; Kim et al, 2008). The four main splice signals are the 5’ splice sites (ss) and the 3’ss, located at the upstream and downstream exon-intron junctions, respectively, the branch site (BS), and the polypyrimidine tract (PPT), which is located upstream of the 3’ss (Figure 1, (Kim et al, 2008; Schreiber et al, 2015)). As common feature in eukaryotes the intron is always defined by a GU starting point and an AG motive at the end (Chen & Manley, 2009) and the intronic adenosine residue that forms the branched lariat structure (Braunschweig et al, 2013).

However in metazoans additional regulatory elements for the exon and intron identification are necessary, which are defined as exonic or intronic splicing enhancers (ESE, ISE), or silencers (ESS, ISS) (Ast, 2004). Specific binding of splicing regulatory proteins (such as serine-arginine protein family (SR), and heterologous nuclear RNP (hnRNP, negative regulator)) to these splicing regulatory elements assists in the placement of the spliceosome on the appropriate splice site (Kim et al, 2008). Generally, the splice site choice is defined by the quantity of positive and negative signals, leading to splicing in case of predominant positive signals (Nilsen & Graveley, 2010).

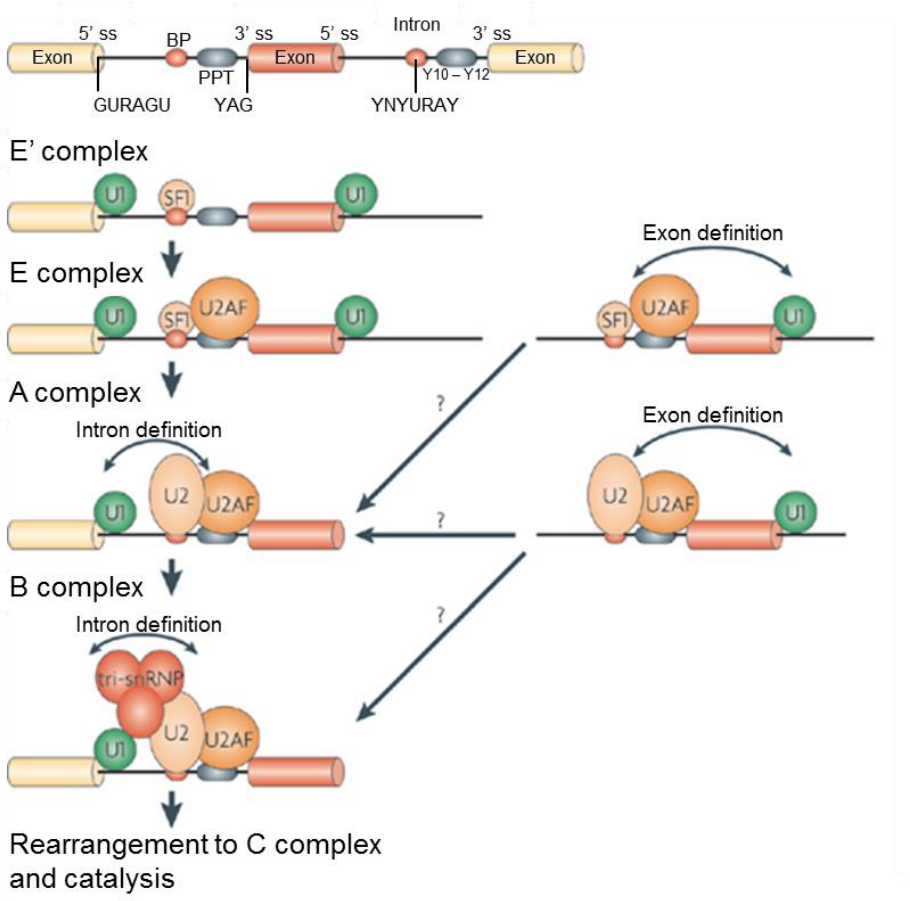

Figure 1: Pre-mRNA splicing by the spliceosome.
A) The four basal splice signals of pre-mRNA are depicted: 5'splice site (ss), branch site (BP), polypyrimidine tract (PPT), 3'ss. The exons (yellow, red) are separated from the intron (black solid line).The consensus sequences are indicated (Y: Pyrimidine, N: any nucleotide, R: Purine). The PPT, located between the BP and the 3'ss, is a pyrimidine-rich stretch. **B)** Mechanism of spliceosome assembly: The spliceosome consist of five snRNPs U1, U2, U4/U6 and U5 (colored circles). The U4/U5 and U6 snRNPs are recruited as a pre-formed tri-snRNP. Additional the splice factor 1 (SF1) and the U2 auxiliary factor (U2AF) are involved in assembly. The stepwise interaction of the snRNPs, SF1 and U2AF forming theE' complex, E-complex, Pre-spliceosomal A complex and the final spliceosomal B complex is shown. Adapted by permission from Macmilan Publisher Ltd: [Nat. Rev. Mol. Cell] (Chen & Manley, 2009), © (2009).

The essential steps of the spliceosome assembly are shown in Figure 1. First, ATP-dependent binding of the U1 snRNP occurs, through base-pairing interactions of the 5' end of the U1 snRNP to the 5' ss of the intron (Wahl et al, 2009). The earliest assembly phase of the spliceosome also involves binding of splice factor 1 (SF1) to the BP and interplay of the U2 auxiliary factor (U2AF, heterodimer of $U2AF^{65}$/$U2AF^{35}$, (Cartegni et al, 2002)) with the PPT and the terminal end of the 3'ss (AG) (Chen & Manley, 2009). Together these molecular interactions yield the spliceosomal E complex and play crucial roles in the initial recognition of the 5'ss and the 3'ss of an intron (Wahl et al, 2009). By exchange of the SF1 with the U2 snRNP the pre-spliceosomal A complex is built in an ATP-dependent manner. Subsequent to the A complex formation, the U4/U6 and U5 snRNPs are recruited as a preassembled tri-snRNP, forming the B complex (final spliceosome) (Hoskins & Moore, 2012). To facilitate the first transesterification the spliceosome requires major conformational and compositional rearrangements to become catalytically active, leading to the consecutive release of the U1 and U4 snRNP unit. Thereby the 2'-hydroxyl group of adenosine at the BP attacks the phosphate at the 5' ss (5' exon/intron boundary), leading to phosphodiester bond cleavage of the 5' exon from the intron and the formation of a lariat intron-3'-exon intermediate (Hoskins & Moore, 2012) . The second transesterification step is the attack on the phosphate at the 3'end of the intron by the 3'-hydroxyl of the detached exon, ligating the two exons under release of the intron (Black, 2003). After the second catalytic step the spliceosome dissociates, releasing the mRNA as well as the U2, U5 and U6 snRNPs to be recycled for additional rounds of splicing (Wahl et al, 2009).

Alternative splicing is a process by which different pairs of splice sites are selected in a pre-mRNA transcript to produce distinct mRNA and protein isoforms (Braunschweig et al, 2013). This helps to explain the fact that animals of different complexity levels have a similar number of genes (humans: 19.000, *Drosophila melanogaster*: 14.000, *Caenorhabditis elegans*: 20.000) (Nieto Moreno et al, 2015). Indeed, the proportion of genes affected by alternative splicing is much higher in humans (95%), than in *Drosophila melanogaster* (46%) or *Caenorhabditis elegans* (25%) (Nieto Moreno et al, 2015).

In general the five most common mechanisms of alternative spicing are exon skipping also known as cassette exon, alternative 5'ss or 3'ss selection, intron retention and mutually exclusive events (Figure 2, (Ast, 2004)).

In case of exon skipping, the prevalent method in higher eukaryotes, a cassette exon is spliced out of the transcript together with its flanking introns (Keren et al, 2010). Alternative ss selection occurs when two or more ss are recognized at one end of an exon (Keren et al, 2010). As rarest splicing event in vertebrates and intervertebrates (less than 5%) intron retention leads to a mature mRNA transcript with a remaining intron (Keren et al, 2010).

Nevertheless, it is clear that introns are important for facilitating alternative splicing, thereby promoting protein diversity, which is associated with tissue-specific functions in eukaryotes (Wong et al, 2015). Further intronic sequences are also known to harbor non-coding RNAs, which regulate distinct biological processes (Wong et al, 2015).

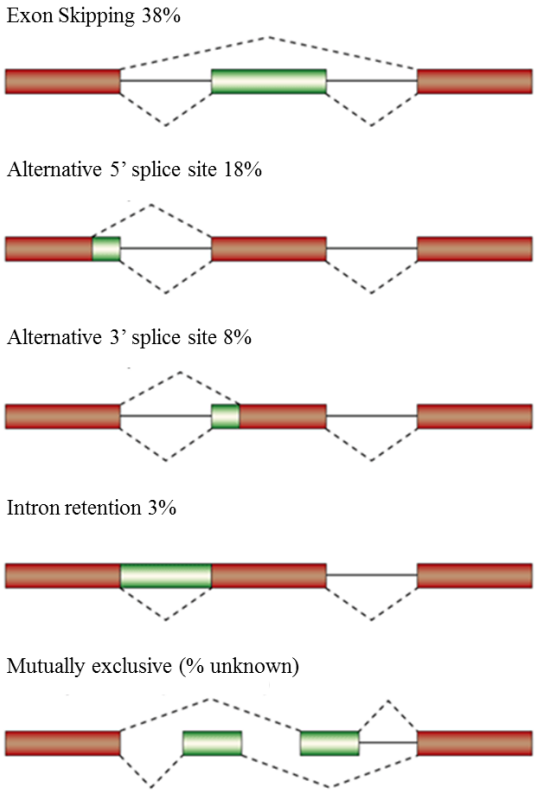

Figure 2: Types of alternative splicing.
Four main subgroups of alternative splicing are: Exon skipping, Alternative splice site selection (5'ss, 3'ss) and Intron retention. Alternatively spliced regions are shown in green, constitutive exons are depicted in red. Introns are represented either by solid lines or dashed lines, which indicate splicing options. The relative abundance of each alternative splicing event conserved in human and mouse is shown in % and related to the % of total alternative splicing events. Adapted by permission from Macmilan Publishers Ltd: [Nat. Rev. Genet.] (Ast, 2004), © (2004).

In particular, alternative splicing is known to affect more than half of all human genes, and has been proposed as primary driver of the evolution of phenotypic complexity in mammals (Wang et al, 2008). Interestingly, when mapping splicing events onto protein structures, about half of the splicing events affect structured and even highly conserved regions (Birzele et al, 2008a).

Such splicing events are called “non-trivial” as they are not easy to explain on a structural level. Often the function of such variants remains elusive. It is commonly assumed that non-trivial splice variants are due to error or noise of the splicing machinery and that the products are subsequently subject to nonsense-mediated mRNA decay (NMD). For example during the pioneer round of translation, the premature termination codons (PTMs), resulting from intron retention, will trigger mRNA degradation by NMD, thereby protecting cells from possible dominant-negative effects of truncated proteins (Jaillon et al, 2008). In this case they would not contribute to the proteome and functional diversity of an organism (Jaillon et al, 2008). However, the expression of a number of such splice variants has been recently confirmed on the protein level in human, indicating high tissue variability (Kim et al, 2014; Wilhelm et al, 2014). Furthermore, for a large fraction of 10% – 15% of non-trivial splice variants, expression and function have been described in the literature (Birzele et al, 2008a). Comprehensive studies on alternative splicing suggest that proteins appear to be much more tolerant to structural deletions, insertions and replacements than previously thought (Birzele et al, 2008a; Csaba et al, 2008). Nevertheless, the role of non-trivial splicing isoforms in the network of cellular proteins is still enigmatic. They might exhibit different functional properties compared to their respective non-spliced, native isoforms and/or could influence the regulation of protein networks in the cell. In addition, from a structural point of view, it is still puzzling whether non-trivial splicing isoforms represent folded proteins and whether their structure is still similar to the structure of the non-spliced, wild-type isoforms.

Non-trivial splicing can be classified into eight different categories comprising different effects to be expected on the structure level (Birzele et al, 2008a). Depending on the affected part during non-trivial splicing these categories are: internal or peripheral β-strands, internal or peripheral αβ motives, conserved coil regions, conserved helices, repetitive elements and large-scale events (affecting more than 50% of the structure (Birzele et al, 2008a).

In summary the possibility to express the antagonist of a protein as an isoform of the native variant would represent an intuitive mechanism to increase functional complexity of an organism by alternative splicing (Birzele et al, 2008a). One non-trivial spliced isoform characterized in this thesis is Rab1A isoform 3 (nt-svRab1A).

As Rab1A is involved in vesicular transport a general overview is described in the following section.

1.2 Vesicular transport process

The cell represents the smallest biological functional unit of all organisms. In general cells can be classified into three structurally and evolutionary different types, archaea, prokaryotes and eukaryotes (Archibald, 2015). Fundamentally, all eukaryotic cells in contrast to archaea and prokaryotes have a membrane-bounded nucleus, a complex endomembrane system, a cytoskeleton and a considerable smaller size (Vellai & Vida, 1999). The presence of intracellular organelles with clear compartmentalization and their own complement of cellular proteins is an additional characteristic of eukaryotes (Figure 8, (Lazar et al, 1997)).

Besides the nucleus, mitochondria, endoplasmic reticulum (ER) (Braakman & Bulleid, 2011), Golgi apparatus (Papanikou & Glick, 2014), lysosomes (Bainton, 1981), peroxisomes (Masters & Crane, 1996; Subramani, 1998) and endosomes are part of the organelle system (Pryer et al, 1992). Due to the existence of a lipid bilayer membrane, organelles are separated from soluble components of the cytosol (Mellman & Warren, 2000). Thus, compared to the cytosol the reaction milieu of organelles can sometimes differ dramatically in chemical characteristics like pH, redox potential, salt concentration and viscosity. Fundamentally in eukaryotic cells, proteins targeted for organelles or the extracellular space typically enter the secretory pathway via the ER already during translation at the ribosome (Braakman & Bulleid, 2011; Lord et al, 2013). The cotranslational translocation process is initiated when a hydrophobic signal sequence or transmembrane sequence is translated and recognized by the signal-recognition particle (SRP) for targeting to the SRP receptor at ER translocation sites (Barlowe & Miller, 2013). In general the ER regulates protein translation, protein translocation across the membrane, protein folding and post-translational modification (Barlowe & Miller, 2013). This organelle also supplies a checkpoint for secretion, providing a level of quality control on protein export, which in general only allows secretion of proteins that are folded and modified correctly (Braakman & Bulleid, 2011). Modification of passenger proteins, for example by glycosylation, sulfation or proteolytic cleavage, occurs further in consecutive Golgi compartments by Golgi-associated processing enzymes (Allan & Balch, 1999), before the passengers are forced into different directions by a sorting process in the most distal Golgi compartment (Lazar et al, 1997). To enable mass exchange with the extracellular space, endocytosis or exocytosis is a common process. In the exocytotic transport, synthesized proteins are transported from the ER, through the Golgi apparatus to the lysosome, to the plasma membrane (PM) or extracellular space (Mellman & Warren, 2000).

Endocytosis involves the receptor-mediated uptake of soluble macromolecular ligands (e.g. hormones, nutrients, viruses) that bind specific cell surface receptors and internalized via coated vesicles (Mellman & Warren, 2000). Alternatively endocytosis accommodates the uptake of large extracellular particles (dead or apoptotic cells, bacteria) or large droplets of fluid by phagocytosis or macropinocytosis (Mellman & Warren, 2000). Both forms of endocytosis are then coupled to the internalization into early endosomes (EEs), from where cargo is either recycled or transported by means of late endosomes (LEs) to the hydrolase-rich acidic lysosome, warranting cargo degradation and redistribution of catabolized material (Wijdeven et al, 2015).

In exocytosis as well as in endocytosis biological material is transported through diverse organelles, processed and prepared for the final function at its destination (Mellman & Warren, 2000; Pryer et al, 1992). To avoid undefined side reactions and by-products during transport, lipids and proteins are forwarded between the respective organelles mainly via vesicle-mediated transport. Thereby individual proteins are transported within the pattern according to a variety of extracellular and intracellular signals that dictate their ability to enter or avoid the various shuttles (Chua & Tang, 2015; Rothman & Wieland, 1996). In general the vesicular transport can be divided into four main steps; vesicle formation and release from the donor membrane (budding) (1), movement towards the acceptor membrane (2), recognition of the acceptor membrane followed by initial interaction between donor vesicles with its partner vesicle/acceptor membrane attachment of the vesicle (tethering) (3) and fusion with the acceptor compartment, releasing the cargo into the organelle lumen or integration of membrane proteins into the target membrane (4) (Bhuin & Roy, 2014; Hutagalung & Novick, 2011). Thereby RabGTPases function as central regulators in tightly controlling these steps in a spatial and temporal manner, by recruiting specific binding partners, such as sorting adaptors, tethering factors, kinases, phosphatases and motor proteins (Park, 2013), which is essential for adequate reactions due to changing environmental influences (Bennett & Scheller, 1993; Bhuin & Roy, 2014; Novick & Zerial, 1997). Further, small G proteins serve multiple cellular processes ranging from structure biogenesis and maintenance, to various aspects of membrane dynamics (Chua & Tang, 2015). As the characterization of nt-svRab1A GTPase is the main part of this thesis; a general overview on structural and functional properties, as well as the involvement of Rab GTPases in vesicular transport are described in detail in the following sections.

1.3 RabGTPases – Members of the Ras superfamily of small G proteins

The Ras superfamily of small guanosine triphosphates (GTPases, molecular mass 20 – 25 kDa) comprises over 150 human members, with evolutionary conserved orthologs found in *D. melanogaster*, *C. elegans*, *S. cerevisia*, *S. pombe*, *Dictyostelium* and plants (Wennerberg et al, 2005). On the basis of amino acid sequence and functional similarities the Ras superfamily can be sub classified into Ras (Ras sarcoma), Rho (Ras homologous), Rab (Ras-related in brain), Ran (Ras-like nuclear) and Arf (ADP-ribosylation factor) families (see Figure 3), as well as the closely related Gα family (Colicelli, 2004; Wennerberg et al, 2005).

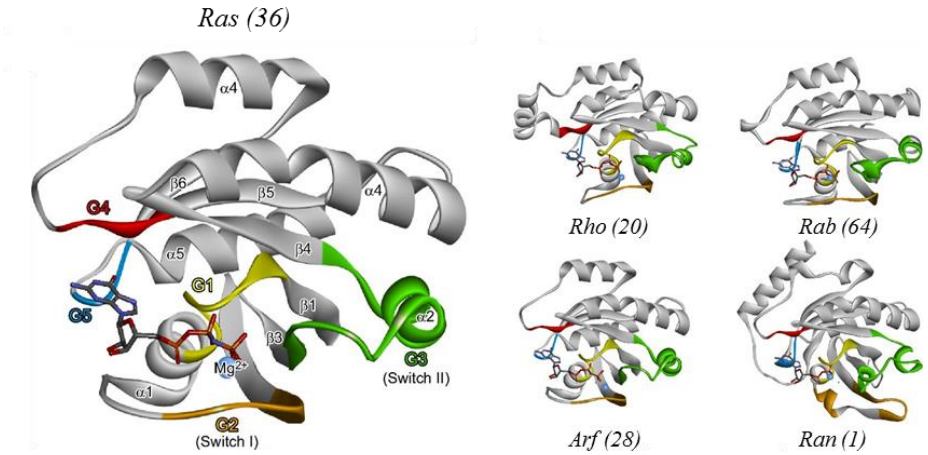

Figure 3: The Ras superfamily – A structural overview.
The 5 different members Ras, Rho, Rab, Arf and Ran of the superfamily are shown. A typical structure of small GTPases is illustrated by the H-Ras in complex with GTP. Conserved sequence motives (G1 – G5), are color coded. Switch I is highlighted in orange, switch II in green. Secondary structural elements are marked (α1 – α5 and β1 – β6). GTP is shown in bond-stick-representation. The number of up to now identified human genes is shown in brackets. Adapted with no permission requirement from [Physiol. Rev.] (Loirand et al, 2013), © (2013).

With more than 60 members the Rab GTPases form the largest branch of the Ras superfamily (Lachance et al, 2014). As founding member of a large superfamily of Ras-related proteins, Ras proteins function as signal transducers and are mutationally activated in many human cancers (Repasky et al, 2004). In general activated Ras proteins are involved in the regulation of cytoplasmic signaling networks which control gene expression and regulation of cell proliferation, differentiation, and survival (Repasky et al, 2004). The proteins of the Rho family, with RhoA, Rac1 and Cdc42, being the best studied (Wennerberg et al, 2005), serve as key regulators of extracellular-stimulus-mediated signaling networks that regulate actin-organization, cell cycle progression as well as gene expression (Etienne-Manneville & Hall, 2002). As most abundant small GTPase in the cell, Ran family members function in nucleocytoplasmic transport of both RNA and

proteins (Weis, 2003). Rab GTPases, which are part of this work, are key regulators of intracellular vesicular transport and the trafficking of proteins between different organelles of the endocytic and secretory pathways (Zerial & McBride, 2001). Like the Rab proteins, the Arf family members are although involved, as major regulators of vesicle biogenesis, in intracellular trafficking (Memon, 2004).

Studying the amino acid sequences of small G proteins from various species showed that the primary structures share 30 – 55% sequence homology. Furthermore all G proteins possess a consensus sequence responsible for GDP/GTP binding and GTPase hydrolytic activity (Valencia et al, 1991). Additional the analysis of small G proteins by crystallography and NMR revealed that all Ras superfamily members share a conserved structure that is an approximately 20 kDa catalytic domain (G domain) (Paduch et al, 2001). Moreover the N- or C-terminal extensions beyond the G domain are unstructured in most cases and are usually not included in the structures (Wittinghofer & Vetter, 2011). Due to the strong sequence deviations in the C-terminal part of Rab proteins (last 27 – 47 amino acids) this region is termed hypervariable region (Li et al, 2014).

A general structural overview on the Ras superfamily is shown in Figure 3 and Figure 9. The main structural characteristics are described in more detail in the following section.

1.3.1 Structural Characteristics of RabGTPases

The structure of small GTPases exhibits six central orientated β-strands (B1 – B6, mostly parallel orientated), which are surrounded by five α-helices (A1 – A5) and connected by five polypeptide loops (G1 – G5, guanine base binding region) (Figure 9). Thus GTPases can be classified as α,β proteins, adopting a mononucleotide binding fold (Leipe et al, 2002), which is typical for guanine nucleotide binding proteins (GNBPs) (Bourne et al, 1991; Vetter & Wittinghofer, 2001). Additional PM1 – PM3 regions are defined (phosphate-/ magnesium-binding region). Contrary to a general rule that within different protein folds secondary structural elements are more conserved than loop regions, the most conserved structural elements of the G domain are the loop regions (Figure 9) (Paduch et al, 2001). Thus the G1 to G5 regions consist of five conserved motives that are critical in GDP/GTP exchange, GTP-induced conformational change, and GTP hydrolysis (Bourne et al, 1991). The consensus sequence motive $GX_4GK(S/T)$ of the G1 loop region (also called the P-loop, phosphate-binding loop, PM1, Walker A motive) coordinates the nucleotide by interaction of the lysine amide-hydrogen of the protein backbone with the α- and β-phosphate of the nucleotide (Leipe et al, 2002; Saraste et al, 1990).

Due to the conserved glycine residues, which adapt sterical unfavorable angle of torsion (unusual to other amino acids) the P-loop region is not affected by conformational changes during GTP hydrolysis (Kraulis et al, 1994). A structural comparison of the GTP- and GDP-bound form, allows to distinguish two functional loop regions, switch I (G2, PM2) and switch II (G3, PM3, Walker B motive (Leipe et al, 2002)) that surround the γ-phosphate group of the nucleotide (Paduch et al, 2001). After nucleotide exchange (GDP to GTP) or the GTP hydrolysis reaction, these switch regions show the strongest conformational changes (Schlichting et al, 1990; Vetter & Wittinghofer, 2001). In order to facilitate nucleotide binding and GTP hydrolysis the presence of a magnesium ion (octahedral coordination) in the catalytic core is essential. Therefore the hydroxyl groups of the serine located in the P-loop region, a highly conserved threonine residue of the switch I region (G2) and an invariant aspartate of the DX_2G sequence in the switch II region (G3) are involved in coordinating the magnesium ion (Bourne et al, 1991). The interaction of the aspartate (G3) with the magnesium ion is critically required for tight nucleotide binding and GTP hydrolysis in most Ras-like and other G proteins (Wittinghofer & Vetter, 2011). In addition the glycine of the DX_2G motive forms a hydrogen bond with the γ-phosphate of the GTP (Bourne et al, 1991). The oxygen of the β-phosphate of the GTP coordinates the magnesium ion.

Thus the strong conformational changes in the switch regions can be described best as a loaded spring mechanism, where release of the γ-phosphate after GTP hydrolysis allows the two switch regions to return into the GDP-specific conformation (Vetter & Wittinghofer, 2001). The discrimination against other nucleotides is achieved by interaction of the NKXD (G4) and TSA (G5) with the nucleobase (Itzen & Goody, 2011; Wittinghofer & Vetter, 2011). Thereby the specificity for guanine is determined by the aspartate side chain of the NKXD motive (G4), which for steric reasons would not tolerate an adenine 6-amino group (Wittinghofer & Vetter, 2011). In general the carboxyl group of the aspartate of the NKXD motive forms hydrogen bonds on the guanine ring, while the asparagine and the lysine residues stabilize the guanine binding site by the formation of hydrogen bonds with the G1 region (Bourne et al, 1991). In contrast to the motives G1 – G4 the amino acids of the G5 region react only indirectly with the guanine nucleotide by stabilizing the aspartate and asparagine side chains of the conserved NKXD region (G4) (Bourne et al, 1991). A detailed sequence analysis by Pereira-Leal *et al.* identified five additional Rab family specific motives, the RabF1 – RabF5 regions (Figure 9) that, based on their primary structure, enable the discrimination from other Ras superfamily members (Pereira-Leal & Seabra, 2000).

Interestingly these regions localize in and around the switch I- and switch II-region and thus mediate interactions with effector and regulator proteins (Pereira-Leal & Seabra, 2000; Pereira-Leal & Seabra, 2001). Four segments which are specifically conserved between subfamily members are designated as RabSF1 – RabSF4 region (Ali et al, 2004). In contrast to the RabF motives, the RabSF regions are localized in the N- and C-terminal region, thus on opposite sides of the Rab protein surfaces.

Due to the strong sequence divergence of the Rab subfamilies, one can hypothesize that the interaction specificity of distinct Rab proteins with respective effectors/regulators (guanine nucleotide exchange factors (GEFs), GTPase activating proteins (GAPs)) is enabled by the RabSF regions (Pereira-Leal & Seabra, 2000; Pereira-Leal & Seabra, 2001). The binding of general regulators, such as Rab escort protein (REP) and Rab GDP dissociation inhibitor (RabGDI), which are nucleotide sensitive, occurs via the RabF regions (Pereira-Leal & Seabra, 2000; Pereira-Leal & Seabra, 2001; Pereira-Leal et al, 2003).

Besides the highly important sequence motives, necessary for nucleotide binding, the biological function of small G proteins strongly depends on posttranslational modifications (Paduch et al, 2001). Thus most members of the Ras-superfamily contain a C-terminal signal sequence (located in the hypervariable region), consisting of cysteine residues, which undergo posttranslational modification like lipidation (termed prenylation), resulting in the reversible attachment of the GTPase with the cell membrane (Berndt & Sebti, 2011; Pereira-Leal & Seabra, 2001). For Ras and Rho family members -CAAX (C: cysteine, A: aliphatic amino acid, X: any amino acid) prenylation motives are common (Pereira-Leal & Seabra, 2000), whereas Rab GTPases are recognized by signal sequences like –XXCC (35%), –XCXC (37%), –CCXX (15%), –CCXXX (8%) or –CXXX (5%) (Farnsworth et al, 1994). In context of the prenylation motive a C15- (farnesyl) or C20- (geranylgeranyl) isoprenoid group is covalently attached to the protein (Pereira-Leal 2001). Rab proteins have been shown to be substrates for prenylation by their specific enzyme Rab geranylgeranlytransferase (GGTase) (Shen & Seabra, 1996). Consequently a geranylgeranyl anchor (C-20 isoprenyl) is covalently attached to the C-terminal cysteine of the Rab proteins by the formation of a stable thioether bond. This is achieved in a concerted action of REP and GGTase (Li et al, 2014). Thereby REP promotes the geranylgeranyl reaction in at least two different ways: by binding the apo-protein substrate and by forming a complex with the GGTase (Farnsworth et al, 1994). In contrary to other prenylation enzymes, like farnesyltransferase (FTase) and GGTase I, the catalytic α,β dimer of Rab GGTase is unable to modify monomeric GTPase substrates (Overmeyer et al, 1998; Pereira-Leal et al, 2003).

Instead, the Rab protein must first bind to the carrier, the REP, to form a stable Rab:REP complex (Overmeyer et al, 1998; Thoma et al, 2001), followed by the formation of a ternary catalytic Rab:REP:GGTase complex (Li et al, 2014). After attachment of hydrophobic geranylgeranyl groups the REP stays bound to Rab, enabling the Rab to remain in solution until it is delivered to the appropriate membrane (Rak et al, 2003).
In conclusion the posttranslational modification of the Rab GTPases is required for their activity as functional regulators for numerous membrane trafficking steps (vesicle budding, targeting, fusion, motility) (Kohnke et al, 2013; Pereira-Leal et al, 2001).

1.4 RabGTPases – Regulators of vesicular transport

1.4.1 Rab-Cycle

The compartmentalization of eukaryotic cells requires the transport of lipids and proteins between distinct membrane-bounded organelles (Stenmark & Olkkonen, 2001). In general this is achieved in a tightly regulated vesicular transport process. Thereby RabGTPases function as central regulators in controlling the vesicle budding, motility and fusion with the acceptor membrane (Novick & Zerial, 1997). Basically each small G protein functions as a precisely engineered molecular switch existing in two interconvertible conformational states (Hall, 1990). Consequently the RabGTPase cycles between membranes and cytosol depending on the nucleotide-bound state (Gavriljuk et al, 2013) and thereby control diverse cellular processes. The Rab cycle is schematically depicted in Figure 4 and described in detail in the following section. The Rab proteins are active in their GTP bound state and become inactivated by hydrolyzing GTP to GDP and, thereby changing its affinities for interaction partners (Bourne et al, 1991). These states are structurally distinguished by the conformations of two structurally flexible loop regions known as switch I (G2) and switch II (G3) which change their conformations dramatically between the active and inactive form (Zhu et al, 2010) (see chapter 1.3.1). The switch regions, particularly switch II, are loosely packed in the GDP-bound state, but become highly ordered and structurally restrained in the GTP form, due to largely structural contacts made by the GTP γ-phosphate (Goody & Itzen, 2013; Zhu et al, 2010).
When bound to GDP the inactive Rab proteins are predominantly distributed in the cytosol bound to GDI (Oesterlin et al, 2012).

In this thermodynamically favored extraction process, the prenylation of RabGTPases is strictly required for stable complex formation with the GDI (nanomolar affinity), whose affinity for unprenylated Rabs is very low (micromolar range or even lower) (Wu et al, 2007). The human genome encodes only two expressed GDI that show tissue-specific expression and that bind to all of the different Rab proteins in their inactive forms (Pfeffer & Aivazian, 2004). They extract the G proteins from membranes and solubilize them in form of the Rab:GDP:GDI complex (Oesterlin et al, 2012; Schoebel et al, 2009). The dissociation of tightly bound GDI from Rabs is believed to require a GDF (GDI displacement factor) (Suh et al, 2009). This then leads to lipid insertion and membrane localization of Rab. PRA-1 (prenylated Rab acceptor, Yip3 in yeast), an integral membrane protein, is so far the only known eukaryotic protein with GDF activity, catalyzing the GDI displacement from endosomal Rab9 (Sivars et al, 2005), Rab5 and Rab7 (Schoebel et al, 2009). Beyond, Oesterlin *et al.* discovered that effective GDI release was achieved by post translational phosphocholination of Rab1 and Rab 35 (Tyr77 (Rab1b), Ser76 (Rab35)) by the enzyme AnkX (Oesterlin et al, 2012).

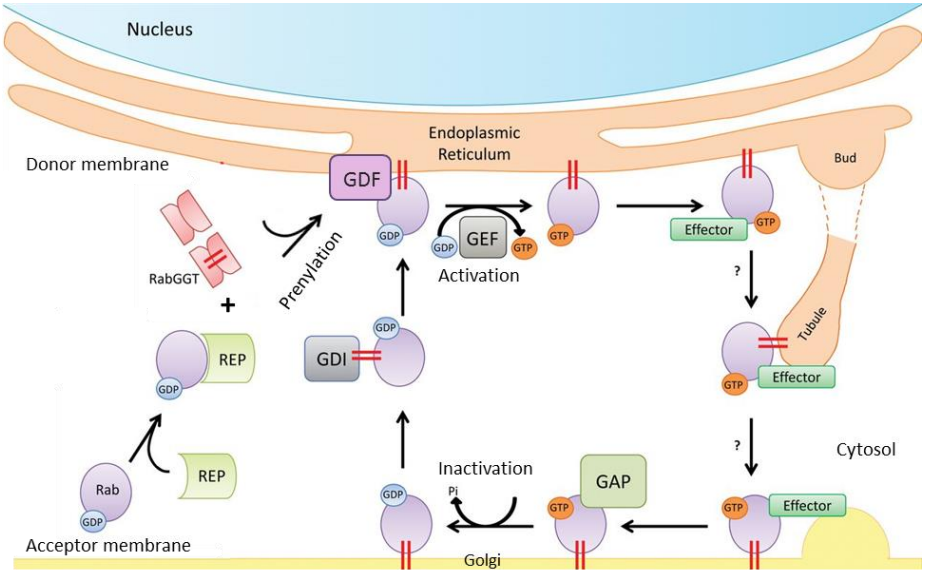

Figure 4: Rab GTPase cycle.
Schematically depicted is the interaction of Rab GTPases with regulatory and effector proteins in vesicular transport. In the cytosol Rab in its inactive GDP bound form is recognized by the Rab escort protein (REP). The binary Rab:REP complex is then identified by the Rab specific Geranygeranyltransferase (RabGGT). This enzyme posttranslational modifies the Rab protein by attaching a prenyl anchor (C20- moiety), necessary for insertion into the donor membrane (e.g. ER). GTPases are activated by guanine nucleotide exchange factors (GEF), catalyzing the GDP to GTP exchange reaction. The activation of the G protein occurs at the donor membrane. In their active GTP bound form Rab proteins can interact with various effector proteins initiating specific processes in vesicular transport (e.g. budding, vesicle movement, tethering and fusion with acceptor membrane). After completion of transport the GTPase is inactivated at the acceptor membrane (e.g. Golgi), by GTPase activating protein (GAP), accelerating the GTP hydrolysis reaction. Recycling of the small GTPase is achieved by a GDP dissociation inhibitor (GDI), which extracts Rab from the acceptor membrane. Additional, the GDI maintains the solubility of the protein during transport by shielding the highly hydrophobic isoprene moiety through binding to its hydrophobic binding pocket. The GDI displacement after re-shuttling of the Rab GTPase is achieved by the GDI dissociation factor (GDF). Adapted from (Sandoval & Simmen, 2012).

After recycling to the respective donor membrane, association of the Rab protein with the intracellular membrane is achieved by post-translational lipidation at its structurally flexible C-terminus (Berndt & Sebti, 2011; Pereira-Leal & Seabra, 2001). Thereby, in a concerted action of GGTase and REP (Li et al, 2014), mostly two cysteine residues are covalently modified with to geranylgeranyl moieties (Wu et al, 2007). Like other prenyltransferases, the GGTase is a heterodimer of α- and β-subunits. It requires an additional unique protein, the REP, representing the Rab protein by formation of the Rab:REP complex to the GGTase (Wu et al, 2007). In the then formed catalytically active ternary Rab:REP:GGTase complex the Rab protein becomes prenylated (Li et al, 2014). After lipidation of the small GTPase the REP stays bound to Rab, enabling the Rab to remain in solution until it is delivered to the appropriate membrane (Rak et al, 2003). The posttranslational modification is necessarily required to ensure stable association of RabGTPase with membranes (Ghomashchi et al, 1995), mainly through the strong hydrophobic character of the C20-isoprenoid.

The transition between the active and inactive state is a slow process by itself, because the intrinsic GTPase activity is low, and GDP release from the active site is slow (Suh et al, 2009). Thus the cycling between both states is mediated by accessory proteins, GEFs and the GTPase activating proteins GAPs (Wiegandt et al, 2015), leading to efficient activation and inactivation of the Rab protein and the tight control of distinct cellular processes on a physiologically relevant time scale. The GEFs specifically stimulate the replacement of GDP on Rab proteins by cytosolic GTP (Schoebel et al, 2011), due to an excess of GTP against GDP in the cell (Barr & Lambright, 2010). The hydrolysis of GTP to GDP is catalyzed by GAPs (Gavriljuk et al, 2013), leading to intrinsic GTP hydrolysis rate acceleration up to 10^5 fold (Gavriljuk et al, 2012). Generally, forward signaling by G proteins is only possible in the active form and is mediated by the interaction with so-called GTPase effector proteins (Goody & Itzen, 2013). That means that active Rabs, attached to the membrane, serve as molecular beacons that attract a diverse set of Rab effectors (e.g., tethering factors, molecular motors, phospholipid modulators, etc.), and thereby determine vesicular trafficking at that membrane (Goody & Itzen, 2013). The most prominent Rab effectors are described in more detail in section 1.4.5. The inactive Rab is removed from the membrane and re-cycled to the donor membrane via the GDI. In doing so the GDI executes his possibility to inhibit the intrinsic GDP dissociation from RabGTPases, which was first observed for the G protein *smg* p25A (bovine Rab3A) (Sasaki et al, 1990), and therefore prevent the inappropriate activation of Rab proteins (Machner & Isberg, 2007).

Due to the three times of magnitude lower affinity of GDI against the GTP-bound form, compared to the GDP-bound state, one can ensure that only inactive Rabs are extracted from the acceptor membrane and maintained in a cytosolic pool until the need for transport at the distinct donor membrane (Wu et al, 2010).

1.4.2 General principles for the GEF catalyzed nucleotide exchange reaction

Small G proteins are activated by GDP/GTP nucleotide exchange stimulated by GEFs (Renault et al, 2003), as the guanine nucleotide release from GNBPs is a slow process itself (Vetter & Wittinghofer, 2001). Despite the highly structural and sequence specific divergence of GEFs, exchange factors share a similar mechanism for the release of the bound nucleotide from the RabGTPase. For the first time the principle of the nucleotide release reaction was shown with Ran and the RCC1 (regulator of chromosome condensation) GEF (Klebe et al, 1995). Thereby two high affinity, binary complexes (GTPase:GDP/GTP and GTPase:GEF) and a ternary complex (GEF:GTPase:GDP/GTP) were identified. The mechanism of GEF action involves a series of fast reaction steps, which lead from a binary protein-nucleotide complex via a trimeric GNBP-nucleotide-GEF complex to a binary nucleotide-free complex (GNBP:GEF) (Vetter & Wittinghofer, 2001). This is stable in the absence of any nucleotide. Compared to the binary complex the reduced affinity predominantly results from an increased dissociation rate of the GEF and the nucleotide from the ternary complex (Itzen & Goody, 2011). This is achieved by displacement of the magnesium ion, leading to a dramatically acceleration of GDP in presence of a GEF (Itzen & Goody, 2011; Klebe et al, 1995). In most of the cases the GEF interacts with the switch II region (Ras:Sos complex also interaction with switch I) and an additional phosphate binding motive (P-loop or switch I), though weakening the affinity of the nucleotide bond. As already described in chapter 1.3.1, the interaction of an invariant aspartate of the DX_2G sequence in the switch II region (G3) with the magnesium ion is critically required for tight nucleotide binding in most Ras-like and other G proteins (Wittinghofer & Vetter, 2011). The divalent magnesium ion binds with micro molar affinity on Ras GTPases and thus decelerates the GDP dissociation velocity by four orders of magnitude (Hall & Self, 1986). This clarifies the conserved binding of various GEFs to the switch II region, thus altering the affinity for the nucleotide. Consequently, the magnesium ion, as well as the P-loop is displaced by amino acids of the GEF.

Affinity studies showed that the β-phosphate –P loop interaction is the most important element for tight binding of the nucleotide (Vetter & Wittinghofer, 2001). Thus structural disturbance of the P-loop is most likely the major reason for the drastically decreased affinity (Vetter & Wittinghofer, 2001). However, the structures reported so far, only show the stable reaction intermediate and do not necessarily indicate how GEFs approach the G protein and how they form the low-affinity ternary complex, in which the nucleotide affinity decreases by five orders of magnitude (Vetter & Wittinghofer, 2001). In the nucleotide free complex the P-loop is stabilized either by interaction of the highly conserved lysine from the P-loop with acidic residues from either the GNBP itself (switch II) or with an invariant glutamic acid finger from the GEF (Goldberg, 1998). The induced conformational changes, mainly in the switch I and switch II region, result in opening the nucleotide binding pocket and finally releasing the nucleotide (Barr & Lambright, 2010; Renault et al, 2003; Vetter & Wittinghofer, 2001). Consequently, the nucleotide free G protein gets activated by binding *in vivo* to GTP, which is present in the cell in higher concentration as GDP (Klebe et al, 1995).

1.4.3 Rab GEFs – a heterogeneous group

In general GEFs are multi-domain proteins or subunits of multimeric protein complexes. The TRAPP (transport protein particle) complexes I and II from *S. cerevisiae* contain six core subunits (Bet3, Bet5, TRAPP subunit 20 (Trs20), Trs23, Trs31, Trs33) from which four subunits (Bet3, Bet5, Trs23, Trs31) mainly catalyze the nucleotide exchange reaction of Ypt1 and Rab1, thus affecting both ER-Golgi transport and intra-Golgi transport (Barrowman et al, 2010). In contrast to GAPs, most of the GEFs do not possess a unique region that enables the identification via the amino acid sequence. Nevertheless, in a vast majority of Rab specific GEFs, it was possible to identify two sequence motives, the DENN- (differentially expressed in normal and neoplastic cells, see Marat *et al*. for Rab specificity of DENN GEFs) (Marat et al, 2011) and the VPS9-domain (vascuolar protein sorting, GEFs for Rab5, Rab21, Rab22) (Carney et al, 2006). The DENN-domain, consists of the subdomains uDENN (upstream DENN), DENN and dDENN (downstream DENN) (Marat et al, 2011). For influencing the Rab specific localization, a partial co-localization of the GEF with the respective Rab can be expected. For example Yoshimura *et al.* identified the co-localization of DENND1A/1B with its sub-strate Rab35 to clathrin coated vesicles at the plasma membrane (Yoshimura et al, 2010).

VPS9-domain protein GEFs are specific for different members of the Rab5 subfamily (Barr & Lambright, 2010). Best characterized is Rabex-5 (Rabaptin-5-associated exchange factor for Rab5), in which VPS9-domain proteins form a complex with the Rab5 effector Rabaptin-5 and due to their specific nucleotide exchange activity for Rab5 were termed Rabex-5 (Kalin et al, 2015).

An exceptional position is taken by the protein DrrA/SidM (defect in Rab recruitment A) from *Legionella pneumophila*, being the first bacterial GEF identified (Machner & Isberg, 2006). The bacterium recruits the host cell GTPase Rab1 to its surrounding vacuole as well as material from the host cell ER in order to generate a Legionella-containing vacuole (LCV), necessary for replication of the pathogenic bacteria (Machner & Isberg, 2006). Besides, its function as GDF, DrrA is a highly specific GEF of Rab1 GTPase (Ingmundson et al, 2007) and therefore was used in this thesis. In general the GEF activity of the DrrA can be assigned to the amino acids 340 – 533 (Schoebel et al, 2009). By Schoebel *et al.* it was shown that the DrrA GEF domain has two binding sites which basically contact the P-loop and the switch regions of Rab1B (Figure 5, (Schoebel et al, 2009)).

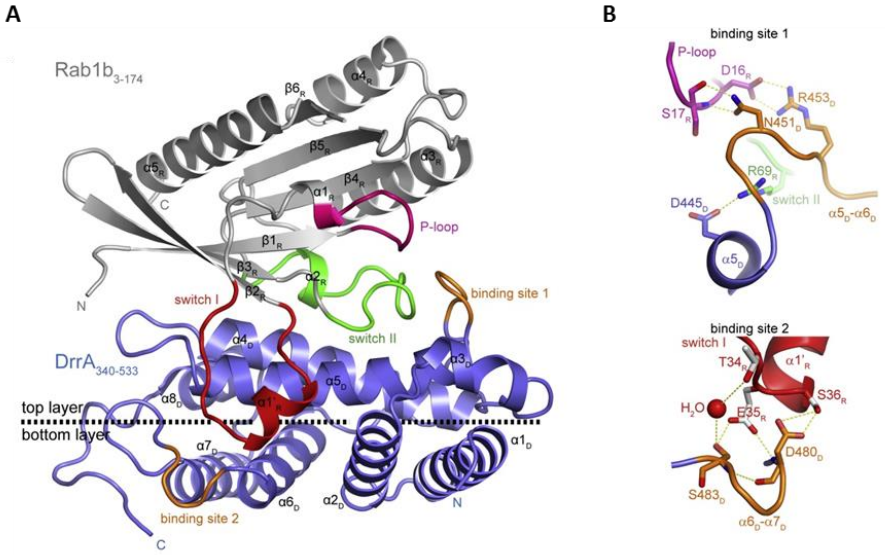

Figure 5: Interaction motive of DrrA GEF with Rab1 GTPase.
A) Crystal structure of $Rab1B_{3-174}$:$DrrA_{310-533}$ complex. DrrA is shown in grey. Due to DrrA binding crystal structure depicts solvent exposed nucleotide binding pocket of Rab1B formed by P-loop (magenta), switch I (dark red) and switch II (green). Binding sites of DrrA GEF to the Rab protein are highlighted in orange. **B)** Detailed view of the interaction of DrrA with the two binding sites of GTPase. Binding site one involves P-loop and switch II (top), binding site two involves switch II (bottom). Yellow dashes indicate polar interactions. Adapted by permission from Elsevier: [Mol. Cell] (Schoebel et al, 2009).

In particular the amino acids asparagine $N451_D$ and arginine $R453_D$ of the GEF binding site 1 interact with the P-loop (Serine $S17_R$, aspartic acid $D16_R$).

In addition, arginine $R69_R$ (switch II) interacts strongly with a negatively charged pocket of the GEF (Schoebel et al, 2009).

Further, the residues aspartic acid $D480_D$ and serine $S483_D$ from binding site 2 contact the switch I region (threonine $T34_R$, glutamine acid $E35_R$, serine $S36_R$) (Figure 5B, (Schoebel et al, 2009)). Mutational studies highlighted the important role of the amino acids asparagine $N451_D$ and arginine $R453_D$ for the DrrA GEF activity. In contrast to other Rab GEFs the DrrA additionally increases the intrinsic nucleotide release by more than five orders of magnitude, hence representing a highly efficient GEF (Schoebel et al, 2009). DrrA has a maximum exchange rate of 7.6 s^{-1}, whereas the maximum rate of nucleotide exchange is only 0.012 s^{-1} for VSP9 and 0.17 s^{-1} for TRAPP (Chin 2009, Esters 2001). By this DrrA outperforms the host GEFs to confer pathogenicity (Schoebel et al, 2009). A comparison of the yeast Ypt1:DrrA complex depicted that DrrA catalyzed nucleotide exchange is not possible until GDI dissociated from Rab1, due to the competition for the same binding site. A rebinding of the GDI to the activated Rab protein can be excluded, because of a three orders of magnitude lower affinity for the Rab:GTP form.

1.4.4 Rab GAPs – a highly conserved group

The duration of the active state of G proteins is limited by GAPs, which accelerate the slow intrinsic rate of GTP hydrolysis by more than 10^5-fold (Gavriljuk et al, 2012; Pan et al, 2006). In general the GAPs bind with micromolar or sub-micromolar affinity to the active G protein (e.g. Ras:GTP), and several orders of magnitude less strongly to the inactive form (e.g. Ras:GDP) (Goody & Hofmann-Goody, 2002). Among eukaryotic organisms Rab GAPs contrary to GEFs, consist of a highly conserved Tre2-Bub2-Cdc-16 (TBC) domain (Frasa et al, 2012). In this thesis the Rab1 specific GAP TBC1D20 was used (Frasa et al, 2012). In the following, the structural and catalytical features of the TBC GAPs are described in brief.

One of the best characterized TBC-domains is Gyp1p (GAP for Ypt1p) containing 16 helices distributed between an N-terminal subdomain ($\alpha1_T$ – $\alpha8_T$) and a C-terminal subdomain ($\alpha9_T$ – $\alpha15_T$) (Rak et al, 2000) (see Figure 6A). Three signature motives (RXXXW, IXXDXXR, YXQ, located in the N-terminal subdomain) were identified, in which IXXDXXR and YXQ are crucial for the hydrolytic activity of the GAP (see Figure 6B, (Barr & Lambright, 2010)). The RXXXW motive appears to be important for the structural integrity of the TBC domain (Gavriljuk et al, 2012). The transition state between the Rab GTPase and the GAP is stabilized by polar/electrostatic

interactions, resulting from the "arginine- (IXXDXXR motive) and glutamine-finger" (YXQ motive, *trans*-glutamine) (Frasa et al, 2012; Pan et al, 2006).

Thereby the arginine and the glutamine interplay with the β-phosphate of GTP so that γ-phosphate of GTP easily hydrolyze and dissociate from Rab (Park, 2013). Thus, a general feature of GTP hydrolytic reactions by TBC-domain containing Rab GAPs is a dual-finger catalytic reaction mechanism. Further, the presence of the conserved glutamine in the DX_2GQ (G3, switch II, *cis*-glutamine) of all known TBC domain substrates and its interaction with backbone atoms of the YXQ GAP motive is likely to be an additional characteristic for the GAP reaction (Langemeyer et al, 2014). Thereby it may stabilize the Rab-GAP complex rather than playing a direct role in the catalysis (Langemeyer et al, 2014). Consequently, Rab is pulled out of the active site, leaving the active site accessible for the catalytic GAP residues allowing $Q144_T$ of GAP to move into the active site (Gavriljuk et al, 2012). In contrast to the intrinsic reaction, the attacking water molecule can now be stabilized in the correct position for nucleophilic attack, which is probably the key contribution of RabGAP to catalysis (Gavriljuk et al, 2012). Evidently, the *cis*-glutamine participates directly in transition-state stabilization for the intrinsic reaction but is co-opted by the *trans*-glutamine finger in the reaction catalyzed by the TBC domain (Pan et al, 2006). Nevertheless, there are also examples (LepB GAP), where GAP deactivates the Rab protein via the *cis*-glutamine (*trans*-glutamine for TBC-GAPs), so opening the possibility for further mechanistic GAP reaction pathways (Mihai Gazdag et al, 2013).

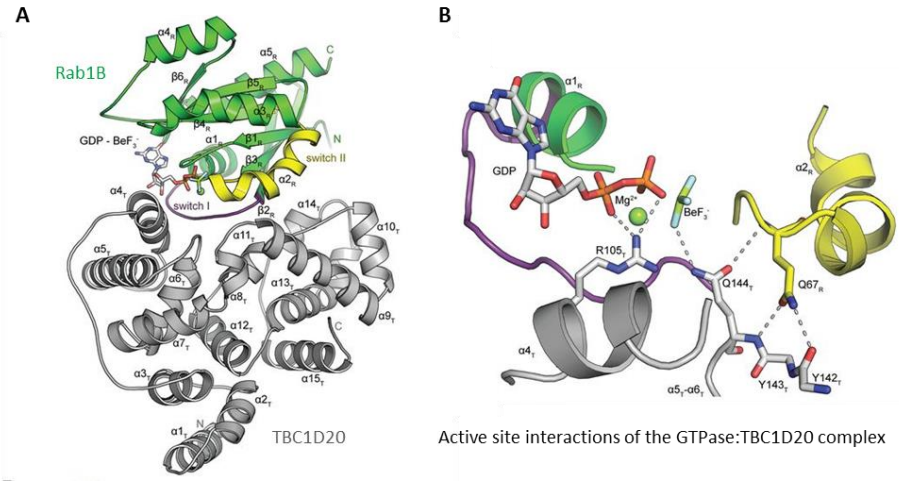

Figure 6: Structure and interaction motive of TBC-domain containing GAPs.
A) Three-dimensional TBC-domain structure in complex with Rab1b:GDP:BeF_3^-. GDP:BeF_3^- is shown in ball-stick-representation. TBC1D20 is depicted in grey, secondary structural elements are marked (N-terminal subdomain: $\alpha1_T$ – $\alpha8_T$, C-terminal subdomain $\alpha9_T$ – $\alpha15_T$). Major parts of the Rab1b protein are shown in green, switch regions are color coded (switch I: magenta, switch II: yellow). **B)** Active site interactions of TB1D20 GAP (grey) and Rab1b protein (green). Switch I region is colored in magenta, switch II in yellow. Functional groups involved in active site interactions are indicated by labeling. Adapted by permission from PNAS: (Gavriljuk et al, 2012).

1.4.5 Rab effectors involved in the vesicular transport

To ensure that vesicles, generated from a donor compartment are delivered to their correct acceptor compartment and vice versa, a tight regulation is required, which is mainly achieved by the interaction of Rab GTPases with effector proteins (Cai et al, 2007). The basis for effector recognition only in the active state of the Rab protein, results from structural different conformations in both states, as well as the presence of effector specific sequence elements (see chapter 1.3.1). GTP hydrolysis leads to a conformational change in the switch regions, being less ordered in the GDP state, thereby making the GTPase unrecognizable to its effectors (Gonzalez Jr & Scheller, 1999). A hydrophobic patch that is more exposed in the GTP state is also a common feature in many GTPase effector interactions (Itzen & Goody, 2011). Also, GTPase effector proteins show a much higher affinity for the GTP state compared to the GDP form (Goody & Itzen, 2013). As a general feature, all known Rab effector complexes involve interactions of one (e.g. Rab3a:Rabphilin3A), or more commonly two α-helices (arising from homodimeric coiled coil structures, e.g. Rab5:Rabaptin5) of the effector with a region of the GTPase encompassing switch I, switch II and the interswitch regions in addition to specific interactions outside this area (Itzen & Goody, 2011). Common to all Rab effector interactions seen is the involvement of a so-called hydrophobic triad, consisting of a phenylalanine at the beginning of the interswitch region, a tryptophan in the second β-strand of the interswitch region and a tyrosine near the end of switch II (Itzen & Goody, 2011).

In contrast to the high degree of conservation within the Rab GTPase family, Rab effector sequences are unrelated, resulting in the possibility that a single Rab GTPase can have more than one effector (Segev, 2001a). However, effector proteins can also be shared between related Rab proteins, providing concerted action of different Rab proteins within one pathway (Jordens et al, 2005). In general different Rab effectors act during vesicle formation (cargo selection, budding, coat formation) (1), movement (2), tethering (3), and fusion with the acceptor compartment (4), with each pathway having its own unique set of effectors (see Figure 7, (Hutagalung & Novick, 2011)).

Vesicle cargo selection is predominantly determined by components of coat complexes (COP I (coat protein complex I), COP II (coat protein complex II, composed of small GTPase Sar1, Sec23/Sec24 and Sec13/Sec31) or clathrin) by recognition of specific elements of the cargo to be transported (Hutagalung & Novick, 2011).

Mammalian cells contain about ten distinct COPs, each driving a distinct transport step through its particular specificity for a target organelle and for a cognate set of cargo molecules (Mancias & Goldberg, 2005). The COP proteins are mainly involved in the early secretory pathway (ER to intermediate compartment (IC) to Golgi) (Guo & Linstedt, 2013). COP I primarily acts from the Golgi to the ER and between the Golgi cisternae (recruited by Arf1, being activated by the GEF GBF1 (Golgi-specific brefeldin A resistant factor 1); GBF1 is activated by Rab1b (Guo & Linstedt, 2013; Monetta et al, 2007)), while COP II mediates traffic form ER to Golgi (recruited by Rab1 (Ypt1p in yeast)) (Cai et al, 2007; Papanikou & Glick, 2014). Sorting and concentration of cargo takes place in specialized ER domains (in the rough ER) called ER Exit Sites (ERES) or transitional ER (tER), where COP II coated vesicles bud from ERES (Garcia et al, 2011; Watson & Stephens, 2005). Following budding, COP II vesicles uncoat and fuse to create larger membrane structures termed vesicular tubular clusters (VTCs) that move along microtubules towards the central Golgi complex (Lanoix et al, 1999). Dissociation of the COP II complex is accompanied by assembly of the COP I complex marking the change in identity of the membrane from ER exit site to IC (Guo & Linstedt, 2013).

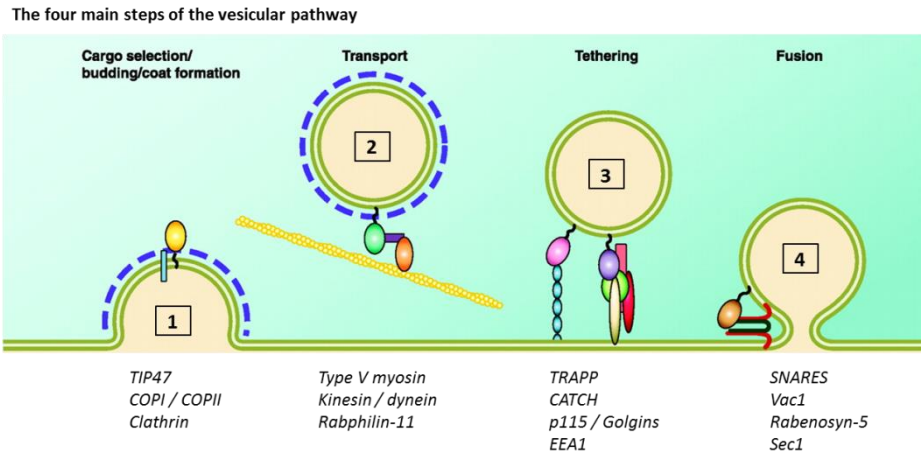

Figure 7: Involvement of different Rab effectors during vesicular transport.
In the active GTP bound form Rab proteins recruit and interact with a variety of effector proteins, thereby mediating different functions of the vesicular transport cascade. The four main steps of vesicular transport are: 1) Cargo selection/budding/coat formation, 2) vesicle transport, 3) vesicle uncoating/ tethering and 4) vesicle fusion. Examples of effectors involved are listed below each step. Adapted with no permission requirement from [Physiol. Rev.] (Hutagalung & Novick, 2011), © (2011).

The movement along actin- or microtubule-based cytoskeletal structures is achieved by type V myosin motor proteins or myosin VI motor proteins (Lipatova et al, 2008). In case of transport to sites of cell growth and for polarized secretion, Rab 11 (Ypt31/32 in yeast) interacts in its active form with Myo2 (type V) via the globular tail domain (GTD) (Lipatova et al, 2008).

The final step is the fusion of transported vesicles at their destination membrane that requires the coordinated action of Rab GTPases, tethering /complexes and SNAREs (soluble *N*-ethylmaleimide-sensitive factor attachment protein receptors, e.g. Sec22, syntaxin, VAMP (vesicle associated membrane protein)) (Jahn & Scheller, 2006)). Thereby the cooperation between Rabs and tethering factors (bridge membranes by binding to GTPases and SNAREs) is necessary for vesicle capture and is tightly coupled to vesicle fusion (Cai et al, 2007). In eukaryotes two different classes of tethers, elongated coiled-coil tethers (large hydrophilic dimeric proteins) like golgins, and multisubunit tethering complexes (MTC, three to ten subunits differing in size per subunit (50 – 140 kDa)) exist (Brocker et al, 2010). In general, MTCs seem to couple the recognition of membranes via Rab GTPases with the subsequent SNARE-mediated membrane fusion (Brocker et al, 2010). MTCs can be divided into two general groups CATCHR (complexes associated with tethering containing helical rods), involved in secretory pathway tethering, and those of the endolysosomal pathway, additional to the eukaryotic specific TRAPP complex (Brocker et al, 2010; Cai et al, 2007). For successful fusion, membrane-embedded SNARE proteins, consisting of a cytosolic coiled-coil domain, are needed on both the vesicles and the target membrane (Brocker et al, 2010). The current knowledge is that v-SNARE usually consists of a tail-anchored SNARE having a single SNARE motive (Hong, 2005). T-SNARE on the other hand consists of either two or three polypeptides (syntaxin: t-SNARE heavy chain, SNAP-25: two t-SNARE light chains) (Hong, 2005). Many SNAREs reside predominantly or even selectively, in specific subcellular compartments (Jahn & Scheller, 2006). For instance the syntaxins (1, 2, 4), SNAP 23 and 25 localizes at the plasma membrane, whereas VAMP is found on synaptic and neurosecretory vesicles and syntaxin-5 and VAMP4 in the Golgi apparatus (Hong, 2005). Some other SNAREs have an even more widespread distribution, including those who are involved in endosomal trafficking (Jahn & Scheller, 2006).
SNAREs from opposing membranes finally bring the two bilayers into close proximity by folding into specific four-helix-bundle complexes, which due to the released free energy, lead to subsequent fusion and lipid mixing of these bilayers (Jahn & Scheller, 2006).

1.4.6 Localization and involvement of RabGTPases in the cell

In order to maintain organelle homeostasis, the traffic of vesicles which fuse with a given compartment needs to be balanced with the flow of vesicles which bud from it (Vitale et al, 1998). Thus, in the exocytic and endocytic pathways of eukaryotic cells, Rab GTPases are essential regulators involved in most of the membrane transport events between various compartments within the cell (Segev, 2001a; Zerial & McBride, 2001). For a general overview on localization of RabGTPases see Figure 8.

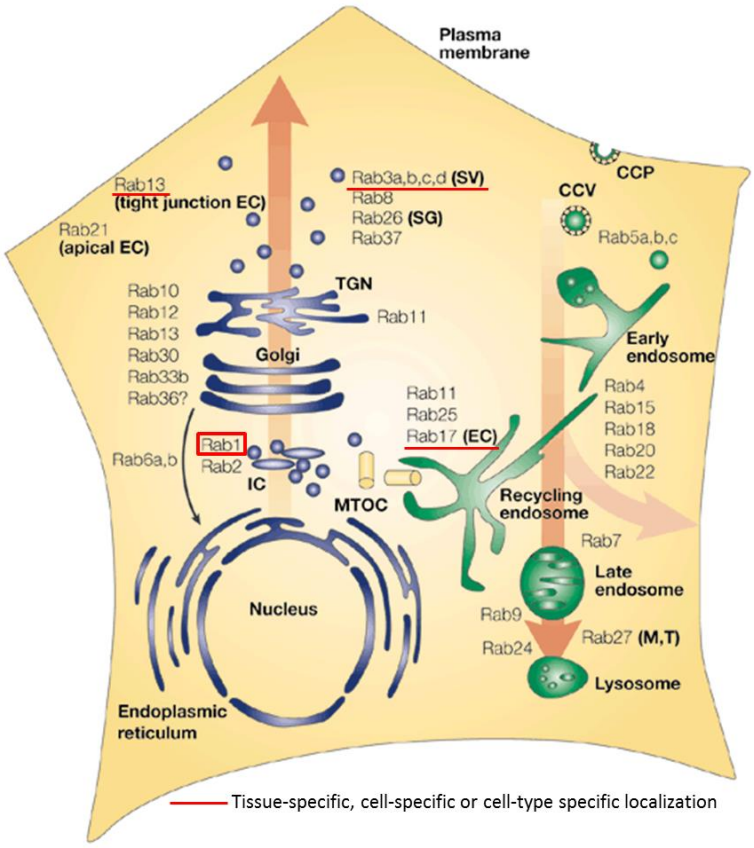

Figure 8: Intracellular localization of Rab proteins.
Summarized are the different localizations of Rab GTPases in mammalian cells. Rab1 (red frame) is involved in ER to Golgi transport. Rab1A and Rab1B isoforms are localized at the ER-Golgi interface and also within the Golgi-complex. Some proteins are tissue- (e.g. Rab17 in epithelia cells (EC)) or cell-specific (e.g. Rab3 in synaptic vesicles (SV)) others show cell-type-specific localization (e.g. Rab13 in tight junctions) (underlined in red). MTOC: microtubule-organizing center, IC: ER-Golgi intermediate compartment, TGN: *trans*-Golgi network, SG: Secretory granules, T: T-cell granules, M: MelanosomesAdapted by permission from Macmilan Publisher Ltd: [Nat. Rev. Mol. Cell] (Zerial & McBride, 2001), © (2001).

In the anterograde transport, cargo proteins move from the ER, through the Golgi apparatus (transport from *cis*-, to medial-, to *trans*-cisternae to *trans*-Golgi network (TGN)) to the PM (Segev, 2001a). Contrary, in retrograde transport, resident proteins and membrane components are retrieved from an acceptor compartment and returned to the appropriate donor partition (Segev, 2001a).

In the endocytic pathway, proteins are internalized into EEs, and transported by means of LEs to the lysosome (Segev, 2001b). As regulators of the exocytic transport Sec4 and Ypt1 (Yeast protein transport, Rab1 in human) were the first members identified in yeast (Hall, 1990). A conserved role was shown for human Rab1 (Ypt1 in yeast), while the closest homologue of Sec4, Rab8 (TGN to basolateral membrane), plays a role at a more specialized, transport step (Segev, 2001a). Rab1 especially mediates the vesicular transport step from ER to Golgi (Aivazian et al, 2006; Machner & Isberg, 2006), also Rab2 plays a role in ER to Golgi transit (Segev, 2001b). Though, Rab1A and Rab1B isoforms are localized at the ER-Golgi interface and also within the Golgi complex (Monetta et al, 2007). The intra-Golgi transport depends on the action of Rab6 (Bhuin & Roy, 2014). As described already in section 1.4.5 COP II vesicles are involved in the anterograde transport. Thereby Rab9 was determined as key GTPase in recruiting its effector TIP47 (tail-interacting protein, periilipin-3, cargo selection protein) for binding cargo receptors via their cytoplasmic mannose-6-phosphate tail (Aivazian et al, 2006). Rabphillin-11 a Rab11 effector, was shown to bind Sec13, a component of the COP II complex (Segev, 2001a). Besides the involvement of Rab11 in vesicular motility in secretory transport (see chapter 1.4.5), Rab5 was identified in regulating the movement of early endosomes on microtubules (Nielsen et al, 1999). Additional Rab3 is associated with secretory vesicles and has a role in regulated secretion of hormones and neurotransmitters (Fischer von Mollard et al, 1994). Further, Ypt/Rabs as well as Rab5 take part in the vesicular docking process. The Rab1 effector p115 (general vesicular transport factor, vesicle-docking protein) may tether vesicles to Golgi via its interaction with Golgi proteins, whereas EEA1 (early endosome antigen-1) and Vac1 (effectors of Rab5) are implicated in vesicular docking (Aivazian et al, 2006; Segev, 2001a). In the final step EEA1 then interacts with two distinct t-SNAREs, followed by the interplay of Vac1 and Rabenosyn (effector of Rab5) with Sec1 like proteins, being responsible for the regulation of SNARE complex formation (Segev, 2001a).

Rab6 has been implicated in intra-Golgi transport, and more recently, in Golgi-to-ER retrograde transport (Segev, 2001b). Rab11 has been implicated in both exocytosis and endocytosis, being on the one hand involved in TGN to PM and recycling to the Golgi and on the other hand in recycling from endosomes to PM (Segev, 2001b).

Coordination of entry and exit from individual compartments is predicted to be important for maintenance of the morphology of intracellular compartments while allowing bidirectional transport (Segev, 2001a).

To make this possible GTPases couple discrete protein transport steps by interaction with other GTPases either by coordinated GTPase activation or by coordinated GTPase function (Segev, 2001a). For example Rab5-mediated entry into early endosomes might be coupled with Rab4-mediated exit, as Rabaptin-5 (Rab5 effector) binds Rab4 (Segev, 2001b; Vitale et al, 1998).

As Rab5 and Rab3A function in the endocytic and exocytic pathways respectively, the observed interaction between their two effectors Rabphilin-3 (Rab3 effector) and Rabaptin-5 (Rab5 effector) might serve to coordinate these pathways (Segev, 2001b).

In conclusion, certain Rab effectors play a dominant role in small G protein localization (Aivazian et al, 2006). Importantly, the overall specificity of Rab localization is contributed to by multiple components, such as GDFs, the proximity of Rab-specific GEFs, and subsequent effector interactions (Aivazian et al, 2006).

2 Aims of the Study

The aim of the project was to analyze the consequences of non-trivial alternative splicing events on the conformation and function of different human proteins in a bioinformatics and biochemical approach. In particular, a large scale survey of splicing structures with respect to structural switches should elucidate the associated functional consequences as well as the conformational diversity implied by splicing. Preliminary work by Birzele *et al.* showed that the tolerance of proteins to structural deletions, insertions and replacements appeared to be higher than previously expected (Birzele et al, 2008a; Birzele et al, 2008b). In addition analysis on the effects of alternative splicing on the protein structure of isoforms have shown an unexpected complexity of alternative splicing events on the protein structure level (Csaba et al, 2008; Tress et al, 2007; Yura et al, 2006). Thus, it should be investigated, whether non-trivial splicing isoforms potentially exhibit different functional properties compared to the respective wild-type protein and how these functional changes would influence the regulation of protein networks in the cell. Stable non-trivial splice variants, which show altered structural behavior compared to their wild-type protein, would also lead to an increase in the conformational diversity of the proteome. Nevertheless, a common assumption is that alternative transcripts are prone to nonsense mediated decay (NMD) (Lareau & Brenner, 2015) or protein degradation immediately after their translation. This would be a major aspect against the contribution of non-trivial splice variants to proteome diversity. Thereby the generated isoforms might as well represent artifacts of the transcriptional machinery, which finally will not fold into stable proteins and cannot contribute any novel function to the proteome.

In conclusion, as until now it remains elusive to what extent the respected non-trivial spliced isoforms are structured and present on the protein level in the cell this was addressed in the thesis.

The bioinformatics studies and data evaluation were performed in cooperation with the bioinformatics group of Prof. Ralf Zimmer form the LMU.

Prior the biochemical characterization of selected splice variants the bioinformaticians identified potential non-trivial splicing candidates, based on comprehensive bioinformatics analysis of known transcripts and structures. Specifically designed high-throughput experiments (e.g. next generation sequencing (NGS) measurements) were applied. Further annotation studies were conducted and with a view to investigate the evolution of the respective nt-sv isoforms conservation analysis across various organisms were executed.

Interesting non-trivial isoforms were then expressed and further investigating with regard to their structure and function by a combination of theoretical (structure prediction, structure modeling) and experimental techniques (structure determination, functional characterization).

One non-trivial spliced isoform, studied exemplary in this thesis in detail, is Rab1A isoform 3 (nt-svRab1A). Three Rab1A splice isoforms are annotated in Swissprot/Uniprot (Figure 10A), all being structurally non-trivial. These variants show a high conservation across various organisms and their transcripts can be detected in a number of sequencing data sets in a variety of human tissues and in other species (Figure 10B) (Wilhelm et al, 2014)).

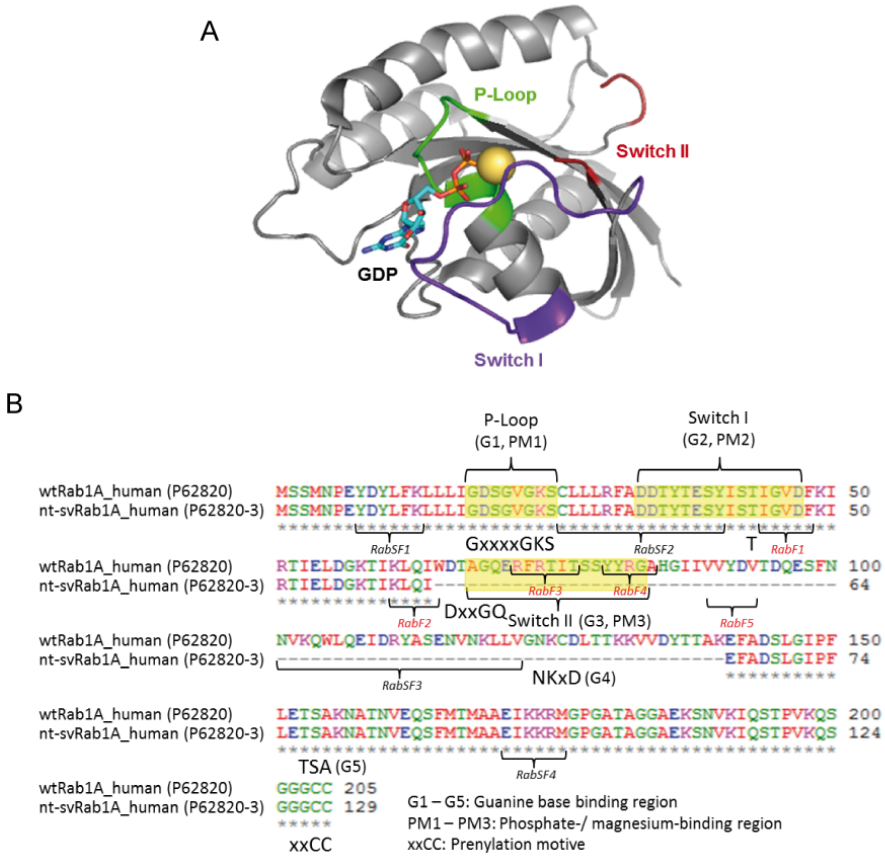

Figure 9: Structural Characteristics of RabGTPases.
A) Ribbon plot of the conserved sequence elements of the G-domain. P-loop: green, switch I: blue, switch II: red. The nucleotide and the magnesium ion is shown in ball-and-stick representation. **B)** Alignment of wtRab1A type with its non-trivial splice variant (nt-svRab1A) (Uniprot ID's are shown in brackets). G1 – G5 motives, as well as PM1 – PM3 regions are marked. Yellow squares highlight P-Loop, switch I and switch II region. Conserved sequence elements are indicated. Additional the RabF (red) and the RabSF (black) regions are shown.

Nt-svRab1A is of special interest as to the deletion of 37% of the residues of the wt protein, it represents a very small variant and lacks most of the proposed binding sites for binding partners and effector proteins (Figure 9).

Additionally, the mRNA for nt-svRab1A is especially expressed in normal breast organoids and not present in HER2 positive breast samples (Eswaran et al, 2013), which might indicate a correlation of the splicing event and breast cancer development. To further elucidate the physiological relevance of this variant, in a combined bioinformatics and experimental approach, the evolutionary conservation of nt-svRab1A as well as its structural and functional properties has been analyzed in this thesis.

3 Material and Methods

3.1 Devices and Materials

3.1.1 Devices

Balances:

Sartorious special accuracy weighing machine AX224, max. 210 g
(Sartorious AG, Göttingen, Germany)

Analytical balance SI4001, max. 4000 g, d = 0,01 g
(Denver Instrument, Göttingen, Germany)

Cell Disruption Apparatus Basic Z:
(Constant Systems Ltd., Low March, United Kingdom)

Centrifuges:

Eppendorf tabletop centrifuge 5418
(Eppendorf, Netheler, Hinz GmbH, Hamburg, Germany)

Eppendorf tabletop centrifuge with cooling unit 5402
(Eppendorf, Netheler, Hinz GmbH, Hamburg, Germany)

Rotilabo® centrifuge with butterfly-rotor
(Carl Roth GmbH & Co. KG., Karlsruhe, Germany)

Rotina 420 R centrifuge with cooling unit
(Hettich Zentrifugen, Tuttlingen, Germany)

Avanti J25 and J-26XP centrifuge with JA10 and JA25.50 rotors
(Beckman Coulter, Brea, USA)

Chromatography systems:

ÄKTA Pure
ÄKTA Prime
Fraction collector F9-R
Superloops (various volumes)
(GE Healthcare Europe GmbH, Freiburg, Germany)

Diaphragm vaccum pump:
(Vacuubrand GmbH & Co., Wertheim, Germany)

Gel electrophoretic device:

Hoefer Mighty Small II dual gel caster
LKB-GPS 200/400 power supply
EPS 301 power supply
(Amersham Pharmacia Biotech, Uppsala, Sweden)

Homogenizer Ultra Turrax DIAX 900:
(Heidolph Instruments, Kelheim, Germany)

HPLC system:

FP-1520 fluorescence detector
UV-1575 UV-VIS detetor
HPLC-pump 2080
(Jasco Labor- und Datentechnik GmbH, Groß-Umstadt, Germany)

Incubator:
(mytron Bio- und Solartechnik GmbH, Heilbad Heiligenstadt, Germnay)

Imaging systems:
ImageQuant LA S 4000 detection system
(GE Healthcare Europe GmbH, Freiburg, Germany)

Typhoon 9200 Variable Mode Imager
(GE Healthcare Europe GmbH, Freiburg, Germany)

Magnetic stirrer Heidolph MR3001:
(Heidolph Instruments, Kelheim, Germany)

Mixer Heidolph Polymax 2040:
(Heidolph Instruments, Kelheim, Germany)

pH meter 538 MultiCal:
(WTW, Weilheim, Germany)

Realtime PCR Cycler:
Stratgene Mx3000P
(Agilent Technologies Deutschland GmbH, Munich, Germany)

Shaker Certomat S:
(B. Braun Biotech International GmbH, Melsungen, Germany)

Spectroscopic instruments:
Absorption spectrometer:
Biotech Ultrospec 3000 UV-VIS spectrophotometer
(Amershan Biosciences Europe GmbH, Freiburg, Germany)

Cary 50/100 Bio UV-VIS spectrophotometer
(Varian Inc., Palo Alto, USA)

Ultrospec 1100 pro UV-VIS spectrophotometer
(Amersham Biosciences Europe GmbH, Freiburg, Germany)

Jasco V-550 UV-VIS spectrophotometer
(Jasco Labor- und Datentechnik GmbH, Groß-Umstadt, Germany)

Nanodrop ND-1000 UV-VIS spectrophotometer
(PEQLAB Biotechnologie GmbH, Erlangen, Germany)

Circular dichroism spectropolarimeter:
Jasco J-715 spectropolarimeter with PTC 343 Peltier device
(Jasco Labor- und Datentechnik GmbH, Groß-Umstadt, Germany)

Fluorescence spectrophotometer:
Fluoromax-2 with PTC 343 Peltier device
(Spex Industries Inc., Metuchen, USA)

Jasco FP-8500 FDP spectrofluorimeter with polarizers
(Jasco Labor- und Datentechnik GmbH, Groß-Umstadt, Germany)

Thermomixer 5436:
(Eppendorf, Netheler, Hinz GmbH, Hamburg, Germany)

Vortex Heidolph Reaxtop:
(Heidolph Instruments, Kelheim, Germany)

Western Blotting system:
FastBlots system
(Biometra, Göttingen, Germany),

3.1.2 Materials

Chromatography columns:

Analytical HPLC column:
$TSKG2000SW_{XL}$ column (7.8 mm ID x 30 cm, 5 µm particle size)
(Tosoh Bioscience, Stuttgart, Germany)

Reversed Phase HPLC column:
C_{18}ProntoSIL column (120-5-C18, 5 µm particle size)
(Bischoff Analysetechnik und –geräte, Leonberg, Germany)

Preparative columns:
His SpinTrap™ column, 1 mL
HisTrap™*-FF* column, 1 mL and 5 mL
Resource™*-Q* column, 6 mL
16/60 Superdex 200 pg column
PD10 desalting column
(GE Healthcare Europe GmbH, Freiburg, Germany)

Consumables:
Amicon centrifugal filter unit Amicon®Ultra-15, Amicon®Ultra-4
(MerckMillipore, Darmstadt, Germany)

BioLite MicroWell Plates (different well types)
(ThermoFisher Scientific Inc., Braunschweig, Germany)

Cell culture flasks (T25 and T75)
(Sarstedt AG & Co., Nümbrecht, Germany)

Cellulose acetate fliter
(Satorius Stedim Biotech GmbH, Göttingen, Germany)

Dialysis membranes Spectra/Por (various MWCOs)
(Spectrum Laboratories Inc., Houston, USA)

Falcon Tubes Greiner, PP (15 mL and 50 mL)
(Greiner Bio-One GmbH, Frickenhausen, Germany)

Micro-concentrator Microcon YM-3 (MWCO = 3000 Da)
(MerckMillipore, Darmstadt, Germany)

Microtubes Rotilabo®, PP, 500 µL
(Carl Roth GmbH & Co. KG., Karlsruhe, Germany)

Nitrocellulose membrane Roti®-NC
(Carl Roth GmbH & Co. KG, Karlsruhe, Germany)

Nunc™Lab-Tek™ II CC2™-Chamber Slide System (2 and 4 well)
(ThermoFisher Scientific Inc., Braunschweig, Germany)

PCR tubes, PP, 0.2 mL
(nerbe plus GmbH, Winsen, Germany)

Reaction tubes (volumes 0.5 mL, 1.5 mL and 2.0 mL)
(nerbe plus GmbH, Winsen, Germany)

Whatman™ 3MM Chromatography papers
(GE Healthcare Europe GmbH, Freiburg, Germany)

Cuvettes:

Cuvettes (one-way), PS, 10 x 4 x 45 mm
(Sarstedt AG & Co., Nümbrecht, Germany)

Hellma® precision quartz cuvette Suprasil, path length 10 mm
(UV-VIS spectroscopy)

Hellma® precision quartz cuvette Suprasil, path length 2 mm
(CD spectroscopy)

Hellma® precision quartz cuvette Suprasil, path length 10 mm, center 15 mm
(Fluorescence spectroscopy)

(Hellma GmbH & Co. KG., Nürnberg, Germany)

3.2 Chemicals

Standard chemicals not listed here, were purchased from Carl Roth GmbH & Co. KG (Karlsruhe, Germany) or Merck KGaA (Darmstadt, Germany). Chemicals were obtained in p.a. grade (pro analysi). Chemicals were used without further purification. All solutions and buffers were prepared with double-distilled water. For cell culture experiments sterilized chemicals and solutions were used.

Acrylamid/Bisacrylamide sol. (38/2, 40% w/v)	Serva Electrophoresis GmbH, Heidelberg, Germany
Agarose	Serva Electrophoresis GmbH, Heidelberg, Germany
Ammonium persulfate (APS)	Carl Roth GmbH & Co. KG, Karlsruhe, Germany
Ampicillin sodium salt (Amp)	Sigma Aldrich Chemie GmbH, Steinheim, Germany
BisSulfoSuccinimidylSuberate (BS^3-H12/D12)	Creative Molecules Inc., California, USA
Brefeldin A from Penicillium brefeldianum	Sigma Aldrich Chemie GmbH, Steinheim, Germany
Bromphenol Blue sodium salt	Sigma Aldrich Chemie GmbH, Steinheim, Germany

Desoxynucleotide triphosphates (dNTPs)	Promega Cooporation, Madison, USA
Dimethylsulfoxid, Hybri-Max™	Sigma Aldrich Chemie GmbH, Steinheim, Germany
DiSulfoSuccinimidyGlutarate (DSSG-H6/D6)	Creative Molecules Inc., California, USA
1,4-Dithiothreit (DTT)	Carl Roth GmbH & Co. KG, Karlsruhe, Germany
Ethylenediaminetetraacetic acid, di-sodium salt dihydrate (EDTA)	Merck KGaA, Darmstadt, Germany
Glycerol 99%	Carl Roth GmbH & Co. KG, Karlsruhe, Germany
Guanosine 5‘-diphosphate sodium salt (GDP)	Sigma Aldrich Chemie GmbH, Steinheim, Germany
Guanosine 5‘-triphosphate sodium salt hydrate (GTP)	Sigma Aldrich Chemie GmbH, Steinheim, Germany
2-[4-(2-hydroxyethyl)piperazin-1yl] ethanesulfonic acid (HEPES)	Carl Roth GmbH & Co. KG, Karlsruhe, Germany
Isopropyl-β-*D*-thiogalactopyranosid (IPTG)	Serva Electrophoresis GmbH, Heidelberg, Deutschland
Kanamycin sulfate	Sigma Aldrich Chemie GmbH, Steinheim, Germany
LB medium	Serva Electrophoresis GmbH, Heidelberg, Germany
2’-(or-3’)-O-(*N*-Methylanthraniloyl) Adenosine 5’-diphosphate disodium salt (MANT-ADP)	Invitrogen molecular probes, Darmstadt, Germany
2’-(or-3’)-O-(*N*-Methylanthraniloyl) Adenosine 5’-triphosphate trisodium salt (MANT-ATP)	Invitrogen molecular probes, Darmstadt, Germany
2’-(or-3’)-O-(*N*-Methylanthraniloyl) Guanosine 5’-diphosphate disodium salt (MANT-GDP)	Invitrogen molecular probes, Darmstadt, Germany
2’-(or-3’)-O-(*N*-Methylanthraniloyl) Guanosine 5’-triphosphate trisodium salt (MANT-GTP)	Invitrogen molecular probes, Darmstadt, Germany
β-Mercaptoethanol (pure)	Merck KGaA, Darmstadt, Germany
Protease Inhibitor Mix HP or Mix M	Serva Electrophoresis GmbH, Heidelberg, Germany
Serva Blue R	Serva Electrophoresis GmbH, Heidelberg, Germany

Serva DNA stain G	Serva Electrophoresis GmbH, Heidelberg, Germany
SYPRO®Orange protein gel stain in DMSO	Invitrogen molecular probes, Darmstadt, Germany
N,N,N',N'-Tetramethyl-ethane-1,2-diamine (TEMED)	Carl Roth GmbH & Co. KG, Karlsruhe, Germany
Thapsigargin	Sigma Aldrich Chemie GmbH, Steinheim, Germany
Tris-(hydroxymethyl)aminomethane (Tris)	Carl Roth GmbH & Co. KG, Karlsruhe, Germany
Tween 20	Merck KGaA, Darmstadt, Germany

3.3 Enzymes, Standards and Kits for Molecular Biology

3.3.1 Enzymes

DNase I
(Roche Diagnostics GmbH, Mannheim, Germany)

Pwo DNA Polymerase
(Roche Diagnostics GmbH, Mannheim, Germany)

Restriction enzymes
(New England Biolabs, Ipswich, USA)

Taq DNA Polymerase
(Promega Coorporation, Madison, USA)

T4 DNA Ligase
(New England Biolabs, Ipswich, USA)

3.3.2 Standards and Kits

Low Range-molecular weight marker
(Biorad Laboratories, Munich, Germany)

peqGold protein marker IV
(peqlab, Erlangen, Germany)

Quickload 1 kb DNA ladder, 50.0 µg/µL
(BioLabs Inc., Lawrenceville, USA)

Pierce™ Bovine Serum Albumin Standard, c = 2.00 mg/mL
(ThermoFisher Scientific Inc., Braunschweig, Germany)

WesternBright ECL Spray for western blot detection
(Advasta, Menlo Park, USA)

Gel filtration calibration low and high molecular weight marker kit
(Sigma Aldrich Chemie GmbH, Steinheim, Germany)

Wizard® Plus SV Minipreps DNA Purification System
(Promega Cooporation, Madison, USA)

Wizard® Pure Yield ™ Plasmid Midiprep System
(Promega Cooporation, Madison, USA)

Wizard® SV Gel and PCR Clean-Up System
(Promega Cooporation, Madison, USA)

ER-ID™ Red Assay Kit (GFP-Certified™)
(Enzo Life Sciences, New York, USA)

M-PER® Mammalian Protein Extraction Kit
(ThermoFisher Scientific Inc., Braunschweig, Germany)

MEM-PER™ Plus Membrane Protein Extraction Kit
(ThermoFisher Scientific Inc., Braunschweig, Germany)

RIPA Lysis and Extraction Buffer Kit
(ThermoFisher Scientific Inc., Braunschweig, Germany)

3.4 Primers

All primers listed below were synthesized at Eurofins MWG Operon (Germany).

Table 1: Primers used for molecular biology techniques.

Primer	Sequence (5‘ to 3‘)
wtRab1A_forward (SUMO fusion construct)	gatcagggatccatgggtagc
wtRab1A_reverse (SUMO fusion construct)	gatcagctcgagttaacaacaac
nt-svRab1A_forward (SUMO fusion construct)	gatcagggatccatgggtagc
nt-svRab1A_reverse (SUMO fusion construct)	gatcagctcgagttaacaacaac
wtRab1A_forward (mRNA studies in human tissue samples)	ctgctgctgattggtgatagcggtg
wtRab1A_reverse (mRNA studies in human tissue samples)	cattgctttttctgcaccgcctgc
nt-svRab1A_forward (mRNA studies in human tissue samples)	ctgctgctgattggtgatagcggtg
nt-svRab1A-reverse (mRNA studies in human tissue samples)	cattgctttttctgcaccgcctgc
wtRab1A-GFP_forward (*in vivo* studies)	gatcagctcgagatgggtagcagcatgaatccggaatatgattac
wtRab1A-GFP_reverse (*in vivo* studies)	gatcaggtcgacccacaacaaccaccaccgctctg
wtRab1A-ΔGFP_forward (*in vivo* studies)	gatcagctcgagatgggtagcagcatgaatccggaatatgattac
wtRab1A-ΔGFP_reverse (*in vivo* studies)	gatcaggcggccgcttaacaacaaccaccaccgctctg
nt-svRab1A-GFP_forward (*in vivo* studies)	gatcagctcgagatgggtagcagcatgaatccggaatatgattac
nt-svRab1A-GFP_reverse (*in vivo* studies)	gatcaggtcgacccacaacaaccaccaccgctctg
nt-svRab1A-ΔGFP_forward (*in vivo* studies)	gatcagctcgagatgggtagcagcatgaatccggaatatgattac
nt-svRab1A-ΔGFP_reverse (*in vivo* studies)	gatcaggcggccgcttaacaacaaccaccaccgctctg

3.5 Bacterial Strains and Plasmids

In Table 2 the in this work used bacterial strains are listed. For plasmid DNA amplification *E. coli Mach1* cells were utilized. *JM109, XL1 Blue* and *BL21(DE3) E. coli* strains served in protein expression.

Table 2: Used *E.coli* strains listed with corresponding genotypes.

E. coli strain	Genotype	Origin
JM109	*end*A1 *rec*A1 *gyr*A96 *thi*, *hsd*R17 (r_k–, m_k+) *rel*A1 *sup*E44 Δ(*lac-pro*AB) [F′ *tra*D36 *pro*AB *laq*I^{q}ZΔM15]	Promega (Madison, USA)
XL1-Blue	*recA1 endA1 gyrA96 thi-1 hsdR17 supE44 relA1 lac* [F´ *proAB lacI^{q}ZΔM15* Tn*10* (Tet^r)]	Stratagene (La Jolla, USA)
BL21-CodonPlus(DE3)-RIL	F$^-$ *ompT hsdS*(r_B^- m_B^-) *dcm*$^+$ *Tet^R gal* λ(DE3) *endA* Hte [*argU ileY leuW Cam^R*]	Stratagene (La Jolla, USA)
BL21 Star (DE3)	F$^-$ *ompT hsdS*$_B$(r_B^- m_B^-) *gal dcm rne131* (DE3)	Invitrogen (Darmstadt, Germany
Mach1™-T1^R	F$^-$ *φ80(lacZ)ΔM15 ΔlacX74 hsdR(r_K–, m_K+) ΔrecA1398 endA1 tonA*	Invitrogen (Darmstadt, Germany)

The following expression plasmids were used in this work. The mutated residues are numbered according to the protein sequence annotated in the UniProt database. Detailed information about the different cloning sites can be obtained in chapter 3.8.2. The correct sequence of all cloning constructs was further verified by sequencing at Eurofins MWG Operon (Ebersberg, Germany).

Table 3: Plasmid constructs used in this work.

Construct	Plasmid (selection marker)	Origin
wtRab1A	pProEx HTa (Amp^R)	GeneArt (Regensburg, Germany)
nt-svRab1A	pProEx HTa (Amp^R)	GeneArt (Regensburg, Germany)
wtRab1A	pET-SUMO (Kan^R)	This work
nt-svRab1A	pET-SUMO (Kan^R)	This work
wtRab1A	pcDNA3.1$^{(+)}$ (Amp^R)	This work
wtRab1A-CysMut (C204A, C205A)	pcDNA3.1$^{(+)}$ (Amp^R)	GeneArt (Regensburg, Germany)
nt-svRab1A	pcDNA3.1$^{(+)}$ (Amp^R)	This work
nt-svRab1A-CysMut (C128A, C129A)	pcDNA3.1$^{(+)}$ (Amp^R)	GeneArt (Regensburg, Germany)
wtRab1A-GFP	pAcGFP1-N1 (Kan^R)	This work
wtRab1A-ΔGFP	pAcGFP1-N1 (Kan^R)	This work
nt-svRab1A-GFP	pAcGFP1-N1 (Kan^R)	This work
nt-svRab1A-ΔGFP	pAcGFP1-N1 (Kan^R)	This work

3.6 Media and Antibiotics for the Cultivation of *E. coli*

All solution and media used for the work with *E. coli* bacteria were immediately autoclaved (121 °C, 20 min) or sterile filtered after preparation. If not indicated elsewhere, all solutions and media were stored at RT. Antibiotics stocks (1000x) were passed through a sterile filter (0.22 µm), aliquoted and stored at -20°C.

LB media:	For the preparation of 1L of *E. coli* medium 20 g of LB-powder were mixed with 1L of distilled water.
Antibiotics:	Ampicillin: 100 µg/mL Kanamycin: 35 µg/mL or 50 µg/mL (1000x antibiotic stocks were prepared)

3.7 Software, Databases and Web-based Tools

Adobe Illustrator CS2	Adobe Systems (San Jose, USA)
Borwin	Jasco (Groß-Umstadt, Germany)
CDNN	Applied Photophysics (Böhm et al, 1992)
EndNote X7	Adept Scientific (Herts, UK)
NEBCutter V2.0	New England Biolabs Inc. (Ipswich, USA)
Microsof Office 2010	Microsoft Corporation (Redmond, USA)
OligoAnalyzer 3.1	Integrated DNA Technologies (Coralville, USA)
Origin 2015	OriginLab (Northampton, USA)
PDB	www.rcsb.org/pdb
ProtParam	ExPASy bioinformatics Resource Portal (Swiss Institute of Bioinformatics, Basel, Swiss)
PubMed	www.ncbi.nlm.nih.gov/pubmed
PyMOL 1.7	Schrödinger LLC (New York, USA)
ImageJ 1.47V	http://imagej.nih.govij
UniProt	www.uniprot.org

3.8 Molecular Biological Methods

All solutions used for molecular biological methods were sterlie. The most frequently used techniques are briefly described in the following sections.

3.8.1 Polymerase Chain Reaction (PCR)

PCR is a common method to amplify a gene or DNA fragment of interst by the use of specific primers. Herby the target DNA in the first step is denatured, followed by primer annealing and amplification of the desired construct by the use of heat stable polymerases. The specific primers needed for each amplification were desinged with the OligoAnalyzer 3.1 tool (Integrated DNA Technologies, see chapter 3.4) and synthesized by Eurofins Genomics (Ebersberg, Germany).
A typical pipetting scheme is depicted below:

Component	**Volume [µL]**
Reaction buffer (10x)	10.0
Template DNA	1.00
dNTPs (10mM)	2.00
Forward Primer (100 pmolµL^{-1})	1.00
Reverse Primer (100 pmolµL^{-1})	1.00
Nuclease-free water	84.5
Polymerase P_{wo} (1UµL^{-1})	0.50

For most of the PCR's the following cycling programme was used:

Melting	95 °C for 45 s (2 min before first cycle)
Annealing	60 °C for 45 s (depending on primers)
Amplification (according to the manual of polymerase, in general 1 min per 1000 bp)	72 °C for 1min (5 min after last cycle)
Cycles	35

The PCR products were fruther analyzed by agarose gel electrophoresis (see chapter 3.8.5). Therefor 9 µL of sample were mixed with 1 µL of DNA-loading buffer (10x). Successfully amplified DNA constructs were then purified by the use of the Wizard® SV Gel and PCR Clean-Up System according to the manufacturer's instruction (Promega, Madison, USA).

3.8.2 Restriction Digest

For the insertion of the diverse amplified DNA fragments into the desired vectors, the purified DNA fragments and the used vectors, first needed to be enzymatically digested using restirction enzymes (New England BioLabs Inc., Massachussetts, USA).
The standard digestion protocol is shown below:

Preparative approach	**Volume [µL]**
Reaction buffer (10x)	6.0
Template DNA	50
Restriction enzyme 1 (20.000 UmL^{-1})	2.0
Restriction enzyme 2 (20.000 UmL^{-1})	2.0

The reaction was either performed over night at 4 °C (preparative approach) or incubated for at least 2.5 h at 37 °C (analytical approach). The full length genes, encoding human nt-svRab1A and wtRab1A were synthesized by GeneArt (Regensburg, Germany). For heterologous expression in *E. coli*, codon optimized gene constructs were used. After amplification of the wtRab1A coding sequence by PCR, NcoI-HF® and XhoI restriction enzymes were used for cloning into the pProEX HTa vector (Invitrogen molecular probes, Darmstadt, Germany). For successful purification of the nt-svRab1A protein the nt-svRab1A coding sequence needed to be re-cloned into the pET SUMO vector (Bepperling et al, 2012). The PCR amplified nt-svRab1A coding sequence was inserted between the BamHI and XhoI site of the pET SUMO vector.
To study the mRNA levels of the Rab1A proteins in different human tissue samples the coding sequences of both proteins were cloned into the pcDNA3 vector (Invitrogen molecular probes, Darmstadt, Germany), by insertion between the BamHI and XhoI restriction site.
In order to perform *in vivo* studies of the Rab1A proteins in eukaryotic cells, re-cloning into the pAcGFP1-N1 vector (Clontech, California, USA) was required. For this the wtRab1A as well as the nt-svRab1A coding sequence was inserted between the XhoI and SalI restriction sites of the vector. Additionally Rab1A protein constructs without a C-terminal GFP fusion were obtained by the use of XhoI and NotI-HF® restriction enzymes. For each of the used restriction enzymes, reaction buffers were applied according to the suppliers' instructions. Afterwards the digested costructs were purified by the use of the Wizard® SV Gel and PCR Clean-Up System according to the manufacturer's protocol (Promega, Madison, USA).

The analytical approach was used to analyze the cloning result. Therefore the following reaction scheme was utilized:

Analytical approach	**Volume [µL]**
Reaction buffer (10x)	1.5
DNA	10
Restriction enzyme 1 (20.000 UmL^{-1})	0.3
Restriction enzyme 2 (20.000 UmL^{-1})	0.3
Nuclease-free water	2.9

The reaction was incubated for 2.5 h at 37 °C. Then the 15 µL were mixed with 1.5 µL of DNA-loading buffer (10x) and the positive insertion of the DNA fragment into the plasmid was analyzed by agarose-gel electrophoresis (see chapter 3.8.5).

3.8.3 Ligation

After the enzymatical digest of the insert DNA and the corresponding vector, the insert DNA was ligated into the desired vector DNA using T4 DNA ligase. A typical reaction scheme is depicted below:

Component	**Volume [µL]**
T4 DNA ligation buffer (10x)	2.0
Insert DNA $_{digested}$	10
Vector DNA $_{digested}$	1.0
ddH_20	6.0
T4 DNA ligase ($3U\mu L^{-1}$)	1.0

The reaction was carried out at 4 °C over night and 10 µL of each ligation was used fruther for transformation of chemical competent *E. coli* Mach 1 cells (see chapter 3.8.8). Positive clones were selected and the respectively contained correctly ligated plasmids were isolated using the Wizard® Plus SV Minipreps DNA Purification System (Promega, Madison, USA, see chapter 3.8.4). The accuracy of all recombinated plasmids was verified by sending them to MWG Eurofins Genomics (Ebersberg, Germany) for sequencing. The plasmid DNAswere stored at – 20 °C.

3.8.4 Isolation of Plasmid DNA from *E. coli*

The principle of the method is selective alkaline denaturation of high molecular weight chromosomal DNA while covalently closed circular DNA remains double-stranded (Birnboim & Doly, 1979). Hereby disruptive cellular components, like proteins and lipids, are separated by precipitation. The purification of the plasmid DNA from water-soluble componentens e.g. carbonhydrates, is achievied through interaction of the plasmid DNA with the silica column material. The plasmid DNA was isolated using the Wizard® Plus SV Minipreps DNA Purification System (Promega, Madison, USA) according to the manufacturer's instruction. The main steps are described breifly in the following stion. Initially 3.0 mL *E. coli* over night cultures were harvested (2 x 1.5 mL, 3 min, RT, 5000 rpm, eppendorf centrifuge 5418, rotor FA-45-18-11), followed by a resuspension step of the cell pellet. Next the alkaline lysis reaction of the cells was performed. After a neutralization step the lysed cells were centifuged (10 min, RT, 14.000 rpm, eppendorf centrifuge 5418, rotor FA-45-18-11) to collect the cleared lysate. In the next step the plasmid DNA was trasferred onto the binding column. After a washing step the plasmid DNA was eluted using 50 µL of nuclease-free water. For the preparation of plasmid DNA for *in vivo* experiments the Pure Yield ™ Plasmid Midiprep System was alternatively used according to the manufacturer's instruction. Therby an endotoxin removal step is included, which is necessary for not damaging the mamalian cells used in the *in vivo* experiments.

3.8.5 Agarose Gel Electrophoresis

This method allowss to separate DNA-strands according to their size in an electrical field. Due to the negatively charged phosphate-groupes of the DNA, migration of the DNA towards the anode occurs. Given that smaller DNA molecules migrate faster through the agarose gel matrix than DNA molecules of higher size, separation is achieved. Plasmid DNA was further analyzed by agarose gel electrophoresis after analytical restiction digest (see chapter 3.8.5), by verification of the approximate size of the DNA fragments. Additionally this method was employed for the purification of PCR products or plasmid DNA by gel extraction, using the Wizard® SV Gel Clean up Kit. In general 1.0 – 2.0 % agarose gels (including 1.0 µL DNA Stain G added, Serva, Heidelberg, Germany) were used. As running buffer 1x TAE was utilized. For the sample preparation 10 µL of sample was mixed with 1.0 µL of DNA loading buffer (10x). Electrophoresis was performed for 30 min at a constant voltage of 100 V. Afterwards the DNA fragments were visualized under UV-light with a *ImageQuant300* system.

The different DNA fragments were assigned by comparing them to a 1 kb DNA standard ladder (New Engal BioLabs Inc., Massachusetts, USA).

Used solutions:

1.00– 2.00 % Agarose solution:

1.00 g or 2.00 g Agarose

100 mL TAE running buffer (1x)

1.00 µL DNA Stain G

TAE running buffer (50x):

2.00 M Tris/Acetate, pH 8.0

50.0 mM EDTA

DNA loading buffer (10x):

50.0 %(v/v) Glycerine

0.20 % (w/v) Bromephenol blue

0.20 % (w/v) Xylencyanol

10.0 mM EDTA, pH 8.0

3.8.6 Cultivation and Storage of *E. coli* cells

The cultivation of *E. coli* cells was either performed in LB liquid media or on LB plates. Selection of the strains was obtained by addition of the appropriate antibiotic to the media (final concentration: LB_{Amp} = 100 µgmL^{-1}, LB_{Kana} = 35 µgmL^{-1} or 50 µgmL^{-1}). The cultures were constantly shaken and incubated over night at 37 °C. For the preparation of the desired cloning construct one single colony was transferred into 3 mL of LB liquid media containing antibiotic. Afterwards the mini cultures were incubated over night in an rotation-incubator at 37 °C. Liquid cultures were inoculated 1:100 with fresh over night cultures. The OD was monitored at 600 nm with an Vis spectrometer.

For long-term storage 500 µL of glycerol (50 % solution, sterile) were added to 500 µL of bacterial suspension, frozen in liquid nitrogen and stored at – 80 °C.

3.8.7 Preparation of chemical competent *E. coli* cells

Chemical competent *E. coli* cells were prepared by incubating 50 mL of LB liquid media (Serva, Heidelberg, Germany), containing the desired antibiotic, with 100 µL of a freshly prepared over night culture at 37 °C. After a OD_{600} of 0.5 – 1 was reached 1 mL of a sterile 1M $MgCl_2$ solution was added and the culture was incubated for additional 10 min at 37 °C under constant shacking. Before centrifugation of the cells (10 min, 4 °C, 5000 rpm, Hettich Rotina 420R centrifuge, 4723 Rotina 4 place swing out rotor), the bacterial culture was incubated on ice for 60 min. The cell pellet was then resuspended in 10 mL of solution A and incubated for additional 60 min on ice. Next the solubilized pellet was centifuged (10 min, 4 °C, 5000 rpm, Hettich Rotina 420R centrifuge, 4723 Rotina 4 place swing out rotor). In the last step the cells were resuspended with 2 mL of solution A containing 15 % glycerol, aliquoted, frozen in liquid nitrogen and stored at – 80 °C.

Solution A (250 mL):

3 M NaAc, pH 5.5	3.25 mL
1 M $CaCl_2$	25.0 mL
2.8 M $MnCl_2$	6.25 mL
H_2O	215.5 mL

3.8.8 Transformation of chemical competent *E. coli* cells

For the transformation of chemical competent *E. coli* cells different strains were used according to requirements. For the isolation of plasmid DNA the *E. coli Mach1* strain was used, whereas *BL21DE3Cd+* (Stratagene, La Jolla, USA) and *JM109* (Promega, Madison, USA) strains served as bacterial strains for protein expression. Each transformation was performed with 1.00 µL (~200 ng) of the desired plasmid DNA and 200 µL of chemical competent *E. coli* cells. The cell/DNA mixtrue was incubated for 30 min on ice, followed by a 1 min heat shock at 42 °C. Hereby the heat shock leads to the uptake of the plasmid DNA into the chemical competent *E. coli* cells. Then the reaction was cooled for 2 min on ice. Next 1.00 mL of LB liquid media was added to the cells and the reaction was incubated for 60 min at 37 °C with agitation. 100 µL of cell suspension was plated on an LB plate containing the desired selection marker. The remaining cell suspension was added into a LB liquid culture containing the respective antibiotic. The LB plate and LB liquid culture was then incubated at 37 °C over night. Due to the used selection marker only the *E. coli* cells which were succesfully transformed with the respective plasmid DNA are able to grow.

3.9 Protein Purification

In general, all purification steps were carried out at – 4 °C. The purity of the Rab1A proteins was evaluated in each chromatographical step by SDS-PAGE analysis (see chapter 3.10.1). All purified proteins were dialyzed against the desired buffers and stored at – 80°C (wtRab1A) or alternatively at – 4 °C (nt-svRab1A). By the use of MALDI-TOF mass spectrometry (MS) the identity and the correct molecular mass of the purified proteins were verified.

3.9.1 Protein Expression and Cell Disruption

For expression of the wtRab1A protein the pProEX HTa vector, containing an N-terminal His_6-Tag followed by an N-terminal TEV-protease cleavage site was used. Thus the wtRab1A protein was expressed with a cleavable N-terminal His-Tag. In contrast to wtRab1A expression, the pET SUMO vector system (Bepperling et al, 2012), containing an N-terminal His_6-SUMO-Tag was utilized for nt-svRab1A purification. By introduction of the SUMO solubility Tag the yield of soluble nt-svRab1A protein could be significantly improved.

The nt-svRab1A protein was expressed in *E. coli BL21 Codon Plus (DE3)-RIL* cells. For wtRab1A expression *E. coli JM109* cells were used. Cells were grown in either 6L of LB medium supplemented with 100 mg ampicillin (wtRab1A) or in 12L of LB medium provided with 35 mg kanamycin (nt-svRab1A) at 37 °C. Protein expression was induced with 1mM IPTG at an OD_{600} of 0.6. Before harvesting of the cells by centrifugation at 6000 rpm (Beckman Coulter Avanti J-26 XP centrifuge, JA-10 rotor, 30 min, 4 °C), the cells were further cultivated in an incubator at 37 °C for 16 h. The supernatant was discarded and the cell pellet was washed with buffer A. For lysis the cells were resuspended in IMAC buffer A, supplemented with DNase I (Roche, Basel, Switzerland) and Protease Inhibitor Mix HP (Serva, Heidelberg, Germany). Alternatively the cell suspension was stored in presence of Protease Inhibitor Mix HP at – 80°C until cell disruption. Lysis of the cells was performed in a Basic Z cell disrupter operated at 2.3 kbar (Constant Systems, Warwick, UK). Next the insoluble material was separated from the supernatant by centrifugation for 60 min at 18.000 rpm at 4 °C (Beckman Coulter Avanti J-26 XP centrifuge, JA-25.50 rotor).

At last the cleared lysate was applied onto a 5 mL HisTrap™ FF-column (GE Healthcare, Munich, Germany) for protein purification.

IMAC Buffer A:

50.0 mM Hepes, pH 8.0
500 mM LiCl
1.00 mM $MgCl_2$
10.0 µM GDP
10.0 mM Imidazole
2.00 mM β-Mercaptoethanol

3.9.2 Chromatographical Methods for Protein Purification

For purification of the various proteins different chromatographical methods were used. The most frequently operated techniques are described briefly in the following section.

3.9.2.1 Immobilized Metal Ion Chromatography (IMAC)

Affinity chromatography facilitates protein purification via a reversible interaction of a matrix associated ligand. Thereby the biochemical interplay is mainly achieved by electrostatic or hydrophobic interaction. In general elution of the desired protein is accomplished by variation of the pH, the ionic strength, the polarity or either by addition of a competitive ligand e.g. imidazole. To facilitate easy regeneration of the column material in presence of metal ions as ligands, metal ions must have a much higher affinity for the matrix material than for the substance to be separated (Porath et al, 1975). For the purification of both Rab1A His-tagged proteins, a pre-packed Ni-Sepharose HisTrap™ FF-column was used. The column material consists of highly cross-linked agarose beads that carry immobilized chelating moieties, charged with Ni^{2+}-ions. Here the presence of the Ni^{2+}-ions leads to a high affinity for His-tagged proteins.

3.9.2.2 Ion Exchange Chromatography (IEC)

Due to electrostatic attraction IEC leads to a reversible ionic interaction of reverse charged particles. Thus IEC can be used for the separation of a variety of substances consisting of charged functional moieties predicated on the affinity of these molecules to the column material. Through the charged side chains of the proteins, an interaction between the reverse charged polymeric carrier matrix and the protein is obtained. By application of an anion exchanger, elution of the protein on the one hand can be achieved by continuous reduction of the pH; on the other hand the gradual increase of the salt concentration results in elution of the protein.

Though attenuation of the electrostatic interaction occurs which leads to dissociation of weaker interacting proteins prior to strong interactors from the carrier matrix. For purification of the nt-svRab1A a 6 mL Resource ™ Q-column (GE Healthcare, Munich, Germany) was applied. The pre-packed anion exchanger column is equipped with rigid, monodispers polystyrene/divinylbenzene beads. Quaternary ammonium-ions are used as functional clusters.

3.9.2.3 Size Exclusion Chromatography (SEC)

The application of SEC enables the separation of proteins or analytes according to their size by a diffusion controlled mechanism. Hence chemical or physical interactions do not occur by the use of this chromatographical method. The column material generates a three dimensional network with a defined pore size, which facilitates that proteins with a certain diameter as well as buffer molecules can penetrate into the pores of the column material. All components are eluted isocratically. Common column materials are silica gel or polymeric particles which are utilized due to their chemical inert characteristics and physical stability. In general proteins larger than the defined pore diameter are not subjected to retention and therefore elute simultaneously with the buffer front, whereas proteins with smaller diameter diffuse into the pores leading to a delayed elution. As last purification step of both Rab1A isoforms a 16/60 Superdex 75 pg gel filtration column (GE Healthcare, Munich, Germany) was used.

3.9.3 Purification of Rab1A isoforms

wtRab1A purification:

Purification of wtRab1A was mainly performed according to the protocol from Schoebel *et. al.* (Schoebel et al, 2009). As first step of purification IMAC chromatography was used by applying the cleared lysate onto a 5 mL HisTrap FF-column at a flow rate of 2 mL/min. Before, the column was pre-equilibrated with IMAC buffer A. For removal of unbound components the column was then washed with IMAC buffer A (10 CV) followed by IMAC buffer B (10 CV). 10 mL fractions were collected. The elution of the His-tagged wtRab1A was performed with IMAC buffer C (10 CV), containing a high concentration of the competitive ligand imidazole. 5 mL protein fractions were collected. Remaining protein components were removed by the use of IMAC buffer D (8 CV, 8 mL fractions). Afterwards the wtRab1A containing fractions were pooled and the HisTrap FF-column was re-equilibrated with IMAC buffer A.

Cleavage of the His-Tag was achieved by the addition of TEV protease (ratio 1/250 TEV/protein), followed by overnight dialysis in dialysis buffer. The tag free wtRab1A protein was separated from the His-Tag and the TEV protease by an additional IMAC chromatography. Thereby the flow through, containing the cleaved wtRab1A was collected in 2 mL fractions. Then the fractions were concentrated and loaded onto a 16/60 Superdex 75 pg column. The SEC column was equilibrated with storage buffer. A flow rate of 1 mL/min was used. 4 mL fractions were collected. After analysis by SDS-PAGE (see chapter 3.10.1) the wtRab1A containing protein fractions were pooled concentrated and aliquots were shock frozen in liquid nitrogen and stored at – 80°C.

Nt-svRab1A purification:

Although for nt-svRab1A purification IMAC was used in the first step. Buffers and conditions were kept the same as for wtRab1A purification except that 2 mL fractions were collected in the elution step. After analysis via SDS-PAGE the nt-svRab1A containing fractions were pooled. Next the His-SUMO Tag was cleaved by the addition of SUMO protease (ratio 1/100 SUMO/protein). The overnight dialysis was performed in dialysis buffer. After the second application to the HisTrap FF column, the flow through containing the cleaved nt-svRab1A protein was dialyzed overnight against IEC buffer A. The theoretical pI (isoelectrical point) of nt-svRab1A was calculated as 5.4 (ProtParam, ExPASy bioinformatics Resource Portal). Thus nt-svRab1A was further purified by the use of a 6 mL Resource™ Q anion exchange column. A continuous flow rate of 3 mL/min was applied. Prior to the application of the protein sample, the column was equilibrated with low salt IEC buffer A (5 CV). Next unbound components were removed by a washing step with IEC buffer A (10 CV). 10 mL fractions were collected. The different proteins were eluted in 2 mL fractions with a salt gradient from 0 to 750 mM NaCl over 15 CV. For the removal of strong interacting proteins a washing step with high salt IEC buffer B (10 CV, 2 mL fractions) was included. Afterwards the nt-svRab1A containing fractions were pooled, concentrated and loaded onto a 16/60 Superdex 75 pg gel filtration column, equilibrated with storage buffer. A flow rate of 1 mL/min was used. 4 mL fractions were collected. The purity of the nt-svRab1A containing fractions was analyzed further by SDS-PAGE (see chapter 3.10.1). The concentrated nt-svRab1A protein was aliquoted and stored at + 4 °C.

IMAC buffers:

IMAC buffer A:

50.0 mM Hepes/KOH, pH 8.0
500 mM LiCl
1.00 mM $MgCl_2$
10.0 µM GDP
10.0 mM Imidazole
2.00 mM β-Mercaptoethanol

IMAC buffer B:

50.0 mM Hepes/KOH, pH 8.0
500 mM LiCl
1.00 mM $MgCl_2$
10.0 µM GDP
20.0 mM Imidazole
2.00 mM β-Mercaptoethanol

IMAC buffer C:

50.0 mM Hepes/KOH, pH 8.0
500 mM LiCl
1.00 mM $MgCl_2$
10.0 µM GDP
300 mM Imidazole
2.00 mM β-Mercaptoethanol

IMAC buffer D:

50.0 mM Hepes/KOH, pH 8.0
500 mM LiCl
1.00 mM $MgCl_2$
10.0 µM GDP
500 mM Imidazole
2.00 mM β-Mercaptoethanol

Dialysis buffer:

50.0 mM Hepes/KOH, pH 8.0
100 mM NaCl
1.00 mM $MgCl_2$
10.0 µM GDP
2.00 mM β-Mercaptoethanol

IEC buffers:

IEC buffer A:

20.0 mM Hepes/KOH, pH 8.0
50.0 mM NaCl
1.00 mM $MgCl_2$
10.0 µM GDP
2.00 mM DTT

IEC buffer B:

20.0 mM Hepes/KOH, pH 8.0
1.00 M NaCl
1.00 mM $MgCl_2$
10.0 µM GDP
2.00 mM DTT

Storage buffer:

20.0 mM Hepes/KOH, pH 8.0
50.0 mM NaCl
1.00 mM $MgCl_2$
10.0 µM GDP
2.00 mM DTT

3.9.4 Dialysis and Concentration of proteins

For long-time storage of purified proteins low salt conditions were achieved by dialysis. Additionally several chromatographic methods like IEC require low salt conditions or the removal of diverse buffer components for the binding of proteins to the utilized column. Here dialysis is used as a common method. The necessary changes of the buffer conditions were accomplished by dialysis using semipermeable membranes with a MWCO of 6 – 8 or 12 – 14 kDa (Spectra/Por®, Spectrum Laboratories Inc., California, USA). Dialysis was performed overnight under slow stirring conditions at + 4 °C.

For concentration of volumes smaller than 1.0 mL a micro-concentrator *Microcon YM-3* (MWCO = 3.0 kDa) was utilized. Bigger volumes were concentrated at 3500 rpm (Hettich Rotina 420 R centrifuge, 4723 Rotina 4 place swing out rotor) at 4 °C using *Amicon®Ultra Centrifugal filters* (4 mL, 15 mL, Merck, Darmstadt, Germany) with a MWCO of 3.0 kDa (nt-svRab1A) or 10 kDa (wtRab1A) respectively. Via centrifugation the buffer is pressed through the membrane, whereas the proteins are concentrated upstream of the membrane.

3.10 Protein Chemical Methods

3.10.1 Discontinuous Sodium dodecyl sulfate Polyacrylamide Electrophoresis (SDS-PAGE)

SDS-PAGE is a common method for the determination of the apparent molecular mass of denatured proteins, although it can be applied for the verification of the purity of proteins. By the use of SDS-PAGE proteins can be separated in an electrical field due to their different charges, resulting in different migration velocities. The addition of sodium dodecyl sulfate causes denaturation of the proteins and simultaneously imparts a negative charge to the polypeptide chain. Herby a proportional protein mass to charge ratio is achieved, resulting in a separation by approximate mass during electrophoresis. Though, proteins with smaller molecular mass migrate faster through the gel matrix than proteins with higher molecular mass. The discontinuous SDS-PAGE makes it possible to apply diluted protein samples (Schagger & von Jagow, 1987) and results in more precise protein bands (Fling & Gregerson, 1986). SDS-PAGE was performed as described previously (Laemmli, 1970). For polyacrylamide gels a 5% (w/v) stacking gel solution and a 12.5% (w/v) separation gel solution was used for wtRab1A, whereas a 15.0% (w/v) separation gel solution was utilized for nt-svRab1A. The polymerization of the polyacrylamide gel matrix was achieved by addition of tetramethylethylendiamin (TEMED) and ammonium persulfate (APS) to the stacking gel solution as well as the separation gel solution. Herby APS served as radical initiator for polymerization. Prior to loading, 20 µL of each sample was mixed with 5.0 µL of Laemmli buffer (5x) and incubated at 95 °C for 5 min. Cell pellet samples were resuspended in 1x Laemmli buffer. Thereby a complete denaturation of the protein sample was obtained. The approximate protein mass was verified by the use of a Low Molecular Weight standard (10 µL, peqGold protein marker IV, peqlab, Erlangen, Germany). Electrophoresis was carried out at 35 mA per gel for 30 – 60 min in a Hoefer Mighty Small II Vertical Electrophoresis Chamber (GE Healthcare, Freiburg, Germany) at RT. Gels were Coomassie stained according to the modified protocol of Fairbanks *et al.* (Fairbanks et al, 1971). Consecutively gels were shortly heated in Fairbanks A and Fairbanks D, followed by constant shaking of the gels in Fairbanks D until protein bands were visible.
Alternatively purchased SERVAGel™ TG PRiME™ 8 – 16% (Serva, Heidelberg, Germany) gradient gels or SERVAGel™ TG PRiME™ 4 – 20% (Serva, Heidelberg, Germany) gradient gels were used.

Used Solutions:

Stacking gel solution (5% acrylamide/bisacrylamide):

40.0% (w/v) acrylamide/bisacrylamide	0.63 mL
Stacking gel buffer (2x)	2.50 mL
ddH_2O	1.88 mL
10.0% (w/v) APS	100 µL
TEMED	10.0 µL

Stacking gel buffer (2x):

0.25 M Tris/HCl, pH 6.8

0.40% (w/v) SDS

Separation gel solution (12.5% acrylamide/bisacrylamide):

40.0% (w/v) acrylamide/bisacrylamide	3.13 mL
Separation gel buffer (4x)	2.50 mL
ddH_2O	4.38 mL
10.0% (w/v) APS	100 µL
TEMED	10.0 µL

Separation gel solution (15.0% acrylamide/bisacrylamide):

40.0% (w/v) acrylamide/bisacrylamide	3.75 mL
Separation gel buffer (4x)	2.50 mL
ddH_2O	3.75 mL
10.0% (w/v) APS	100 µL
TEMED	10.0 µL

Separation gel buffer (4x):

1.50 M Tris/HCl, pH 8.8

0.80% (w/v) SDS

Laemmli loading buffer (5x):

0.30 M Tris/HCl, pH 6.8

0.05% (w/v) Bromphenol blue

50.0% (v/v) Glycerol

10.0% (w/v) SDS

5.00% (v/v) β-Mercaptoethanol

Running buffer (10x):

0.25 M Tris/HCl, pH 8.8

2.00 M Glycerol

1.00% (w/v) SDS

Fairbanks A:

25.0% (v/v) Isopropanol

10.0% (v/v) Acetic acid

0.05% (w/v) Coomassie Blue R

Fairbanks D:

10.0% (v/v) Acetic acid

3.10.2 Western Blotting

Western Blotting is a common technique to combine the electrophoretic protein separation with the specificity of immunochemical detection. Herby proteins from SDS-PAGE gels (see chapter 3.10.1) first were transferred onto a nitrocellulose membrane (Roti®-NC, Carl Roth, Karlsruhe, Germany) using a FastBlots system (Biometra, Göttingen, Germany), to make them accessible for antibody detection. The general procedure is described briefly in the following section. Prior to blotting, the membrane, the Whatman™ 3MM Chromatography papers (GE Healthcare, Freiburg, Germany) and the SDS gel were incubated for 2 min in western blot transfer buffer. Next the following components were stacked from bottom to top and placed between the plate electrodes: three layers of Whatman™ 3MM Chromatography paper, nitrocellulose membrane, SDS gel and three layers of Whatman™ 3MM Chromatography paper. Afterwards western blotting was carried out at 1.5 mA/cm^2 (72 mA per gel) for 60 min. To block unspecific binding, the blotting membrane was then incubated for 30 min at RT in 5% (w/v) milk powder PBS-T solution, followed by addition of the primary antibody diluted in 1% (w/v) milk powder PBS-T solution for 60 min at RT. After three washing steps with PBS-T (10 min each) at RT, the blotting membrane was incubated with secondary antibody diluted in 1% (w/v) milk powder PBS-T solution. Here the primary rabbit polyclonal IgG antibody Rab1A (Santa Cruz Biotechnology, Heidelberg, Germany) in 1:5000 dilutions, followed by a secondary antibody (horseradish peroxidase-conjugated goat α-rabbit IgG, 1:5000, Sigma-Aldrich, St. Louis, USA) was used. After three additional washing steps with PBS-T solution the specific protein bands were visualized by chemiluminescence using WesternBright ECL Spray (Advansta, California, USA) and an ImageQuant LA S 4000 detection system (GE Healthcare, Freiburg, Germany).

Used solutions:

Westernblot Transfer buffer:

0.200 M Glycine

0.020 M Tris/HCl, pH 8.3

20% (v/v) Methanol

0.037% (w/v) SDS

PBS-Tween20 washing buffer (PBS-T):

1.150 M NaCl

0.004 M KH_2PO_4

0.160 M Na_2HPO_4 x H_2O, pH 7.4

0.100% (v/v) Tween20

3.11 Spectroscopic Methods

All recorded spectra were reference corrected. As reference the respective buffers of the experiment were used.

3.11.1 Ultraviolet-Visible Absorption Spectroscopy (UV-VIS)

When absorption occurs by radiation with light from the ultraviolet or visible range, valence electrons (mostly π-electrons) are excited and lifted from the ground state (HOMO) into an energy-rich excited state (LUMO). The required wavelength necessary to overcome the energy difference between both energy levels can be calculated from the Plank-Einstein relation (Equation 1, (Atkins & de Paula, 2006)).

Plank-Einstein relation:

$$\Delta \boldsymbol{E} = \boldsymbol{h\nu} = \boldsymbol{h}\frac{\boldsymbol{c}}{\boldsymbol{\lambda}} \qquad \textbf{(Equation 1)}$$

ΔE = energy difference [J]

h = Plank constant [Js]

ν = frequency [Hz]

c = speed of light [ms^{-1}]

λ = wavelength [nm]

Absorption of proteins in the range of λ = 230 – 300 nm is mainly induced by the aromatic side chains Tyr (λ_{max} = 275 nm, ε_{max} = 1400 $M^{-1}cm^{-1}$) and Trp (λ_{max} = 280 nm, ε_{max} = 5600 $M^{-1}cm^{-1}$), whereas Phe (λ_{max} = 258 nm, ε_{max} = 200 $M^{-1}cm^{-1}$) as well as disulfide bridges (λ_{max} = 250 nm, ε_{max} = 300 $M^{-1}cm^{-1}$) contribute only little to absorption due to their low sensitivities (Creighton & Chasman, 1997). The absorption of peptide bonds is observable at a wavelength smaller than 230 nm.

UV spectroscopy was used to determine the protein concentration. Thereby the protein concentration was calculated according to the Beer-Lambert law (Equation 2).

$$\boldsymbol{A = -log_{10}\frac{I}{I_0} = \varepsilon \cdot c \cdot d} \qquad \textbf{(Equation 2)}$$

A = Absorbance

I = emitted radiation intensity

I_0 = inclined radiation intensity

ε = molar extinction coefficient [$M^{-1}cm^{-1}$]

c = protein concentration [$molL^{-1}$]

d = path length [cm]

The theoretical molar extinction coefficients (ε_{280} for proteins at λ = 280 nm) were calculated online with the ProtParam tool (ExPASy bioinformatics Resource Portal).

The protein concentrations of both Rab1A proteins were determined using a Bradford protein assay, which involves the binding of the dye Coomassie Brilliant Blue G-250 to hydrophobic amino acid side chains of the protein (Bradford, 1976). This results in an wavelength shift of the dye maximum from λ = 465 nm (red) to λ = 595 nm (blue) (Bradford, 1976). The increase in absorbance at λ = 595 nm can be traced spectro-photometrical. The assay was performed according to the standard protocol (Bradford, 1976).

3.11.2 Circular dichroism Spectroscopy (CD)

Circular dichroism describes the capability of optical active substances (consisting of asymetric carbon atoms) to absorb left circulary polarized (LCP) or right circulary polarized (RCP) light to different extent (Kelly et al, 2005). Molar circular dichroism can also be devised by applying the Beer-Lambert law (Equation 3).

Thus CD is defined as the difference in extinction coefficients for both types of circular polarized light.

$$\Delta A = A_L(\lambda) - A_R(\lambda) = [\varepsilon_L(\lambda) - \varepsilon_R(\lambda)] \cdot c \cdot d = \Delta\varepsilon \cdot c \cdot d \qquad \textbf{(Equation 3)}$$

ΔA = delta Absorbance

ε_L = molar extinction coefficient for LCP light [$M^{-1}cm^{-1}$]

ε_R = molar extinction coefficient for RCP light [$M^{-1}cm^{-1}$]

c = protein concentration [$molL^{-1}$]

d = path length [cm]

Hence CD spectroscopy is a common method for the characterization of the structure and stability of biopolymers. Due to the differential absorption of backbone amide goups in asymetric sondary structures Far-UV CD spectroscopy (λ = 170 nm – 250 nm) is used to deduce the sondary structure characteristic (Johnson, 1990) of an protein. In the Far-UV region characteristic minima for α-helical elements occur at 208 nm and 222 nm. β-sheets provide a less distinct minimum at 218 nm, additional to a visible maximum at 196 nm. Information about the tertiary structure can be gained by measurements in the Near-UV region (λ = 250 nm – 300 nm) (Johnson, 1990). CD spectroscopy is measured as ellipticity θ in degrees.

For quantitative analyis of the respective protein the conversion of the measurement signal to the mean residue ellipticity is required (Equation 4).

$$\theta_{MRW,\lambda} = \frac{\theta_\lambda \cdot 100 \cdot MRW}{c \cdot d} = \frac{\theta_\lambda \cdot 100 \cdot M_r}{c \cdot d \cdot N_{aa}} \qquad \textbf{(Equation 4)}$$

θ_{MRW} = mean residue ellipticity at wavelength λ [$degcm^2dmol^{-1}$]

θ = measured ellipticity at wavelength λ [mdeg]

MRW = mean molecular weight of the amino acid

c = protein concentration [gL^{-1}]

d = path length [dm]

M_r = molecular weight [$gmol^{-1}$]

N_{aa} = number of amino acid residues

For secondary structure analysis Far-UV-CD spectra were recorded at a final protein concentration of 0.3 mg/mL in quartz cuvettes with 0.02 dm pathlength (Hellma, Müllheim, Germany) at 10 °C. As buffer PBS (pH 8.0) was used. The measurements were performed with a Jasco J-715 spectropolarimeter (Jasco, Großumstadt, Germany) equiped with a PTC 343 peltier unit. Parameters for acquirements were set to a wavelenght range of 260 – 200 nm, 20 nms^{-1}, 16 accumulations. Far-UV spectra were buffer-corrected and the mean residue ellipticity was calculated with equation 4. Structural element contents were deduced using the CD spectra deconvolution software CDNN from Applied Photophysics.

3.11.3 Fluorescence Spectroscopy

Fluorescence spectroscopy offers the possibilty to analyze structural as well as dynamical properties of biomolecules. The absorption of light from a suitable wavelenght leads to the excitation of the electrons of the molecule from its ground state to one of the various vibriational states of an higher energy state. The back transition of the excited electrons into the ground state induces the partial emission of former absorbed energy mainly as elecromagnetic radiation. Fluorescence competitive processes like internal conversion (dissipation of excitation energy into vibronic levels), intersystem crossing (Disexcitaiton via phosphorescence or radiationless transision) or quenching result in incomplete emission of the excitaiton energy (Qu et al, 2007). Similar to absorption spectroscopy the fluorescence intensity is essentially determined by the molecular environment of the protein or the used solvent. Additional fluorescence is negatively influenced by an increase in temperature or a decrease in solvent viscosity (Skoog & Leary, 2013). Given that proteins mostly contain aromatic amino acids like Trp (λ_{max} = 355 nm), Tyr (λ_{max} = 304 nm) or Phe (λ_{max} = 282 nm), which contain a delocalized π-electron system, they can be analyzed by their intrinsic fluorescence properties (Chattopadhyay & Raghuraman, 2004). Thereby the fluorescence behaviour of proteins is significantly determined by Trp, which has the highest quantum yield and is able to quench Tyr or Phe fluorescence by resonance energy transfer (Creighton & Chasman, 1997). Though Trp excitation occurs in the emission region of Tyr and Phe. Besides these intrinsic fluorescence properties various fluorophores exist for specific applications like the investigation of binding characterisitcs.

3.11.3.1 Fluorescence measurements in presence of MANT-Nucleotides

The nucleotide binding of GDP, GTP and ADP to the Rab1A proteins was investigated by the use of fluorescent-labeled MANT-nucleotides (Invitrogen molecular probes, Darmstadt, Germany). Thereby a fluorescent methylanthraniloyl (MANT) group is attached to the ribose moiety (Pisareva et al, 2007; Pisareva et al, 2006). By direct excitation of the MANT-fluorophore changes upon binding are observable at the respective emission maximum. The measurements were performed according to Murthy *et. al* (Murthy & Lorand, 2000). Fluorescence emission spectra were recorded with a spectrofluorometer FP-8500 (Jasco, Großumstadt, Germany) at $\lambda_{exc.}$ = 360 nm at 20 °C.

In a total volume of 150 µL a protein concentration of 1.00 µM (nucleotide-free, see chapter 4.4.1) and a MANT-GXP/Mg^{2+} or MANT-AXP/Mg^{2+} concentration of 0.50 µM was used (Murthy & Lorand, 2000). Spectra were recorded in PBS buffer (pH = 8.0). Measurements were conducted for the Rab1A proteins and the MANT-GXP's and MANT-AXPs alone, as well as a combination of the wtRab1A protein or the nt-svRab1A and the MANT-nucleotide (MANT-GDP, MANT-GTP, MANT-ADP or MANT-ATP).

Determination of the binding affinites for nt-svRab1A to the respective MANT-nucleotides was assesed by fluorescence spectroscopy titration experiments. Therefore changes in fluorescence intensity were examined to monitore binding of MANT-GXP's and MANT-AXP's to nt-svRab1A. As starting solution MANT-GXP or MANT-AXP/Mg^{2+} (0.5 µM) in 150 µL of PBS buffer (pH 8.0) was incubated in quarz cuvettes (light path 10 mm) at 20°C. The concentration of the respective Rab1A protein (nucleotide free) was increased stepwise until saturation was achieved. Fluorescence emission spectra between 380 - 560 nm (Ex 360 nm) were recorde and buffer corrected. Shown are normalized fluorescent intensities at 444 nm. For the determination of the apparent K_D's a quadratic fit equation was used.

3.11.3.2 Fluorescence Anisotropy Spectroscopy

Fluorescence anisotropy spectroscopy is a common method to examine kinetics and binding constants of protein interactions. The basic principal is that the emission of light by a fluorophore has unequal intensities along the different axes of polization depending on its orientation (Lacowicz, 2006). In contrast to immobilized fluorophores, the free movement of fluorophores in solution causes a decrease in the degree of polarization prior the re-emission of photons.
Thus fluorescence anisotropy describes the extent of depolarization and can be calculated by equation 5.

$$r = \frac{I_{\parallel} - I_{\perp}}{I_{\parallel} + 2I_{\perp}} \qquad \textbf{(Equation 5)}$$

r = anisotropy

$I_{\parallel}$ = parallel fluorescence intensity

$I_{\perp}$ = perpendicular fluorescence intensity

Although the measured anisotropy signal is dependent on the rotational movement of the fluorophore in solution. The Perrin equation (equation 6) directly correlates the measured anisotropy to the rotational correlation time, describing how fast the motion in solution occurs. The rotational correlation time is dependend on the viscosity of the solvent, the size and shape of the fluorophore and also affected by the temperature (equation 6). Given that the intrinsic anisotropy r_0 as well as the fluorescence lifetime τ of the fluorophore are constant, anisotropy can be measured as a function of time and increases upon binding.

$$\boldsymbol{r = \frac{r_0}{1+\frac{\tau}{\theta}} = \frac{r_0}{1+\frac{\tau}{\frac{\eta V_m}{RT}}}} \qquad \textbf{(Equation 6)}$$

r = anisotropy

r_0 = intrinsic anisotropy of the molecule

τ = fluorescence lifetime [ns]

θ =rotational correlation time [ns]

η = viscosity of the solvent [$kgs^{-1}m^{-1}$]

V_m = molar volume of the fluorophore [m^3mol^{-1}]

R = gas constant [$Jmol^{-1}K^{-1}$]

T = temperature [K]

As comparison to the, via changes in fluorescece intensity, identified apparent K_D's for binding of nucleotides, additional studies of the MANT-GXP's and MANT-AXP's to the Rab1A proteins were carried out by fluorescence anisotropy spectroscopy. Changes in fluorescence anisotropy (Δr values) were monitored with a spectrofluorometer FP-8500 (Jasco, Großumstadt, Germany) supplied with polarizors at 20 °C. Measurements were perfomed at an excitaiton wavelenght of $\lambda_{exc.}$ = 365 nm and MANT-GXP or MANT-AXP, association was followed at an emission wavelenght of $\lambda_{em.}$ = 448. As instrument settings a bandwidth for excitation and emission of 5 nm, high sensitivty and a time interval of 1 s was adjusted. Samples were measured with a fluorescence quartz cuvette of 10 mm pathlength (Hellma, Müllheim, Germany). As starting solution MANT-GXP/Mg^{2+} or MANT-AXP/Mg^{2+} (0.1 µM) in 1 mL of PBS buffer (pH 8.0) was prepared and incubated for 5 min at 20 °C. The respective Rab1A protein 0.15 µM, (nucleotide-free) was added after a stable signal was reached. The concentration was increased stepwise until saturation was achieved.

Preparation of nucleotide-free Rab1A protein

The preparation of free Rab1A protein was in general performed according to Goody *et al.* (Goody et al, 2012). To the GXP bound wtRab1A or nt-svRab1A protein 5 mM EDTA (5x more molar excess than $MgCl_2$ in the protein solution) was added and incubated for 2 h at room temperature. Free nucleotide was removed by loading the sample on a PD10 desalting column (GE Healthcare, Munich, Germany). The PD10 column was equilibrated with buffer A. The protein containing fractions were then dialyzed against the desired measurement buffer equipped with 1 mM $MgCl_2$ (pH = 8.0) at 4 °C. After concentrating of the protein samples the measurements were immediately performed. To verify the complete removal of bound nucleotide additional reversed phase HPLC measurements were performed and compared with nucleotide containing standard (GDP, GTP, ADP or ATP) measurements.

PD10 equilibration buffer A:

20 mM Hepes/KOH, pH 8.0
50 mM NaCl
2.0 mM (w/v) DTT

3.12 Structural and Functional Analysis

3.12.1 Analytical Size Exclusion Chromatography (HPLC)

The basic prinicple of high performance liquid chromatography (HPLC) is that by pumping a liquid (mobile phase) over the stationary phase under high pressure conditions, analytes are separated into their subcomponents (Aitzetmüller et al, 2012). Thereby high resolution separation of the different components is achieved by diverse interaction of the analytes with the functional groups of the stationary phase (Rimmer, 2011). With the proportional correlation of retention time and the logarithmic molecular weight of the subcomponents, the determination of the apparent molecular weight of all oberservable peaks is possible. For the calculation a calibration curve of standard proteins is used.

In this thesis HPLC was used as analytical size exclusion chromatography to analyse the quaternary structure of both Rab1A proteins. Measurements were performed with a $TSKG2000SW_{XL}$ column (Tosoh Bioscience, Stuttgart, Germany) operated at 20 °C. Under native conditions a constant flow rate of 0.5 mL/min was utilized. Prior the sample application the column was equilibrated with PBS buffer (pH 8.0) containing 1 mM $MgCl_2$. 2 µg protein were applied to the column.

Measurements under denaturing conditions were performed with a constant flow rate of 0.2 mL/min using the native buffer with addition of 3 M guanidinium chloride. Prior to the SEC runs under denaturing conditions the protein samples were incubated for 1.5 h at room temperature in the presence of 3 M guanidinium chloride.

Elution profiles were recorded using fluorescence detection ($\lambda_{exc.}$ = 280 nm, $\lambda_{em.}$ = 330 nm) with a FP 920 fluorescence detector (Jasco, Großumstadt, Germany). For calibration standard proteins of the gel filtration calibration low and high molecular weight marker kit (Sigma-Aldrich, St. Louis, USA) or the gel filtration standard (Bio-Rad, Hercules, USA) were applied.

Additional HPLC measurements were carried out with Rab1A proteins in prese of the nucleotide GDP (10 µM). Prior to application onto the column, the nucleotide free samples were incubated for 1.5 h at 20 °C with 1 mM $MgCl_2$ and GDP. Control experiments were performed with carboanhydrase (Sigma-Aldrich, St. Louis, USA) in absence and presence of GDP (10 µM).

Although the interaction of the two Rab1A proteins was studied by HPLC. Therefor a protein concentration of 10 µM each (ratio 1/1) was used. Before the measurement the mixture was incubated for 1.5 h at 20 °C.

3.12.2 Reverse Phase HPLC

GTP hydrolysis and ATP hydrolysis was assayed as a function of time by reversed phase analytical high performance liquid chromatograohy (HPLC) using a C_{18} ProntoSIL column (120-5-C18, 5 µm, Bischoff Analysetechnik und –geräte GmbH, Leonberg, Germany) in the presence of tetrabutylammonium bromide (Simon et al, 1996). For the measurements a constant flow rate of 1.0 mL/min was used. Prior the HPLC measurements a nucleotide exchange reaction of GDP against GTP was performed according to Goody *et al.* (Goody et al, 2012) in the presence of EDTA (c_{final} = 5 mM, 5x more molar excess than $MgCl_2$ in solution) and a 20 fold molar excess of GTP or ATP with regard to the protein. After 2 h contact time at room temperature the removal of free nucleotide was performed by loading the sample on a PD10 desalting column (GE Healthcare, Munich, Germany) equilibrated with buffer (20 mM Hepes, 50 mM NaCl, 2 mM DTT, pH 8.0). The protein containing fractions were then concentrated and samples were taken after desired time points. The hydrolysis reaction was started by the addition of $MgCl_2$ (c_{final} = 1 mM) to the sample. Measurements in presence of $TBC1D20_{(1-362)}$ were performed using a protein to GAP ratio of 1/100.

3.12.3 Protein Cross-linking combined with Mass Spectrometry

Further evaluations on the quaternary strucutre of nt-svRab1A were conducted by chemical protein cross-linking experiments. Proteins or other molecules can be intramolecular or intermolecular combined via the formation of a covalent bond. Crosslinking reagents consist of bifunctional or multi-functional reactive end groups which are capable to form stable covalent bonds with the desired functional groups (e.g. sulfhydryls, primary amines) of the protein. A number of different crosslinkers are available depending on the application.

Here the isotopically–coded crosslinkers DSSG-H6/D6 or BS^3-H12/D12 (Creative Molecules Inc., USA) was used. In a total volume of 40 µL nt-svRab1A protein (137 µM) or wtRab1A (10 µM) was mixed with 10 equivalents (eq.)., 12 eq. or 15 eq. of cross-linker respectively. The reaction was incubated for 30 min at RT, followed by addition of 10 µL of Laemmli-buffer (5x) for quenching. For the separation of the cross-linking bands SDS-PAGE of the samples were performed. Afterwards the intramolecular and intermolecular cross-link bands were cutted out of the SDS gel, digested with trypsin and analyzed further by mass spectrometry using a liquid chromatography-mass spectrometer LC-MS (LTQ Orbitrap XL, Thermo Scientific, Rockford, USA). Sample preparation was carried out as described previously (Bepperling et al, 2012). The data was processed using the MassMatrix software (Xu & Freitas, 2009).

3.12.4 Thermal Shift Assay (TSA)

Thermal Shift Assay is a common method to analyze the thermal denaturation of a protein in the prescence of a fluorescent dye like SYPRO®Orange (Invitrogen molecular probes, Darmstadt, Germany). In a non-polar environment (denatured protein with hydrophobic patches) these dyes are fluorescently active, whereas quenching effects predominantly occur in aqueous solution (Niesen et al, 2007). The temperature at which a protein unfolds is measured by an increase in fluorescence of a dye with affinity for hydrophobic parts of the protein, which are exposed by unfolding of a protein (Lo et al, 2004; Niesen et al, 2007).

For analysis of the Rab1A proteins in the absence and presence of the nucleotides GDP and GTP, TSA measurements were performed. The experiments were carried out in PBS buffer (pH = 8.0) supplied with 1 mM $MgCl_2$. The addition of $MgCl_2$ is necessary as binding of the nucleotides to Rab1A is favored in the presence of divalent magnesium ions (John et al, 1993; Simon et al, 1996).

The denaturation experiment was performed in 71 cycles with a heating rate of 1 °C/min from 20 °C to 95 °C in a real time PCR cylcer (Stratagene Mx3000P, Agilent Technologies, Oberhaching, Germany). A total protein amount of 5 µg was used. Prior to the TSA measurements in the presence of the nucleotides GDP and GTP the nucleotide-free Rab1A proteins were incubated with the respective nucleotide (0.5 µM – 50 µM) and 1 mM $MgCl_2$ in PBS buffer (pH 8.0) for 1.5 h at 20 °C.

3.12.5 Co-Immunoprecipitation Studies (Co-IP) followed by Mass Spectrometry

Co-Immunoprecipitation is a common method to study protein-protein interactions *in vitro* or *in vivo*. The basic principal is that by the use of a specific antibody against the particular protein, all potential interactors that are bound to this target protein are indirectly captured and simultaneously precipitated out of solution. The main steps are described birefly in the following stion. By addition of the antibody (monoclonal or polyclonal) to purified proteins or either cell lysate an immune complex is formed with the target protein. In the netxt step the immune complex is immobilized onto antigen coupled beads (protein A or G). Unprecipitated substances are removed by a washing step. Then the target protein, including its diverse interacting proteins is eluted from the beads. If the used antibody is not covalently linked to the beads, the antibody although elutes with the antigen. Unspecific binding of the target protein to the immobilized beads or unspecific interplay of the used antibody with potential interactors result in negative falsification of the Co-IP experiment and thus need to be prevented.

Co-IP studies of purified protein

The interaction of the Rab1A proteins with the $DrrA_{(340-533)}$ GEF were studied by Co-IP. Experiments were performed in PBS buffer (pH 8.0) using 10 µg of the respective Rab1A protein and the $DrrA_{(340-533)}$ GEF. Prior to the addition of the $DrrA_{(340-533)}$ GEF to the samples, the Rab1A proteins (nt-svRab1A or wtRab1A) were incubated for 2 h with 1 mM $MgCl_2$ and 10 µM GDP (Guanosine 5’ di-phosphate sodium salt, Sigma-Aldrich, St. Louis, USA) in PBS (pH 8.0). After the addition of the $DrrA_{(340-533)}$ GEF to the samples and incubation for 1 h at 4 °C, the rabbit polyclonal IgG antibody Rab1A (Santa Cruz Biotechnology, Heidelberg, Germany) was added and incubated further for 1.5 h at 4 °C. Next protein G-sepharose beads (GE Healthcare, Munich, Germany) were added and the samples were incubated for 3 h at 4 °C. The protein G-sepharose was precipitated by centrifugation at 14000 rpm (Eppendorf centrifuge 5418R, FA-45-18-11 rotor) for 30 s

and washed four times with PBS buffer (pH 8.0). Bound proteins (interaction partners) were eluted with 0.1 M glycine (pH 2.8) and further analyzed by SDS-PAGE. Co-IP studies of the Rab1A proteins with the $Rab1B_{(3-174)}$ variant were performed under similar conditions.

Co-IP studies of the nt-svRab1A and the wtRab1A were performed in a slightly modified way. 20 µg of both proteins were used. To saturate the IgG antibody with nt-svRab1A and to exclude false positive bindings of the later added wtRab1A protein to the antibody, a fivefold molar excess of nt-svRab1A over antibody was used. First, the rabbit polyclonal IgG antibody Rab1A (Santa Cruz Biotechnology, Heidelberg, Germany) and the nt-svRab1A were incubated at 4 °C for 1 h with 1 mM $MgCl_2$ and 10 µM GDP or GTP (Guanosine 5' tri-phosphate sodium salt hydrate, Sigma-Aldrich, St. Louis, USA) respectively. Second Protein G Sepharose beads were added and the samples were incubated for 1 h at 4 °C. After centrifugation of the Protein G Sepharose beads (14.000 rpm, Eppendorf centrifuge 5418R, FA-45-18-11 rotor, 30 s), a washing step for 10 min with 5 % milk powder in PBS buffer (pH 8.0) was included for blocking of free valances of the sepharose. Unbound components were removed by an additional washing step with PBS buffer (pH 8.0). Finally, wtRab1A was added and further incubated for 3 h at 4 °C. The precipitation, elution and further analysis of the samples were kept the same as described above.

Co-Immunoprecipitation (Co-IP) from HeLa lysate samples

For the identification of interaction partners in the HeLa lysate samples, the lysate was spiked with 30 µg of nt-svRab1A or wtRab1A. Preparations were performed in PBS buffer (pH 8.0) with 110 µg HeLa lysate. HeLa lysate was produced according to the manufacturer's M-PER® Mammalian Protein Extraction Reagent protocol (Thermo Scientific, Rockford, USA). The remaining conditions were kept the same as described for Co-IP of purified proteins. The eluate was separated by SDS-PAGE and further analyzed by LC-MS (LTQ Orbitrap XL, Thermo Scientific, Rockford, USA), basically as described previously (Bepperling et al, 2012). Proteins were identified using the Sequest HT algorithm implemented in the Proteome Discoverer 1.4 software, and considered as hits if they were not present in the respective control.

3.12.5.1 Mass Spectrometry

After Co-IP, the Coomassie-stained gel lanes were cut into six individual samples and prepared for liquid chromatography-mass spectrometry analysis as described previously (Bepperling et al, 2012). After reduction, alkylation and trypsin-digestion, peptides were extracted in five repeats of sequential addition of 10 mM NH_4HCO_3, acetonitrile (ACN), 0.1 % formic acid, ACN, and again ACN. The respective supernatants were pooled, and concentrated prior to loading the peptides onto an Acclaim PepMap RSLC C18 trap column. Separation of the peptides was performed on a PepMap RSLC C18 column (both Thermo Scientific, Langenselbold, Germany) at a flow rate of 0.2 µl/min eluting the peptides with a linear, 46 min gradient from 4 % to 30 % ACN supplemented with 0.1 % formic acid directly into a LTQ Orbitrap XL mass spectrometer (Thermo Scientific). Full scans and five dependent MS2 scans (CID spectra) were recorded in each cycle. The MS data derived from each gel slice were searched against the human sequence database downloaded from NCBI using the Sequest HT algorithm implemented into the software "Proteome Discoverer 1.4" (Thermo Scientific). The search was limited to tryptic peptides containing a maximum of two missed cleavage sites. Only monoisotopic precursor ions were used for the search and a peptide tolerance of 10 ppm for precursors and 0.6 Da for fragment masses was preconditioned. Proteins were accepted as identified only when at least two distinct peptides with a target false discovery rate below 1 % according to the decoy search were retrieved from the sample.

3.13 Cell Biological Methods

The influence of the presence of nt-svRab1A *in vivo* was analyzed by over-expression of the isoform in human embryonic kidney 293 cells (*HEK293*). For comparision the wtRab1A protein was over-expressed. For over-expressing nt-svRab1A as well as wtRab1A was ligated into the mammalian pAcGFP-N1 vector (Clontech Laboratories Inc., Mountain View, USA), leading to a C-terminal fusion of GFP (Haas et al, 1996). Therefor the coding sequence of wtRab1A or nt-svRab1A was amplified by PCR and inserted between the XhoI and SalI site of the multiple cloning site of the pAcGFP-N1 vector. Additionally Rab1A protein without the C-terminal GFP fusion were constructed as well (using XhoI, NotI restriction sites). After 24 h post transfection the GFP fusion constructs were further analyzed by fluorescence light microscopy, the constructs without GFP fusion were studied by Western blot.

3.13.1 Cultivation of eukaryotic cells

HEK293 (human embryonic kindey 293), *HeLa (*Henrietta Lacks*,* cervix carcinoma) and *MCF7* (breast adenocarcinoma) cells were cultured in Dulbecco's Modified Eagle Medium (DMEM, Invitrogen molecular probes, Darmstadt, Germany) including 10 % (v/v) Foetal Calf Serum (BioConcept, Allschwill, Switzerland) at 37 °C in a humified atmosphere containing 5 % CO_2. Routinely 25 cm^2 or 75 cm^2 cell culture flasks (TS25, TS75 Sarstedt AG & Co., Nümbrecht, Germany) were used for cultivation. For analysis of the cell viability and examination against potential contamination of the cells, a Leica DM-IRB microscope (Leica Microsystems, Wetzlar, Germany) was utilized. At a confluence of approximately 80 % cells were sub-cultured. Therefor the culturing medium was discarded and the cells were washed with DPBS buffer (Invitrogen molecular probes, Darmstadt, Germany). For detachment of strong adherent cells (HeLa, MCF7) from the layer of the cell culture flask, 1 mL of Trypsin-EDTA 0.5 % (Invitrogen molecular probes, Darmstadt, Germany) was added and the cells were further incubated for 2 min in the incubator. The detached cells were then resuspended in DMEM-FCS medium to inhibit the Trypsin protease reaction. For *HEK293* cells (weakly adherent cells) it was already sufficient to detach the cells by addition of 1 mL of DPBS. The number of living cells was determined by addition of Trypan blue (Sigma-Aldrich, St.-Louis, USA) to 50 µL of detached cells (ratio 1:1). Afterwards the desired amount of cells was transferred into a new flask equipped with fresh culturing medium.

3.13.2 Transfection of eukaryotic cells

Transfection is a commonly used process to insert foreign DNA into eukaryotic cells for expression of a transgene protein. For transient transfection the Lipofectamine®2000 Transfection Reagent protocol (Invitrogen molecular probes, Darmstadt, Germany) was employed. Therefor 3 x 10^4 cells per well were grown on 4-well CC2-coated glass slides (Nalge Nunc International, Rosklide, Denmark,) over night at 37 °C under standard cell culture conditions. Depending on the experiment either the GFP fusion constructs of the Rab1A proteins or the constructs without C-terminal GFP fusion were transfected. Earliest at 24 h post transfection the cells were either analyzed by fluorescence microscopy or Western Blot.

3.13.3 Preparation of eukaryotic cell lysate

For the preparation of eukaryotic cell lysate RIPA buffer was used according to the manufacturer's protocol (Thermo Scientific, Rockford, USA). In brief the desired cells (*HEK293*, *HeLa*, *MCF7*) were grown under standard conditions at 37 °C until approximately 100 % confluence was reached. Then the culture medium was removed, followed by washing steps with cold DPBS. In case of weakly adherent or suspension cells, cells were pelleted by 2500 x g (Hettich Rotina 420 R centrifuge, 4723 Rotina 4 place swing out rotor) for 5 minutes and the supernatant was discarded. Then the cells were washed in cold DPBS and pelleted by centrifugation. After addition of cold RIPA buffer (1 mL per 75 cm^2 containing 5 x 10^6 cells) and incubation the lysed cells were centrifuged at 14.000 x g for 15 minutes at 4 °C. The supernatant was transferred into a new tube. For long-time storage Protease Inhibitor Mix M (Serva, Heidelberg, Germany) was additionally added and the lysate was aliquoted, shock frozen in liquid nitrogen and stored at – 80 °C.

3.13.4 Analysis of membrane binding of Rab1A proteins

Rab1A protein over-expressing *HEK293* cells were lysed and separated into the cytosolic and membrane containing protein fractions using the Mem-PER™ Plus Membrane Protein Extraktion Kit (Thermo Scientific, Rockford, USA). Therefor the wtRab1A or the nt-svRab1A coding sequence was amplified by PCR and inserted between the XhoI and NotI site of the multiple cloning site of the pAcGFP-N1 vector, leading to C-terminal constructs lacking the GFP fusion. As control *HEK293* cells overexpressing the pAcGFP-N1 empty vector were used. Further analysis was performed by Western blot using 4.3 µg of total protein per sample. As loading control GAPDH, detected by a primary mouse monoclonal Anti-GAPDH antibody (Sigma-Aldrich, St-Louis, USA) in 1:10.000 dilution, followed by secondary antibody (horseradish peroxidase-conjugated goat α-mouse IgG, 1:5000, Sigma-Aldrich, St.-Louis, USA) was used.

To study the influence of prenylation on membrane attachment for both Rab1A proteins, C-terminal Cys-mutants (wtRab1A-C204A/C205A, nt-svRab1A-C128A/C129A) were designed and inserted into a pcDNA 3.1 (+) vector. Further analysis of *HEK293* cells, over-expressing the mutated Rab1A proteins was performed by the use of the Mem-PER™ Plus Membrane Protein Extraktion Kit (Thermo Scientific, Rockford, USA), followed by Western blot analysis. 6 µg of total protein per sample was used and tubulin served as loading control.

Tubulin was detected by a primary mouse monoclonal Anti-tubulin antibody (1:10.000, Sigma-Aldrich, St-Louis, USA), followed by detection with secondary antibody (horseradish peroxidase-conjugated goat α-mouse IgG, 1:5000, Sigma-Aldrich, St-Louis, USA).

3.13.5 Co-Localization Experiments

Co-localization studies of the Rab1A proteins with the ER were performed in *HEK293* cells overexpressing the GFP fused Rab1A expression constructs. Prior to the transient transfection of the cells using the manufacturer's Lipofectamine®2000 Transfection Reagent protocol (Invitrogen molecular probes, Darmstadt, Germany), the cells were grown on CC2-coated glass slides (Nalge Nunc International, Rosklide, Denmark, 3 x 10^4 cells/well). For visualization of the ER the ER-ID™ Red Assay Kit (Enzo Life Sciences GmbH, Lörrach, Germany) was used. According to the manufacturer´s instructions the cells were stained with 50 µL of staining solution for 30 min at 37 °C. Further analysis was performed by fluorescence light microscopy.

3.13.6 Secreted Alkaline Phosphatase Reporter Gene Assay (SEAP)

The secretion assay was performed as described elsewhere (Cullen & Malim, 1992; Mukherjee et al, 2011), using the Sreted Alkaline Phosphatase Reporter Gene Assay Kit (Cayman Chemical Company, Ann Arbor, USA). *HEK293* cells were co-transfected with a alkaline phosphatase expression plasmid and the pAcGFP-N1 empty vector, the wtRab1A or the nt-svRab1A expression constructs without the GFP fusion. 24 h post transfection the amount of alkine phosphatase sreted into the culture medium was analyzed by detection of chemiluminescence in a Tecan Genios plate reader (Tecan Group Ltd, Männedorf, Germany).

3.13.7 Analysis of Rab1A protein levels in MCF7 cells under normal and stress conditions

The Rab1A protein levels were analyzed in MCF7 cells under normal and stress conditions. To mimic ER or Golgi stress, cells were either treated with Thapsigargin or Brefeldin A (BFA). According to the manufacturer's instruction a final concentration of 10 μgmL^{-1} (36 µM) BFA was used, 300 nM Thapsigargin were utilized.

To exhibit complete inhibition of the Golgi apparatus, MCF7 cells containing BFA were incubated for 1 h 30 min, cells with Thapsigargin were cultivated further for 3 h under standard cell culturing conditions. As controls untreated cells, with identical incubation times were used. Afterwards the cells were lysed and analyzed further by Western Blot analysis. 40 µg of each lysate sample was used tubulin served as loading control. Tubulin was detected by a primary mouse monoclonal Anti-tubulin antibody (1:10.000, Sigma-Aldrich, St-Louis, USA), followed by detection with secondary antibody (horseradish peroxidase-conjugated goat α-mouse IgG, 1:5000, Sigma-Aldrich, St-Louis, USA).

3.13.8 Fluorescence Microscopy

For fluorescence microscopy a Zeiss Axiovert 200 microscope (Zeiss, Jena, Germay) equipped with a Hamamatsu C4742-95 camera (Hamamatsu, Herrsching, Germany) was used. Images were proccessed with ImageJ.

4 Results Part I – The human nt-svRab1A

4.1 Evolutionary conservation and expression analysis of nt-svRab1A

As starting point for further biochemical analysis of the non-trivial splice variants investigated here, bioinformatical experiments were performed to identify alternative splicing on proteome level. Additionally, on the basis of alternative splicing events mapped on the respective 3D-structures of the native proteins 10 different target proteins (including the non-trivial splice variant of Rab1A, nt-svRab1A) with structurally non-trivial splice variants were selected for examination. In this selection process the following aspects were included: Availability of a crystal structure of the full-length isoform, a well-studied enzymatic function of the wild-type protein and the evidence for the non-trivial spliced isoform *in vivo* on the mRNA level and as far as possible on the protein level. For many potential splice isoforms of Rab1A and other proteins it is still under debate, whether they are really translated and exist on the protein level. Especially for non-trivial splice variants it was expected that most of them are degraded already at the mRNA level by NMD (Jaillon et al, 2008; Lareau & Brenner, 2015; Lareau et al, 2007). On the other hand, for a substantial fraction (10 – 15 %) of non-trivial splice variants, protein products and protein functions have been described (Birzele et al, 2008a; Birzele et al, 2008b). Such a non-trivial splice variant is the spliced isoform of the human Rab1A GTPase, which was analyzed in detail in this thesis.

The results showed that for the *rab1A* gene the existence of up to three annotated human splice variants with up to now unclear function exist (iso-2, P62820-2, iso-3, nt-sv, P62820-3 and iso-4, E7END7 according to Uniprot, Figure 10A). In addition the annotation of the rab1A splice variants in other genomes was possible (iso-4 in bos, iso-2 in mouse, and iso-3 (nt-sv) in mouse, and puffer fish; Figure 10B, circles). With a view to investigate the evolution of the respective non trivial isoforms, the conservation of the respective isoforms in orthologous genes of 10 model organisms, using the annotated protein coding transcripts from the ENSEMBL database (Cunningham et al, 2015), was studied. This analysis indicated that the gene structure (exon-intron structure, splice sites) of *rab1A* is highly conserved (with high sequence similarities) in a number of species and would allow for the non-trivial isoforms iso-2, iso-3 (nt-svRab1A) and iso-4 to exist (Figure 10B, boxes). The isoform of interest (iso-3, nt-svRab1A) lacks 37 % of the amino acids of the wild-type Rab1A protein and is conserved (annotated) in mouse down to puffer fish with sequence similarities of 98.8 % and 64.4 %, respectively.

Additionally, the conserved gene structure would allow for the formation of splice variant iso-3 (nt-svRab1A) in a large number of animal species including fish and even fly, which misses the intron between exon 3 and 4 (Figure 10A). Only worm and yeasts do not support the splice variant iso-3 (nt-svRab1A) due to their gene structures. This wide range conservation and apparent expression of the iso-3 transcript suggests that the analyzed isoform might serve some evolutionary function.

Moreover, the isoforms and in particular iso-3 (nt-svRab1A) can be detected in a large number of the 174 human next-generation-sequencing (NGS) data sets (Figure 10B).

The isoform of interest (iso-3, nt-svRab1A) lacks 37 % of the amino acids of the wild-type Rab1A protein and is conserved (annotated) in mouse down to puffer fish with sequence similarities of 98.8 % and 64.4 %, respectively. Additionally, the conserved gene structure would allow for the formation of splice variant iso-3 (nt-svRab1A) in a large number of animal species including fish and even fly, which misses the intron between exon 3 and 4 (Figure 10A). Only worm and yeasts do not support the splice variant iso-3 (nt-svRab1A) due to their gene structures. This wide range conservation and apparent expression of the iso-3 transcript suggests that the analyzed isoform might serve some evolutionary function.

Moreover, the isoforms and in particular iso-3 (nt-svRab1A) can be detected in a large number of the 174 human next-generation-sequencing (NGS) (Figure 10B).

In addition, *rab1A* isoforms can be found in many of the 341 NGS data sets of various species (Figure 10B, triangles), although to a much lesser extent due to the much smaller number of available data sets in the respective species.

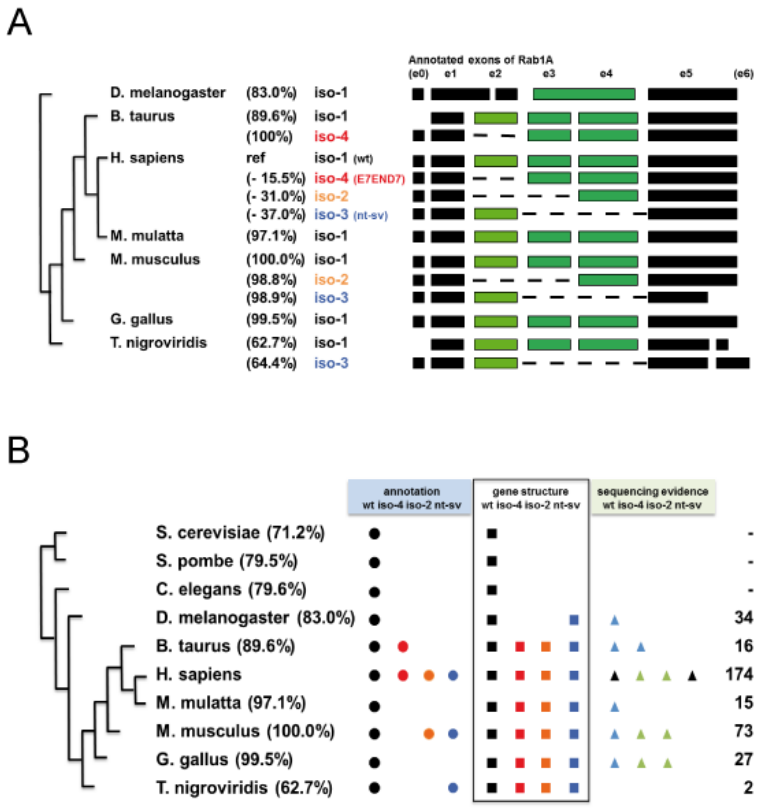

Figure 10: Evolutionary conservation of nt-svRab1A.
A) Conservation of gene structure of *rab1A*, gene (exon – intron) structures and annotated isoforms of *rab1A* in seven species: The (NCBI) taxonomy of the species is shown together with the sequence similarity (as compared to the respective human isoform) of the conserved wild-type (iso-1, 205 AA) and three annotated human isoform sequences of *rab1A*. The splice isoforms iso-2, iso-3 (nt-sv) and iso-4 delete 31 % (64 AA), 37 % (76 AA) or 15.5 % (32 AA) of the residues of the wt sequence, respectively (deleted parts indicated in green). The schematic alignment visualizes the exons in the four *rab1A* isoforms as annotated in the respective species. The wt consists of six exons (e0 – e5), the splice variant iso-4 deletes only exon e2 (light green), iso-2 deletes two exons e2 and e3, and iso-3 e3 and e4 (both dark green, as in fly there is only one corresponding exon). The isoforms are also different with respect to exon e0 and possibly additional C-terminal exons e6 in puffer fish. Moreover the length of the starting and end terminal exons varies slightly between isoforms and species. **B)** Evolutionary conservation of human *rab1A* (reference) and its three annotated splice variants iso-2, iso-4 and nt-sv in ten species: The (NCBI) taxonomy of the ten species is shown schematically together with the sequence similarity of the conserved wild-type (wt) sequence of Rab1A with the human wt sequence. The similarity of the wt sequences ranges from 100 % in mouse down to 62.7 % in puffer fish (*T. nigroviridis*) and is between 71.2 % and 79.6 % in yeasts. The circles indicate whether the respective splice variants (iso-4, iso-2 and nt-sv) are conserved in the shown species: iso-4 (Uniprot: E7END7) is conserved in human and bos, iso-2 (Swissprot: P62820-2) in human and mouse, and nt-sv (Swissprot: P62820-3) in three species (human, mouse and puffer fish). The rectangles visualize whether the gene structure is conserved, i.e. whether the exon-intron structure would allow for the respective splice variant which is always the case except for yeast and worm, whereas fly would allow for only one of the splice variants (nt-sv) due to a missing intron. The triangles and the numbers in the last column (number of available next generation sequencing data sets, 341 in total) indicate whether the wild-type and/or the splice isoforms can be found very often (black), often (light blue) or sometimes (light green) in these NGS data. Figures were kindly provided by the bioinformatics group of Prof. Dr. Ralf Zimmer (LMU).

Overall, the bioinformatics analysis of Rab1 gene-structure and non-trivial splice forms demonstrates a high level of evolutionary conservation of the non-trivial splice forms. Consequently, one can assume their evolutionary relevance, thus counter arguing against non-functional products.

In order to elucidate the role of splice variant iso-3 (nt-svRab1A) in human, it was investigated if, nt-svRab1A encoding mRNA is present in humans, by analyzing 20 total RNA isolates from different human tissue samples. After reverse transcription of the total RNA, the presence of Rab1A isoform 1 (wt) and isoform 3 (nt-svRab1A) was detected by polymerase chain reaction using specific primers (Figure 11A). Hereby the initial presence of the nt-svRab1A mRNA is indicated by a band appearing at 250 base pairs.
In accordance with the proposed presence of nt-svRab1A in different tissues on basis of the human proteome data (Wilhelm et al, 2014), the nt-svRab1A is expressed in 19 out of the 20 tissues tested (Figure 11B). Interestingly, in some tissues tested both the wtRab1A and nt-svRab1A isoforms were detected, showing similar expression levels.
Besides, the mRNA levels for the wtRab1A in many tissues seemed to be under the detection limit in our experiments. Nevertheless, the presence of wtRab1A was confirmed on protein level in the human proteome study (Wilhelm et al, 2014). This might indicate that the stability of the two Rab1A protein isoforms is different, forcing the cell to produce more nt-svRab1A mRNA, to balance the protein amounts of the two isoforms.

A

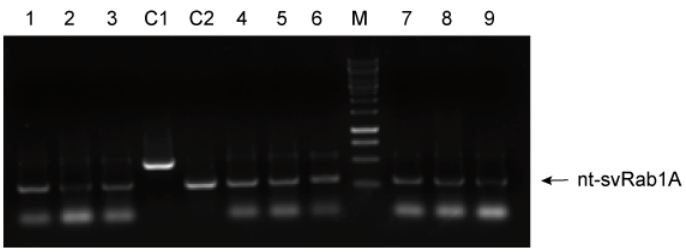

B

Tissue	Wild type		Splice Variant	
	mRNA level	protein level	mRNA level	protein level
Adrenal gland	no	yes	yes	yes
Brain cerebellum	no	yes	yes	yes
Brain whole	no	yes	yes	yes
Fetal brain	yes	not tested	yes	not tested
Fetal liver	no	not tested	yes	not tested
Liver	no	yes	yes	yes
Heart	no	yes	yes	yes
Kidney	no	yes	yes	yes
Lung	no	yes	yes	yes
Placenta	yes	yes	yes	yes
Prostate	yes	yes	yes	yes
Salivary gland	no	yes	yes	yes
Skeletal muscle	yes	no	yes	no
Small intestine	no	no	no	no
Spleen	no	yes	yes	yes
Stomach	no	yes	yes	yes
Thymus	no	no	yes	no
Thyroid gland	no	yes	yes	yes
Trachea	no	no	yes	no
Uterus	no	yes	Yes	yes

Figure 11: Analysis of the mRNA levels of Rab1A proteins in different human tissue samples.
A) Example agarose gel (1 %) of three different tested tissues. As template 1.0 µg, 2.0 µg and 4.0 µg of the respective tissue RNA was used. 1.0 µg of wt or nt-svRab1A DNA was utilized as a control. The respective RNA samples were reverse transcribed into cDNA followed by a polymerase chain reaction. The band at 250 base pairs indicates the presence of nt-svRab1A mRNA (marked by an arrow), whereas the identification of a band at approximately 528 base pairs shows the presence of wtRab1A mRNA. C1: Control wtRab1A, C2: Control nt-svRab1A, 1-9: Tissue samples, Adrenal gland: 1-3, Fetal Liver: 4-6, Liver 7-9. **B)** Overview of the presence of Rab1A on mRNA- (this study) and protein-level (Wilhelm et al, 2014) in 20 different human tissue samples tested.

4.2 Protein purification of wtRab1A and nt-svRab1A

In the following section an overview of the established purification methods on both proteins are presented. A detailed description of the respective purifications steps is shown in Material and Methods (see chapter 3.9). In general, protein purification of both human variants was achieved in a recombinant manner from *E. coli*.

For expression of the wtRab1A protein the pProEX HTa vector, containing a cleavable N-terminal His_6-Tag was used. *E. coli JM109* cells were utilized for expression. Cells were grown in 6L LB_{Amp} medium overnight at 37 °C. Affinity chromatography followed by His_6-Tag removal and SEC allowed the preparation of wtRab1A without any problems (~ 6 mg wtRab1A per liquid culture, Figure 12). After concentration the protein was aliquoted, shock frozen in liquid nitrogen and stored at – 80 °C.

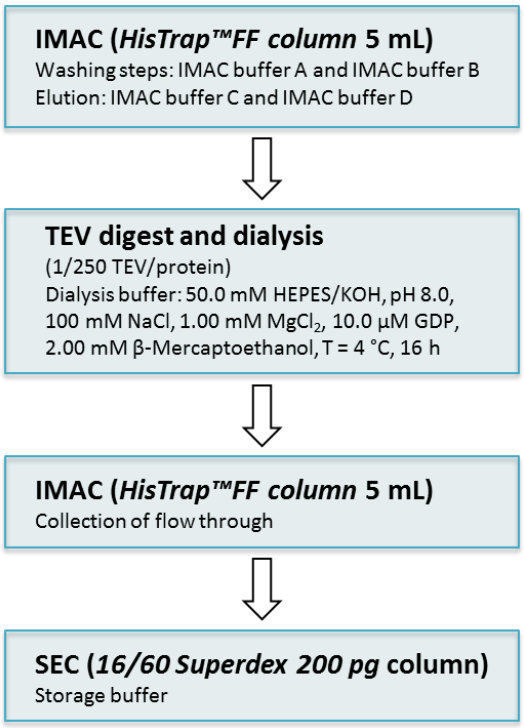

Figure 12: Purification scheme of wtRab1A protein.

First trials in also expressing nt-svRab1A with the pProEx HTa vector construct failed, due to almost 90 % of the protein being detected in the insoluble cell pellet fraction. By reason of a missing crystal structure of nt-svRab1A, purification strategies using refolding techniques could not be applied.

Thus, nt-svRab1A was re-cloned into a pET SUMO vector system. By introducing of the SUMO Tag the yield of soluble nt-svRab1A protein could be significantly improved. *E. coli BL21 (DE3) Cod+* cells were used for expression.

However compared to wtRab1A, nt-svRab1A expression was weaker, making an up-scaling of the cell culturing conditions to 12 L of LB_{Kana} medium (6 L LB_{Amp} medium used for wtRab1A) necessary.

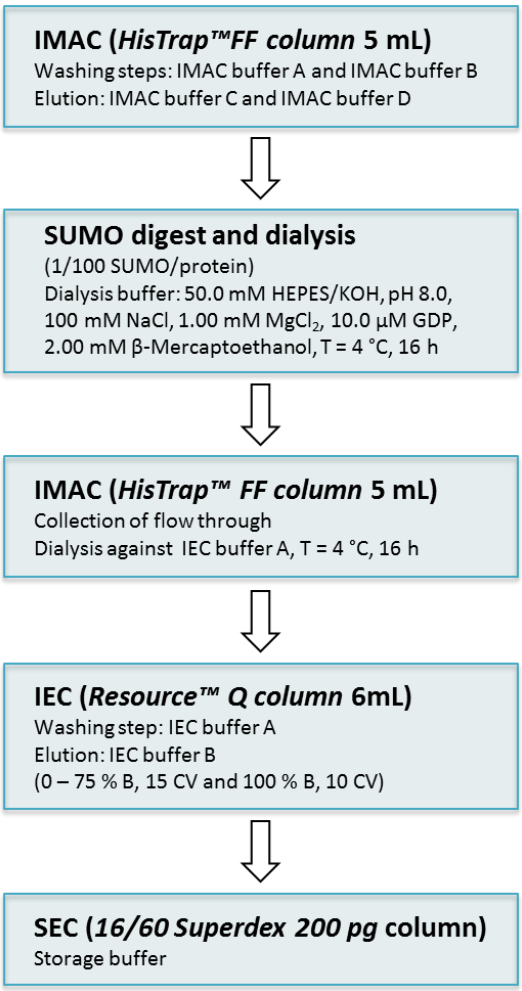

Figure 13: Purification scheme of the nt-svRab1A.

Further, prior SEC, an additional purification step was necessary to achieve the nt-svRab1A in its pure form. Instead, IEC was utilized (Figure 13).
In contrast to wtRab1A it was only possible to store the concentrated nt-svRab1A at +4 °C, due to precipitation of the isoform after thawing.

In summary, it was possible to isolate both proteins in their soluble form. In comparison to wtRab1A, the nt-svRab1A expression levels were significantly lower and throughout the purification, nt-svRab1A was more aggregation prone. This resulted in overall lower yields of the isoform (~ 0.3 mg nt-svRab1A per liquid culture), hence limiting the amount of experiments which could be performed per protein batch.

Because of its aggregation propensity when concentrated by centrifugation, it was not possible to exceed concentrations over 50 µM. In addition long term storage of nt-svRab1A was due to precipitation under various conditions not possible. Consequently, the isoform always needed to be freshly purified prior its use in the different experiments.

4.3 Structural characterization of the nt-svRab1A

As already mentioned previously, an aim of this thesis was to analyze the effect of alternative splicing on the structures of the respective non-trivial isoforms. In particular, it was explored whether splicing leads to conformational diversity. This could be underlined if the comparison of the wild type structure to the non-trivial splice variant one would lead to observable conformational switches.
Thus, in the following section the structure of the nt-svRab1A was examined by the use of structural bioinformatics and biochemical techniques.

4.3.1 Nt-svRab1A is a folded, dimeric protein

Nt-svRab1A lacks 76 amino acids (37 %) of the sequence compared to wtRab1A. This region includes several effector and regulator binding sites (e.g. switch II, Figure 9A). According to the 3D structure of wtRab1A ((Pereira-Leal & Seabra, 2000), PDB ID: 2FOL) important internal contact sites are missing in nt-svRab1A (Figure 9B). In order to analyze whether nt-svRab1A represents a folding competent and structured protein the secondary structure was examined by Far-UV CD spectroscopy. The comparative analysis of the secondary structures by Far-UV CD spectroscopy showed that both proteins are folded (Figure 14A). Calculation of the contents of different secondary structural elements for wtRab1A are in agreement with the proposed 3D structure (PDB ID: 2FOL) and only minor differences were observed in the secondary structure of nt-svRab1A. The observed strong minimum at 205 – 208 nm is due to the peptide like, small size of nt-svRab1A and might hint to a higher flexibility of α-helical elements (Gopal et al, 2012; Kelly et al, 2005).
The overall observed decrease in the β-sheet, as well as in α-helical contents correlates well with the deleted regions of the protein. This indicates that even with 76 of 205 amino acids missing, no profound rearrangement of the secondary structure of nt-svRab1A occurred.

To better understand how, despite the drastic deletion of 76 amino acids, a stable protein structure can be formed without radical rearrangements of the protein core (residues 6 – 64 and 155 – 176) computational modeling experiments were performed in cooperation with the group of Dr. Oliver Lange (TUM). Modeling studies for nt-svRab1A were carried out with Rosetta (Kaufmann et al, 2010; Leaver-Fay et al, 2011). Starting from the crystal structure of wtRab1A (Figure 14B, modeled residues are shown in dark blue), coordinates for major parts of the protein core (residues 6 – 64 and 155 – 176) were copied and the gap of the 76 missing residues were closed in nt-svRab1A, when compared to wtRab1A, by remodeling residues 141 – 154 (Figure 14B). Therefore kinematic loop modeling protocol (Mandell et al, 2009) of Rosetta was used.

Indeed, Rosetta was able to close the 76 residue gap surprisingly well. The 5 % lowest energy loop conformations revealed two distinct clusters of loop conformations for the structure of nt-svRab1A. A representative of each of these two loop conformations were selected for further analysis (Figure 14C).

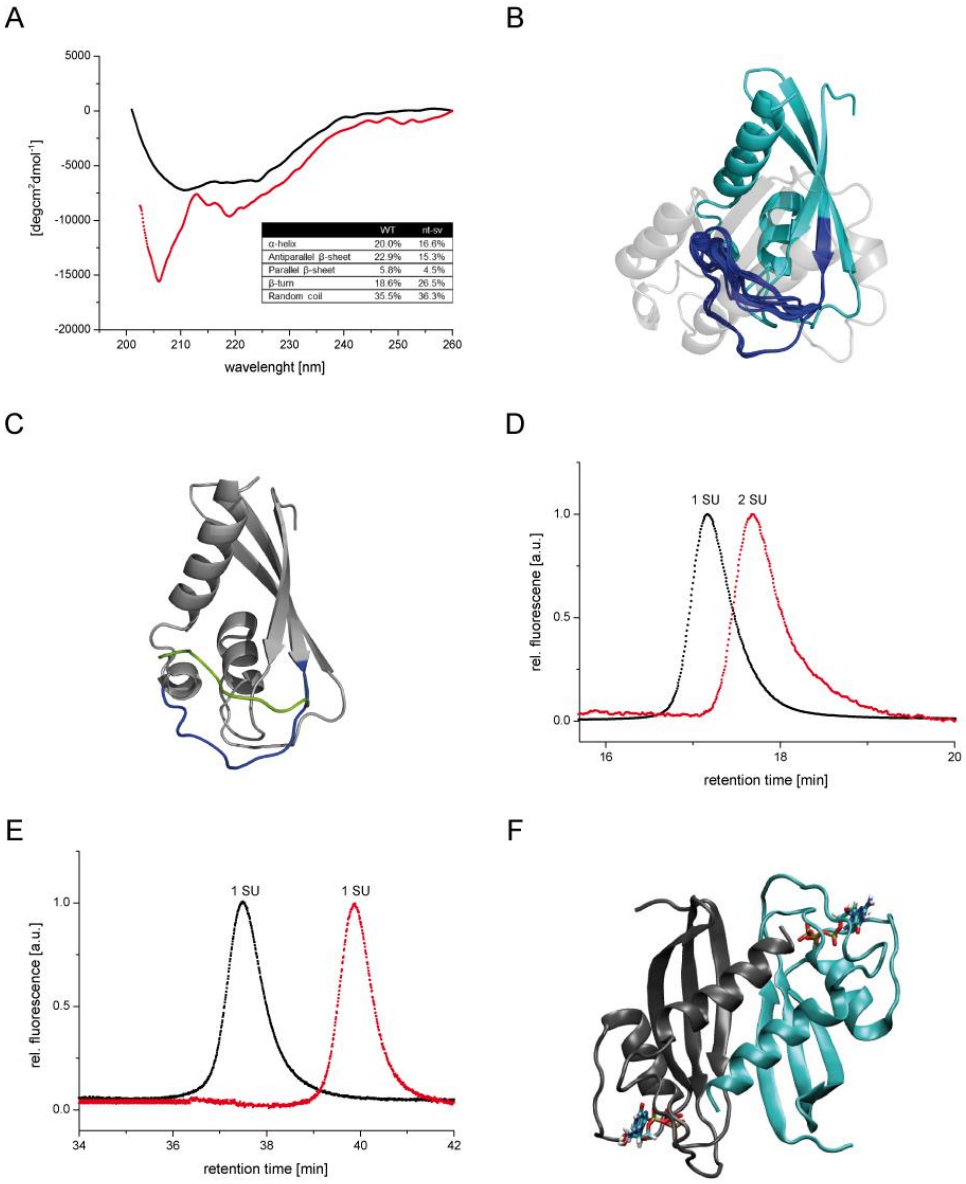

Figure 14: Nt-svRab1A is a structured dimer.

A) Secondary structure analysis: Far-UV CD spectroscopy of wtRab1A (black) and nt-svRab1A (red). 16 accumulations were recorded. *Inset*: calculation of the secondary structural contents according to CDNN (Applied Photophysics). **B)** Loop Modeling of nt-svRab1A: residues 6 – 64 and 155 – 176 were maintained according to the wtRab1A (PDB ID: 3TKL, (Cheng et al, 2012)). The identical residues of wtRab1A and nt-svRab1A are shown in cyan. The newly arranged residues of nt-svRab1A are shown in blue. The residues only present in wtRab1A are depicted in transparent grey. **C)** Two significantly different loop conformations were identified and used for further analysis: Loop Conformation 1 (green) and Loop Conformation 2 (blue). **D)** Quaternary structure analysis: SEC analysis of the nucleotide-free wtRab1A (black) and nucleotide-free nt-svRab1A (red) under native conditions using a TSKG2000SW$_{XL}$ column, operated in PBS buffer with 1 mM $MgCl_2$ at 20 °C. 2 µg of protein was applied at a constant flow rate of 0.5 mL/min. The calculated number of subunits for both Rab1A proteins is depicted. **E)** Quaternary structure analysis: SEC analysis of nucleotide-free wtRab1A (black) and nucleotide-free nt-svRab1A (red) under denaturing conditions using a TSKG2000SW$_{XL}$ column, operated in PBS buffer containing 3M guanidinium chloride and 1 mM $MgCl_2$ at 20 °C. 10 µg of protein per sample was applied at a constant flow rate of 0.2 mL/min. Prior to the measurements the samples were incubated in the 3M guanidinium chloride containing running buffer for 1.5 h at room temperature. The calculated number of subunits for both Rab1A proteins is depicted. **F)** Structural model for the dimerization of the nt-svRab1A splice variant based on the best scoring complex obtained from a systematic protein-protein docking search using the ATTRACT package (Zacharias, 2003). Each partner of the symmetric homo-dimer is indicated as cartoon (grey and cyan for the two nt-svRab1A monomers). Interaction is mediated by burying nonpolar residues at the interface and formation of intermolecular hydrogen bonds between the two beta-strands at the interface. The bound GTP molecules are depicted in atom-colored stick representation.

To assess the stability of the two different loop conformations, molecular dynamics simulations for 100 ns in explicit solvent were carried out for each of the two selected models. Both structural models remained stable throughout the simulation (Figure 15).

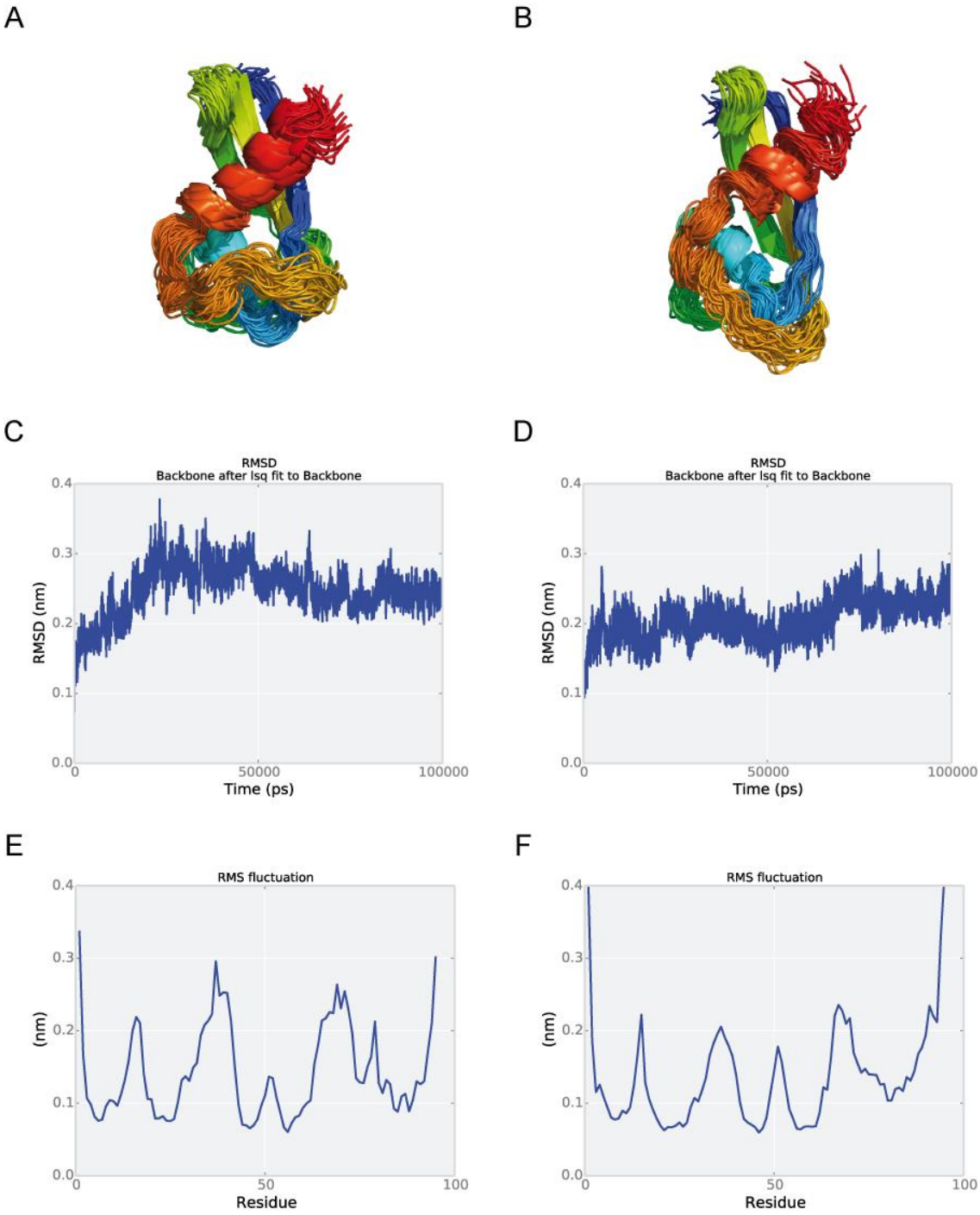

Figure 15: Molecular Dynamic simulations of the two highly different structural loop models.
A, C, E) Docking results for loop conformation 1. **B, D, F)** Docking results for loop conformation 2. **A, B)** Snapshots of the protein structure every 2000th step along the MD trajectory. **C, D)** RMSD relative to the structure in the minimized, equilibrated system along the trajectory. **E, F)** Averaged root mean square fluctuation of atomic positions for each residue in the trajectory. This figure was kindly provided by the group of Dr. O. Lange (TUM).

The levels of RMS fluctuation are slightly higher for loop conformation 1. Without any further experimental data, this structural modeling exercise can by no means provide us with confidence into exact atomic coordinates, but it does quite impressively illustrate that it is indeed possible to form a stable protein core without major structural rearrangement of the secondary structural elements remaining after deletion of the 76 residues.

Next, we analyzed the quaternary structure of both proteins. Size Exclusion Chromatography (SEC) experiments under native conditions showed single peaks for both proteins (Figure 14D). In accordance with the literature the quaternary structure of wtRab1A was determined as monomeric (Pereira-Leal et al, 2003) with an apparent molecular mass of ~27.6 kDa. Nt-svRab1A, however, showed a dimeric quaternary structure with an apparent molecular mass of ~24.0 kDa. Control experiments at denaturing conditions allowed to dissociate nt-svRab1A into a monomer with an apparent molecular weight of ~13.0 kDa (Figure 14E). This is in good correlation to the calculated theoretical mass of 13.9 kDa.

The observation of a dimer indicates that the structure of nt-svRab1A can be stabilized by the formation of an oligomeric quaternary structure under native conditions.

In correlation, the structural model of the nt-svRab1A monomer displays a large exposed hydrophobic surface area due to the lack of 76 amino acids compared to wtRab1A.

In collaboration with the theoretical biophysics group of Prof. Dr. M. Zacharias (TUM), we were able to achieve a working model for the observed dimerization of nt-svRab1A (Figure 14F). Therefore, systematic protein-protein docking searches on the entire surface of the nt-svRab1A protein were carried out, using the ATTRACT docking approach (Zacharias, 2003). With a significant scoring gap relative to alternative solutions the docking search predicted a symmetric dimeric complex structure as the best scoring solution (Figure 14F). The predicted binding geometry resulted in a well packed protein-protein interface which buries the hydrophobic surface area that is solvent exposed in the spliced variant relative to the wtRab1A protein.

To receive an impression whether the bioinformatical proposed nt-svRab1A structure of the dimer may be suitable, chemical cross-linking experiments were performed. As both proteins contain a relative high amount of lysine residues (wtRab1A: 17 (8 %), nt-svRab1A: 11 (9 %)), which are almost uniformly distributed over the whole amino acid sequence, cross-linkers which have the capability of forming a covalent bond between lysine residues were applied. In order to review the available crystal structure of wtRab1A, intra-molecular cross-link experiments were conducted.

Therefore, in a first experimental approach the bifunctional DSSG-H6/D6 linker, connecting distances of 7.7 angstrom was used (Nowak et al, 2005). To exclude side reactions of the linker itself, the linker amount was limited to a maximum of 3 times the lysine equivalents necessary without excess. After addition of the respective quantity of cross-linker to the protein sample and further incubation for 30 minutes at room temperature, the reaction was inhibited by addition of 5x Laemmli.

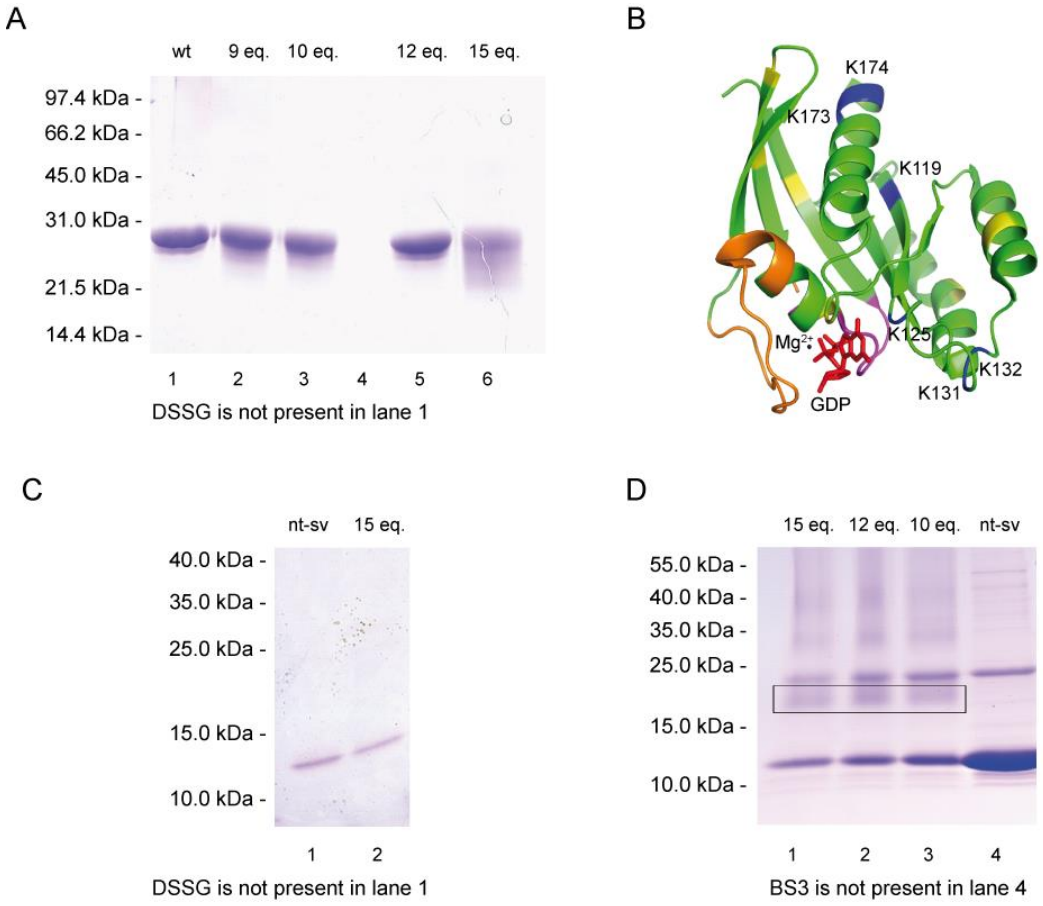

Figure 16: Protein Cross-linking experiments of Rab1A proteins.

A) Coomassie stained 12.5 % SDS-Gel of chemical cross-linking of wtRab1A in presence of DSSG-H6/D6 linker. 10 µM of protein was used in a total volume of 40 µL. The SDS-Gel lanes 2, 3, 5 and 6 display the addition of cross-linker in different equivalents (9 eq., 10 eq., 12, eq. and 15 eq.) to the wt protein. After 30 min incubation time at room temperature the reaction was inhibited by addition of 5x Laemmli. The protein bands in lane 1 and in lane 6 were further analyzed by mass spectrometry **B)** Representation of identified mass spectrometry cross-link results from experiment **(A)** are highlighted in the wtRab1A crystal structure (PDB ID: 2 FOL, P-loop: magenta, Switch I: orange). Detected cross links are shown in dark blue (positions of lysine residues are depicted). Non-cross linked lysine amino acids are shown in yellow. **C, D)** Coomassie stained 4 – 20 % SDS-Gel of chemical cross-linking of nt-svRab1A in presence of DSSG-H6/D6 linker **(C)** or BS3-H12/D12 linker **(D)**. 10 µM **(C)** or 137 µM **(D)** of protein was used in a total volume of 40 µL. The SDS-Gel lanes 2 **(C)** and 1 – 3 **(D)** show the addition of respective cross-linker in different equivalents (10 eq., 12, eq. and 15 eq.) to the nt-svRab1A protein. After 30 min incubation time at room temperature the reaction was inhibited by addition of 5x Laemmli. The desired protein samples were further analyzed by mass spectrometry. The rectangle in **(D)** shows intermolecular cross-linking of nt-svRab1A in presence of BS3-H12/D12 linker.

As one can see from Figure 16A, the wtRab1A protein was successfully intra-molecular cross-linked in presence of DSSG-H6/D6. This was indicated by the smear visible around the respective protein band in presence of cross-linker (e.g. lane 6) compared to its wtRab1A band alone (lane 1). However, no further protein bands with higher molecular weight were detected on the respective SDS-gel (Figure 16A). Thus, no formation of inter-molecular cross-links was observed for wtRab1A.

This is in good accordance to the literature, as common RabGTPases show a monomeric quaternary structure (Pereira-Leal et al, 2003).

By further analyzing the protein bands with mass spectrometry it was possible to define the accurate chemical linked intra-molecular positions and visualize them in the crystal structure of wtRab1A (Figure 16B). After the mass spectrometry measurements the results were further evaluated with the Mass Matrix program (Xu & Freitas, 2009). The proposed hits were then manually verified. The identified matches of cross-links are highlighted in dark blue (K119/K131, K125/K131, K131/K132, K132/K174, K173/K174) in the wtRab1A crystal structure. The predicted Mass Matrix hits of intra-molecular cross-links for the wtRab1A are summarized in Figure 17. The proposed cross-link identified between the lysine 125 and lysine 132 (Figure 16A) could not be verified manually. Additional, several determined interactions (K58/K187, K58/K191, K174/K187, K174/K191, K174/K198, Figure 17), occurred in the not resolved C-terminal region of wtRab1A. Thus, no further structural information could be obtained from these cross-links. Interestingly, three cross-links involved lysine residues that are located within two loop regions (K125, K131, K132, Figure 16B). Even though the theoretically calculated distances between these lysine residues (K125/K131 = 10.85 angstrom, K119/K131 = 28.04 angstrom, K132/K174 = 33.16 angstrom) would be too large for successfully connecting these amino acids with the used DSSG-H6/D6 cross-linker (distance range of 7.7 angstrom). This indicates that the cross-links are conceivably due to the highly flexible loop regions in solution. Hence, the approach of resolving the given crystal structure of wtRab1A by the use of cross-links in loop-regions is hardly possible. One reason is that these loops have a high degree of flexibility in solution, contrary to their rigidity in the mono-crystal. Thus, chemical cross-link interactions between secondary structural elements like α-helices or β-strands are promising candidates for resolving conformations.

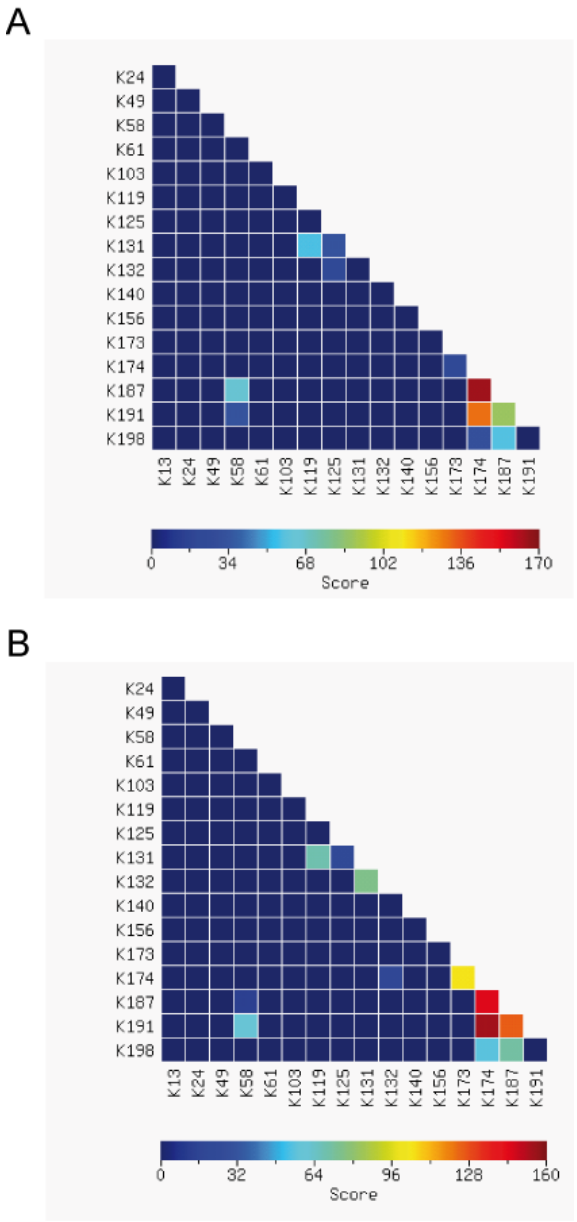

Figure 17: Overview of intra-molecular cross-links of wtRab1A identified by mass spectrometry.
A, B) Heat map of intra-molecular cross links, occurring between primary lysine groups analyzed by Mass Matrix (Xu & Freitas, 2009) for the light chain **(A)** and heavy chain **(B)** of the used DSSG-H6/D6 cross-linker. Mass spectrometry measurements and data evaluation was kindly performed by M. Daake (TUM).

As the lysine residues depicted in yellow are still not cross linked (Figure 16B), the BS3-H12/D12 cross-linker was applied for the identification of more chemically formed intra-molecular bonds. This linker connects lysine residues with a distance of up to 11.4 angstrom. By theoretical calculations 15 potential cross-link interactions were determined. In contrast to wtRab1A no intra- and inter-molecular cross-links were determined for nt-svRab1A in presence of DSSG-H6/D6 (Figure 16C). However chemical interactions occurred by addition of BS3-H12/D12 to nt-svRab1A (Figure 16D).

This is again visible by a smearing of the respective monomeric nt-svRab1A protein band in presence of cross-linker (e.g. lane 1) compared to the nt-svRab1A sample without reactant added (lane 4, Figure 16D). Additionally, protein bands appeared at higher molecular weight, indicating inter-molecular cross-linking of nt-svRab1A.
By further mass spectrometry analysis of the respective protein bands, it was possible to identify a chemically formed dimer of nt-svRab1A (marked by rectangle, Figure 16D). However, up to know the exact cross-link positions could not be assigned.
To evaluate the ability of formation of even higher oligomers, the protein bands at ~35 kDa and ~40 kDa (in presence of cross-linker) need to be analyzed in detail by further mass spectrometry experiments.
As already shown by SEC measurements nt-svRab1A forms a dimer, which was further verified by the performed cross-link experiments.
Due to the still ongoing data evaluation process it was so far not possible to assess, whether the observed structure of the chemically cross-linked dimer fits to the proposed computational model (Figure 14E).

4.3.2 Nt-svRab1A is stabilized in presence of GXP nucleotide

Belonging to the Ras superfamily the activity of Rab1A is mainly regulated by the nucleotide bound. The G protein is inactive when GDP is present and active in its GTP bound form (Dong et al, 2012; Gavriljuk et al, 2013; Haas et al, 2007). Therefore, as starting point computational analysis should indicate whether, one of the major properties of a small GTPase is affected in nt-svRab1A, due to alternative splicing. The docking results suggested that binding of GTP seems to be possible in a manner comparable to wtRab1A for loop conformation 1 (Schöppner et al). In addition, the analysis of the postulated dimer structure tolerates binding of GXP nucleotides (Schöppner et al). Hence, according to the proposed dimeric structure, no interference of dimerization with nucleotide binding appears.
To investigate nucleotide binding experimentally, thermal shift assays (TSA) of both nt-svRab1A and wtRab1A were performed in the absence or presence of GDP and GTP. For these measurements the nucleotide-free variants of both proteins were used. Besides the analysis of nucleotide binding, TSA is a common method to compare the stability of proteins. During the thermal unfolding process of the wtRab1A and nt-svRab1A proteins the change in the fluorescence of the dye Sypro-Orange was monitored.

The calculated midpoints of the thermal transition (melting point) are 35.5 °C for nucleotide-free nt-svRab1A and 43.8 °C for nucleotide-free wtRab1A (Table 4, Figure 18). This difference is in good accordance with the absence of contacts formed by nearly 50 % of α-helices and β-sheets. Furthermore, different shapes of melting curves of both proteins are visible (Figure 18B, D). This suggests that the unfolding processes of nt-svRab1A is less cooperative (Tsao & Dokholyan, 2010).

As expected, wtRab1A is efficiently stabilized in the presence of both nucleotides, indicated by a strong shift of the thermal melting curves to higher temperatures (Figure 18A, C). In comparison to the nucleotide free form of wtRab1A a 13.5 °C higher apparent thermal stability was observable in presence of GDP and a 22.3 °C higher stability was determined when GTP was present (Table 4).

In general the stabilization of nt-svRab1A by nucleotides is less pronounced.

In presence of GDP an increase of 7.5 °C and in presence of GTP of 3.5 °C was calculated (Figure 18B, D). Of note, in contrast to wtRab1A, nt-svRab1A was more efficiently stabilized by GDP.

Table 4: Comparison of the calculated T_m values of wtRab1A and nt-svRab1A in absence and presence of GDP and GTP.

[µM]	T_m [°C]	Δ T_m [°C]	T_m [°C]	Δ T_m [°C]
0	43.5 ± 0.08		35.5 ± 0.12	
GDP 0.5	47.8 ± 0.24	4.00	n.d.	n.d.
GDP 1.0	49.8 ± 0.21	6.00	n.d.	n.d.
GDP 10	51.1 ± 0.17	7.30	36.0 ± 0.08	0.50
GDP 25	51.4 ± 0.09	7.60	40.0 ± 0.21	4.50
GDP 50	57.0 ± 0.17	13.2	43.0 ± 0.12	7.50
GTP 10	63.3 ± 0.16	19.5	38.0 ± 0.17	2.50
GTP 25	65.2 ± 0.09	21.4	39.0 ± 0.19	3.50
GTP 50	66.1 ± 0.17	22.3	39.0 ± 0.09	3.50

Additional SEC measurements of both proteins in presence and absence of GDP were performed. For both Rab1A isoforms a shift to lower retention times was visible after the addition of GDP, equivalent to a slight increase of their apparent molecular masses (Figure 18E). To rule out that the column characteristics are affected by GDP and $MgCl_2$, SEC analysis of carboanhydrase was performed as a control. Here, no peak shifts was observed (Figure 18F).

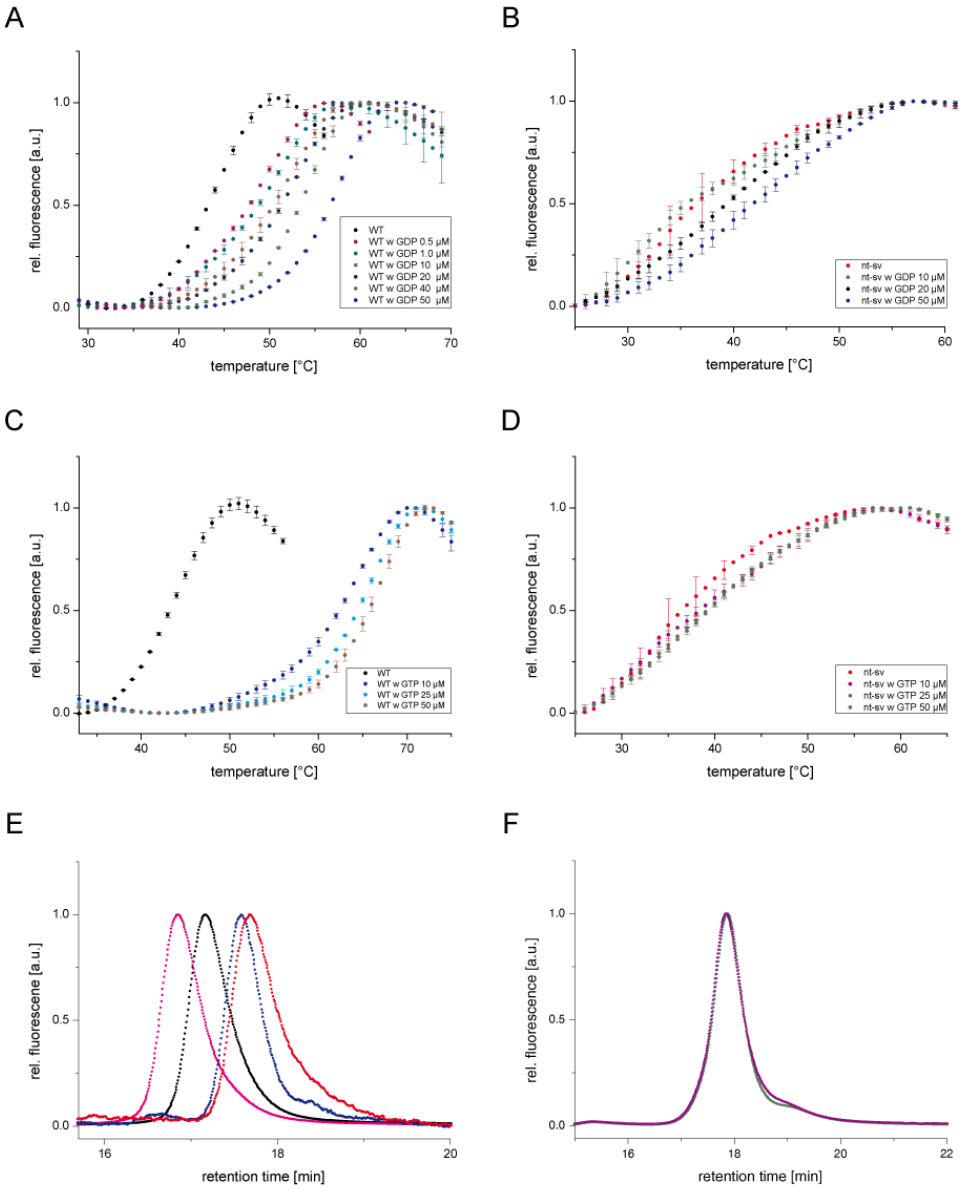

Figure 18: Thermal stability analysis of nt-svRab1A in absence and presence of GXPs.
TSA measurements comparing the GDP **(A, B)** and GTP **(C, D)** binding abilities ofwtRab1A **(A, C)** and nt-svRab1A **(B, D)**. Nucleotide-free wtRab1A and nt-svRab1A was used. In total 5 µg of protein was utilized. The measurements were conducted in PBS buffer (pH 8.0) with 1 mM $MgCl_2$ added. All calculated T_m values are means of at least three samples and the corresponding standard deviations are indicated. The T_m values are summarized in Table 4. **E)** Nucleotide binding studies: SEC analysis of the Rab1A proteins in absence (wtRab1A: black; nt-svRab1A: red) and presence of 10 µM GDP (wtRab1A: magenta; nt-svRab1A: dark blue) using a TSKG2000SW_{XL} column at 20 °C. 2 µg of each protein was employed. PBS buffer (pH 8.0) containing 1 mM of $MgCl_2$ was utilized. Measurements were performed at a constant flow rate of 0.5 mL/min. **F)** Control SEC measurements were performed with Carboanhydrase in absence (green) and presence (purple) of 10 µM GDP using a TSKG2000SW_{XL} column at 20 °C. 2 µg of protein was applied. Measurements were executed at a constant flow rate of 0.5 mL/min in PBS buffer (pH 8.0) equipped with 1 mM of $MgCl_2$.

Thus, the SEC analysis further indicates that the binding of GDP to nt-svRab1A is still possible and results in conformational changes similar to wtRab1A.

Additionally, the SEC analysis demonstrates that nucleotide binding has no influence on the quaternary structure of nt-svRab1A which apparently elutes as dimer also in presence of nucleotide. For further details on nucleotide binding see section 4.4.1.

4.4 Functional characterization of nt-svRab1A

With regard to potentially associated functional consequences resulting from non-trivial splicing, we were interested in comparing the functional characteristics of the nt-svRab1A protein to its wild-type form. One principal point addressed was the analysis whether the non-trivial splice isoform shows impaired functional properties compared to wtRab1A. Besides *in vitro* experiments also *in vivo* studies were performed. In consideration of the *in vivo* results this could imply how identified functional changes influence the regulation of protein networks in the cell.

Basically each small G protein functions as a precisely engineered molecular switch existing in two interconvertible conformational states (Hall, 1990). Consequently the RabGTPase cycles between membranes and cytosol, depending on the nucleotide-bound state (Gavriljuk et al, 2013) and thereby controls diverse cellular processes. Thus, possible changes in the common RabGTPase cycle (see 1.4.1) should be highlighted. This would lead to tremendous consequences for nt-svRab1A itself, showing alterations in the major regulatory tool of small G proteins.

4.4.1 Nt-svRab1A losses its specificity for GXPs

Already the previously performed thermal stability studies showed that in presence of GXP nucleotides nt-svRab1A can be stabilized. Therefore, the nucleotide binding efficiency of nt-svRab1A was investigated in more detail by fluorescence spectroscopy measurements. In all measurements fluorescent –labeled analogs of GXP and AXP, containing a methylanthraniloyl (MANT) group attached to the ribose moiety (Göttle et al, 2007; Pisareva et al, 2007; Pisareva et al, 2006) were used. As illustrated in Figure 19A and B, the addition of MANT-nucleotides (GXP's) to wtRab1A causes significant changes in the emission spectra of the MANT-fluorophore (Murthy & Lorand, 2000). By direct excitation of the MANT-fluorophore, the respective emission maximum at 444 nm increases upon the addition of the nucleotide-free wtRab1A (ratio protein/MANT-GXP = 1 µM/0.5µM). Comparing the relative fluorescence intensity (RFI) of the MANT-GDP value alone (normalized to Δ_{RFI} MANT-GDP = 1) with the RFI values in presence of the Rab1A isoforms, showed that upon binding of MANT-GDP to nt-svRab1A or wtRab1A the RFI value doubles (Δ_{RFI} wt: 2.2, Δ_{RFI} nt-sv: 1.9; Figure 19A,B). Similar effects were observed for the fluorescence measurements in presence of MANT-GTP (Δ_{RFI} wt: 1.9, Δ_{RFI} nt-sv: 1.8; Figure 19B).

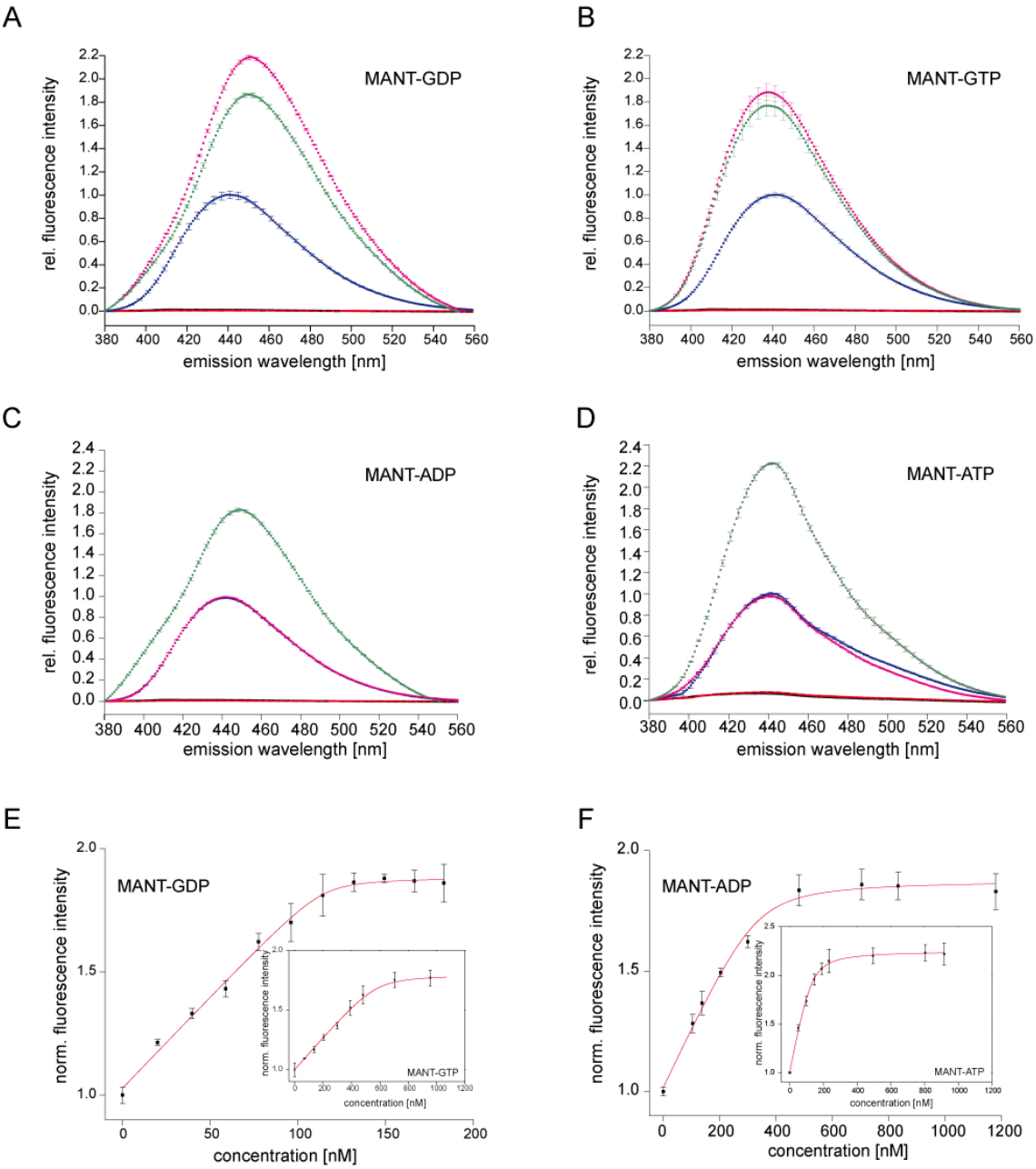

Figure 19: Nt-svRab1A binds nucleotides.

A, B) Binding of MANT-GDP **(A)** and MANT-GTP **(B)** by Rab1A proteins (nucleotide-free): Fluorescence emission spectra (λ_{exc} = 360 nm) for wtRab1A (black), nt-svRab1A (red),MANT-GXP alone (blue, X = GDP or GTP) and a combination of both (wtRab1A w MANT-GXP: magenta, nt-svRab1A w MANT-GXP: green) were determined (Murthy & Lorand, 2000). The spectra are mean values of four independent measurements and the corresponding standard deviations are indicated. **C, D)** Binding of MANT-ADP **(C)** and MANT-ATP **(D)** by Rab1A proteins (nucleotide-free): Fluorescence emission spectra (λ_{exc} = 360 nm) for wtRab1A (black), nt-svRab1A (red), MANT-AXP alone (blue, X = ADP or ATP) and a combination of both (wtRab1A w MANT-AXP: magenta, nt-svRab1A w MANT-AXP: green) were determined (Murthy & Lorand, 2000). Shown are the mean values of the respective measurements and the corresponding standard deviations are indicated. **E, F)** Fluorescence titration measurements comparing the binding ability of nt-svRab1A for MANT-GDP **(E)** and MANT-GTP **(Inset, E)** and for MANT-ADP **(F)** and MANT-ATP **(Inset, F)** examined by changes in fluorescence intensity at 444 nm (λ_{exc} = 360 nm). Measurements were operated in a MANT-GXP/Mg^{2+} or MANT-AXP/Mg^{2+} (0.5 µM) starting solution in 150 µL PBS buffer at 20°C. The concentration of the respective protein was increased stepwise until saturation was achieved. Shown are normalized fluorescent intensity mean values of triplictes and the corresponding standard deviation. For the determination of the apparent K_D's a quadratic fit equation was used.

In nt-svRab1A the guanine base binding region (NKXD, G4; Figure 9B) is missing. From the literature it is known that the G4 and G5 (TSA, Figure 9) regions are responsible for the discrimination against other nucleotides (Itzen & Goody, 2011). Therefore, additional fluorescence emission spectra were recorded in presence of MANT-ADP and MANT-ATP. Contrary to the wt-Rab1A protein, an increase of the delta RFI value in presence of nt-svRab1A was monitored for MANT-ADP (Δ_{RFI} MANT-ADP alone: 1, Δ_{RFI} wt: 1, Δ_{RFI} nt-sv: 1.8; Figure 19C). The MANT-ATP measurements showed similar characteristics, leading to an increase in the delta RFI value only in presence of nt-svRab1A (Δ_{RFI} MANT-ATP alone: 1, Δ_{RFI} wt: 1, Δ_{RFI} nt-sv: 2.2; Figure 19D).

Hence, the non-trivial splicing event leads to an altered nucleotide specificity of nt-svRab1A, as binding of ADP and ATP contrary to the wtRab1A protein is possible as well.

In a next set of fluorescent spectroscopy experiments the apparent K_D values for GXP and AXP nucleotides binding to nt-svRab1A were determined. All titration measurements showed a characteristic binding curve shape upon increasing the concentration of nt-svRab1A (Figure 19E, F). Thus, binding of GDP, GTP, ADP and ATP to the splice isoform is possible. Apparent K_D's of ~0.1 µM for binding of MANT-GDP, ~0.3 µM for binding of MANT-GTP, ~0.2 µM for binding of MANT-ADP and ~0.1 µM for MANT-ATP were determined. The observation of an approximately 3 fold higher binding affinity for MANT-GDP compared to MANT-GTP is in good accordance to our TSA data (Figure 18). These indicated a more effective stabilization of nt-svRab1A in presence of GDP. Nevertheless, in comparison to nucleotide binding affinities of other RabGTPases the resulting apparent K_D's are much lower.

Compared to wild type RabGTPases (K_D values usually in the low nanomolar range) the affinity of nt-svRab1A for nucleotides is ~1000-fold lower (Simon et al, 1996). Besides fluorescent spectroscopy measurements, fluorescent anisotropy measurements resulted in the identification of K_D values in the same range (data not included).

Collectively, these findings display that binding of GDP or GTP, as well as ADP or ATP to the nucleotide-free nt-svRab1A is still possible.

4.4.2 Nt-svRab1A interacts no longer with Rab1 specific DrrA GEF

RabGTPases can fulfill their function only by transitioning between the GDP and GTP bound states. By itself this is a slow process, which in the cell is enhanced and regulated by GAPs and GEFs (Renault et al, 2001; Suh et al, 2009; Vetter & Wittinghofer, 2001).

Several studies identified the *Legionella pneumophila* protein DrrA (defect in Rab1 recruitment A) as a specific GEF of Rab1 (Ingmundson et al, 2007; Machner & Isberg, 2007; Schoebel et al, 2009). DrrA interaction with other Rab1 proteins involves the P-Loop, switch I and switch II (Schoebel et al, 2009). As the switch II region is completely missing in nt-svRab1A, the capability of $DrrA_{(340-533)}$ to interact with nt-svRab1A was examined in the next set of experiments. The respective Co-Immunoprecipitation (Co-IP) results are depicted in Figure 20.

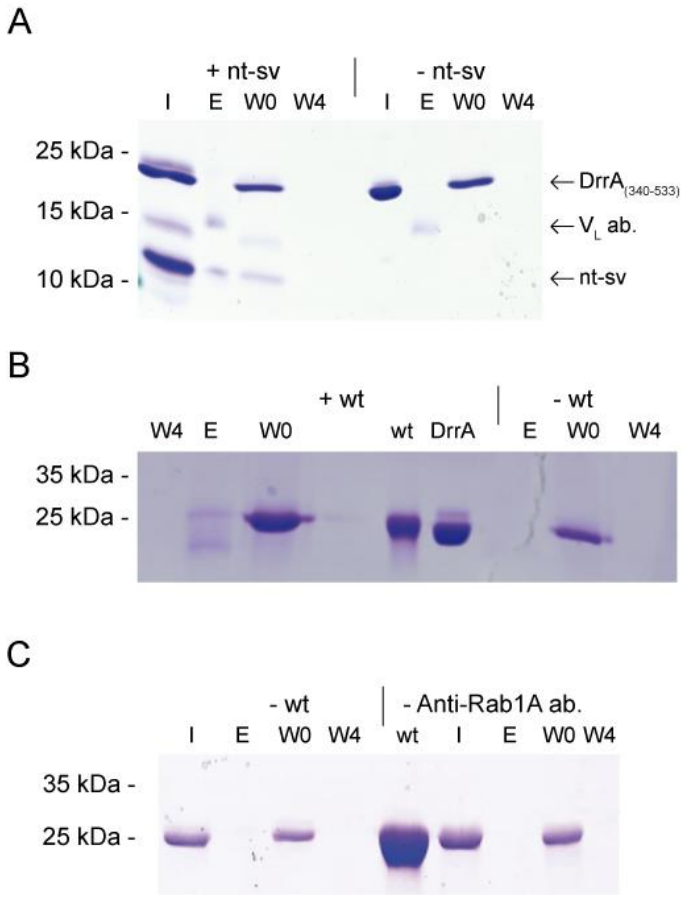

Figure 20: Nt-svRab1A does not interact with $DrrA_{(340-533)}$ GEF.
A, B, C) GEF interaction studies: Coomassie stained SDS-Gel (4 – 20 % nt-svRab1A, 12.5 % wtRab1A) of Co-IP studies of nt-svRab1A **(A)** or wtRab1A **(B)** with $DrrA_{(340-533)}$ GEF. I= Input, E= Elution, W0= Wash 0, W4= Wash 4. 10 µg of each protein was used. C) 12.5 % Control SDS-gel of Co-IP studies with $DrrA_{(340-533)}$ GEF. I= Input, E= Elution, W0= Wash 0, W4= Wash 4.

Co-IP was performed mixing nt-svRab1A/ or wtRab1A and $DrrA_{(340-533)}$ in equal amounts in presence of GDP before incubation with an antibody directed against Rab1A. To exclude unspecific interaction of the GEF with the Rab1A specific antibody or interplay of the used proteins with the protein G sepharose beads, control Co-IPs were conducted (Figure 20C). Therefore Co-IPs without wtRab1A protein or addition of antibody were carried out. In both elution lanes no detectable bands were visible, accordingly unspecific interactions can be excluded (Figure 20C). As expected the Co-IP results showed that in contrast to wtRab1A (Figure 20B), no interaction of nt-svRab1A with $DrrA_{(340-533)}$ was observed (Figure 20A).
Thus, an important level of control is missing in nt-svRab1A, considerable altering the activation process of the splice isoform.

4.4.3 Nt-svRab1A still shows GTP hydrolysis activity but lacks inactivation control by TBC GAP

Rab proteins are switched off by GAPs that stimulate the intrinsic GTP hydrolysis activity (Mihai Gazdag et al, 2013). Most Rab-GAPs accelerate the intrinsic GTP hydrolysis rate up to 10^5-fold (Gavriljuk et al, 2012). Due to the determined structural alterations of the nt-svRab1A the intrinsic GTP hydrolysis activity was evaluated in the following. It was also addressed whether the intrinsic GTP hydrolysis activity can be stimulated in presence of the Rab1 specific GAP TBC1D20 (Gavriljuk et al, 2012; Haas et al, 2007). The GTP hydrolysis rates of wtRab1A and nt-svRab1A with and without GAP (ratio 1/100 protein/GAP) were assayed by reversed phase chromatography (Simon et al, 1996).
Figure 21A and 21B depict that both proteins are capable of hydrolyzing GTP. For wtRab1A a rate constant of $2.0 \times 10^{-5}\ s^{-1}$ was calculated, which is in good accordance to the Rab1B GTP hydrolysis rate ($1.5 \times 10^{-5}\ s^{-1}$) (Gavriljuk et al, 2012) and other Ras proteins (Wittinghofer & Vetter, 2011). The intrinsic GTP hydrolysis rate for nt-svRab1A was determined as 8.0×10^{-5} s-1. Interestingly, compared to the wt protein, nt-svRab1A shows a 4 fold higher intrinsic GTP hydrolysis rate.

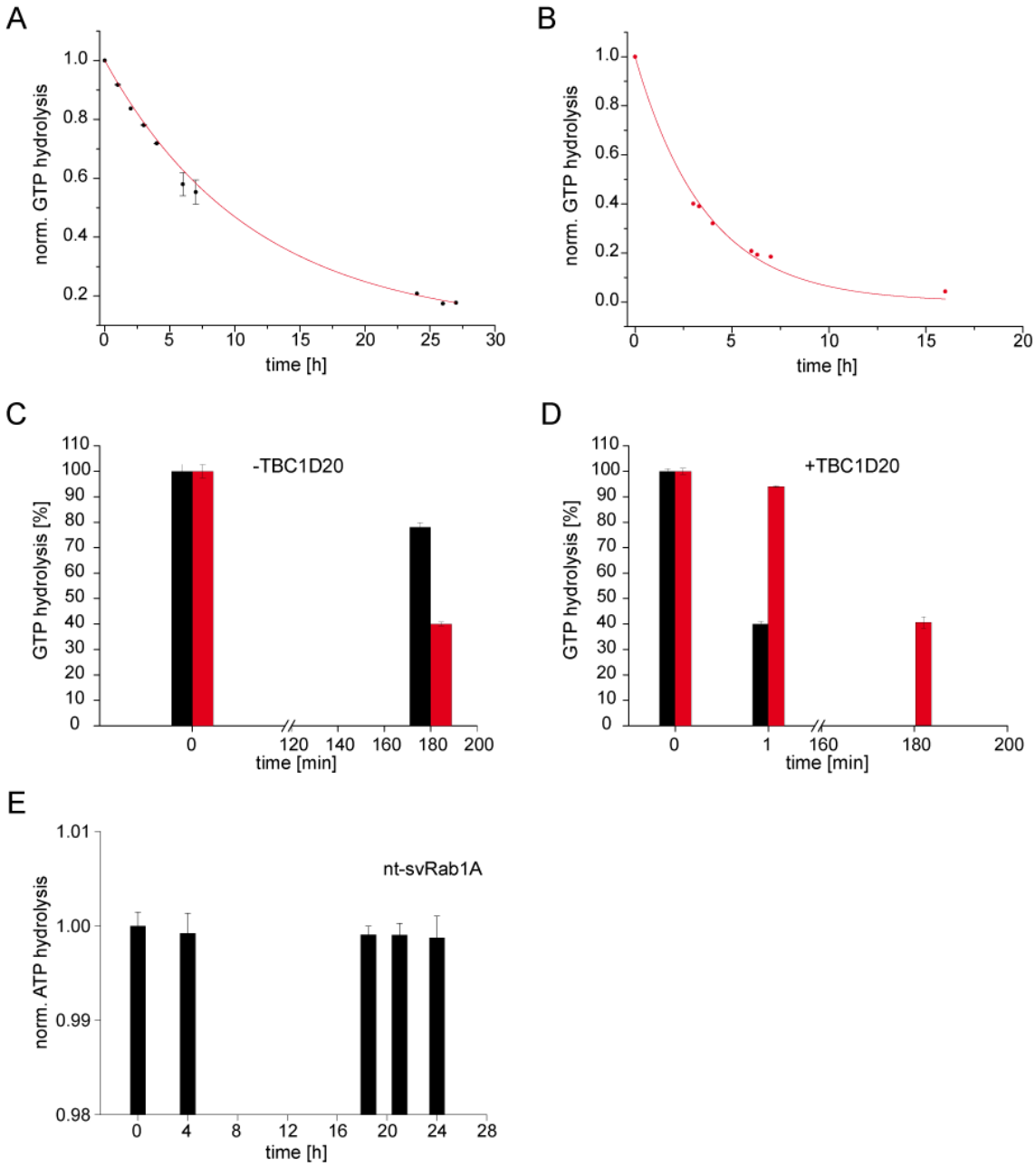

Figure 21: Nt-svRab1A shows intrinsic GTP hydrolysis activity.
A, B) Analysis of the intrinsic GTP hydrolysis of wtRab1A **(A)** and nt-svRab1A **(B)** as a function of time by reversed phase HPLC, using a C_{18} ProtoSIL reversed phase column. The hydrolysis reaction was started by addition of $MgCl_2$ (c_{final} = 1 mM) to the sample. Measurements were performed at a constant flow rate of 1.0 mL/min for 20 min at room temperature. The normalized GTP values were plotted against the different time points. To determine the intrinsic GTP hydrolysis rates of both proteins a first order exponential decay fit equation was used. **(C, D)** The GTP hydrolysis rates of wtRab1A (black) and nt-svRab1A (red), in absence **(C)** and presence **(D)** of the GAP, was assayed as a function of time by HPLC. A C_{18} ProtoSIL reversed phase column was used for the experiments. Measurements were performed at a constant flow rate of 1.0 mL/min for 20 min at room temperature. The hydrolysis reaction in presence of the GAP was started by the addition of $MgCl_2$ (c_{final} = 1 mM) and $TBC1D20_{(1\text{-}362)}$ (ratio protein/GAP = 1/100) to the sample. The normalized GTP values were plotted against the different time points. **E)** Analysis of the intrinsic ATP hydrolysis of nt-svRab1A was monitored as a function of time by reversed phase HPLC, using a C_{18} ProtoSIL reversed phase column. The hydrolysis reaction was started by the addition of $MgCl_2$ (c_{final} = 1 mM) to the sample. Measurements were performed at a constant flow rate of 1.0 mL/min for 15 min at room temperature. The normalized ATP values were plotted against the different time points.

As expected for wtRab1A, the presence of the GAP protein catalyzed GTP hydrolysis (Figure 21D) (Gavriljuk et al, 2012). However, the presence of TBC1D20 did not increase GTP hydrolysis of nt-svRab1A (Figure 21). During the TBC GAP catalyzed mechanism, the conserved glutamine in the DX_2GQ (G3, switch II, *cis*-glutamine) of the Rab protein directly interacts with the backbone atoms of the YXQ GAP motif (Haas et al, 2007; Langemeyer et al, 2014). In addition, the glycine of the DX_2GQ forms a hydrogen bond with the γ-phosphate of GTP (Bourne et al, 1991)

Given that the switch II region is completely absent in nt-svRab1A, this might explain the lacking stimulation of the GTP hydrolysis rate by the GAP protein.

Due to the loss in specificity for guanine nucleotides (4.4.1), additional investigations analyzing the intrinsic ATP hydrolysis ability, were performed. However, even though binding of ATP to nt-svRab1A is still possible (Figure 19D, F), an intrinsic ATP hydrolysis activity was not detected (Figure 21E).

In summary the results on Rab activation (4.4.2) and inactivation further signify that nt-svRab1A seems to be not regulated by GEFs and GAPs.

4.4.4 Nt-svRab1A is no longer regulated by GEFs and GAPs *in vivo*

Rab1A belongs to the family of membrane-associated GTPases which are predominantly activated by membrane-localized GEFs (Sprang & Coleman, 1998). However, previous GEF interaction studies (4.4.2) were executed under *in vitro* conditions, lacking membrane compartments and membrane-related components. Thus, additional Co-IP experiments were performed *in vivo,* elucidating whether membrane-attached GEFs and further known Rab-interacting proteins are now able to bind to nt-svRab1A. *In vivo* conditions were mimicked by the use of HeLa lysate. Co-IPs were carried out in presence of GDP. After precipitation with an antibody directed against Rab1A, the potential interaction partners of nt-svRab1A (Figure 22A) and wtRab1A (Figure 22B) were identified using mass spectrometry.

To exclude false positive hits, the identified interactors were compared with the corresponding results of control Co-IPs performed in the absence of Rab1A antibody (Figure 22). The mass spectrometry results for both proteins are summarized in Appendix 1. The comparison of the interaction partners, determined by Co-IP and MS, of wtRab1A and nt-svRab1A showed that overall a lower number of proteins interact with nt-svRab1A. In total 81 interactors were identified for wtRab1A, while only 12 interactors were identified for nt-svRab1A. 17 proteins interacted with both Rab1A isoforms.

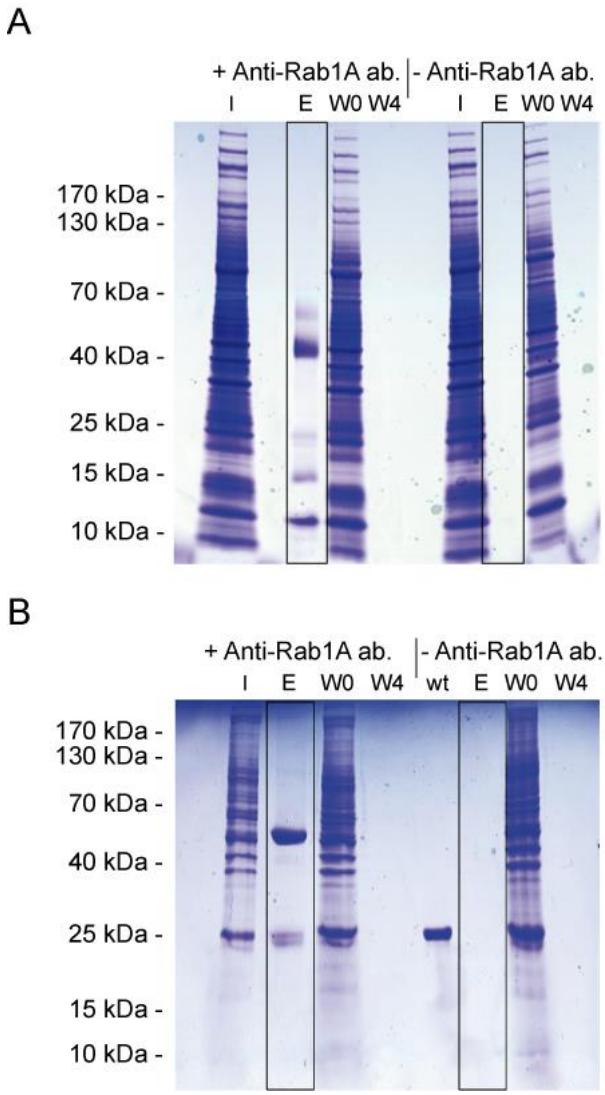

Figure 22: Nt-svRab1A is no longer regulated by a GEF and GAP.
Interaction studies of nt-svRab1A **(A)** and wtRab1A **(B)** using HeLa lysates: Coomassie stained SDS-Gel (nt-svRab1A: 4 – 20 %, wtRab1A: 12.5 %) of Co-IP. 110 µg of HeLa lysate spiked with 30 µg of respective Rab1A protein was used. I= Input, E= Elution, W0= Wash 0, W4= Wash 4. Elution lanes in presence of antibody and control lanes were further analyzed by mass spectrometry (highlighted by rectangles).

These mainly included cytoskeleton components and elongation factor 1-alpha 1, also belonging to the class of G proteins.

Interestingly, 12 proteins were identified which interacted solely with nt-svRab1A. These include Rab1B and isoform 2 of Rab35 (non-trivial spliced form of full-length Rab35), several cytoskeleton components and the transitional endoplasmic reticulum ATPase involved in ER to Golgi transport as well as sequestosome-1, which is involved in the endosomal transport, were identified as interactors of nt-svRab1A.

Additionally, a variety of proteins involved in mRNA splicing (e.g. serine-threonine kinase receptor-associated protein, isoform 2 of polyadenylate-binding protein 1, nuclease-sensitive element-binding protein 1, heterogenous nuclear ribonucleoprotein K) were detected.

However, in agreement with the results described above (4.4.2 and 4.4.3), no GEF or other Rab1A-activating proteins, as well as no other GTPase activating proteins were identified. In summary the results show, that nt-svRab1A lacks controlled activation and inactivation. Thus, due to alternative splicing, one major regulatory tool of the RabGTPases itself is affected in nt-svRab1A. Consequently this leads to a no longer temporally controlled involvement in cellular processes.

4.4.5 Nt-svRab1A interacts with wtRab1A protein and its close homologue Rab1B

With the studies described above it was possible to identify that the quaternary structure of nt-svRab1A is a dimer (4.3.1). Because of this finding, additional experiments should elucidate whether nt-svRab1A might also be able to form dimers or higher oligomers with wtRab1A and other Rab proteins (Romero et al, 2013). SEC measurements of both isoforms mixed in 1:1 ratio were performed. The SEC chromatogram of the mixture of both Rab1A isoforms showed one major peak, appearing at a retention time corresponding to an apparent molecular mass of ~30 kDa (Figure 23A), indicating the formation of hetero-dimers. The visible tailing and the shoulder of the peak suggests minor rests of not in the hetero-dimer incorporated portions of the two parent proteins.

By additional Co-IP experiments, performed with mixtures of both isoforms, this result was further verified. Interestingly, the interaction of nt-svRab1A with wtRab1A was also independent of the presence of GDP (Figure 23B) or GTP (Figure 23C). Thus, nt-svRab1A forms hetero-dimers with wtRab1A.

In chapter 4.4.4 it was possible to identify nt-svRab1A specific interactors from Co-IPs conducted with HeLa lysate samples and analyzed further by mass spectrometry.

The most surprising hit from these experiments was Rab1B, a close homologue of Rab1A. Rab1B is supposed to regulate membrane trafficking and signal transduction systems thereby controlling diverse cellular activities, including gene expression (Romero et al, 2013). However, Rab proteins are supposed to act as monomers and no interactions between different Rab proteins were described so far (Pereira-Leal & Seabra, 2000; Pereira-Leal et al, 2003).

To confirm the interaction between nt-svRab1A and Rab1B, Co-IP experiments using the purified Rab1A isoforms and a C-terminal truncated variant of the Rab1B protein ($Rab1B_{(3\text{-}174)}$) were performed.

Rab1A (wt or nt-sv) and Rab1B$_{(3-174)}$ were mixed in equal amounts in the presence of GDP. After incubation an antibody directed against Rab1A was added. Again, nt-svRab1A interacted with Rab1B$_{(3-174)}$ independently from GDP (Figure 23D). In contrast no interaction of wtRab1A and Rab1B$_{(3-174)}$ was observed (Figure 23E).

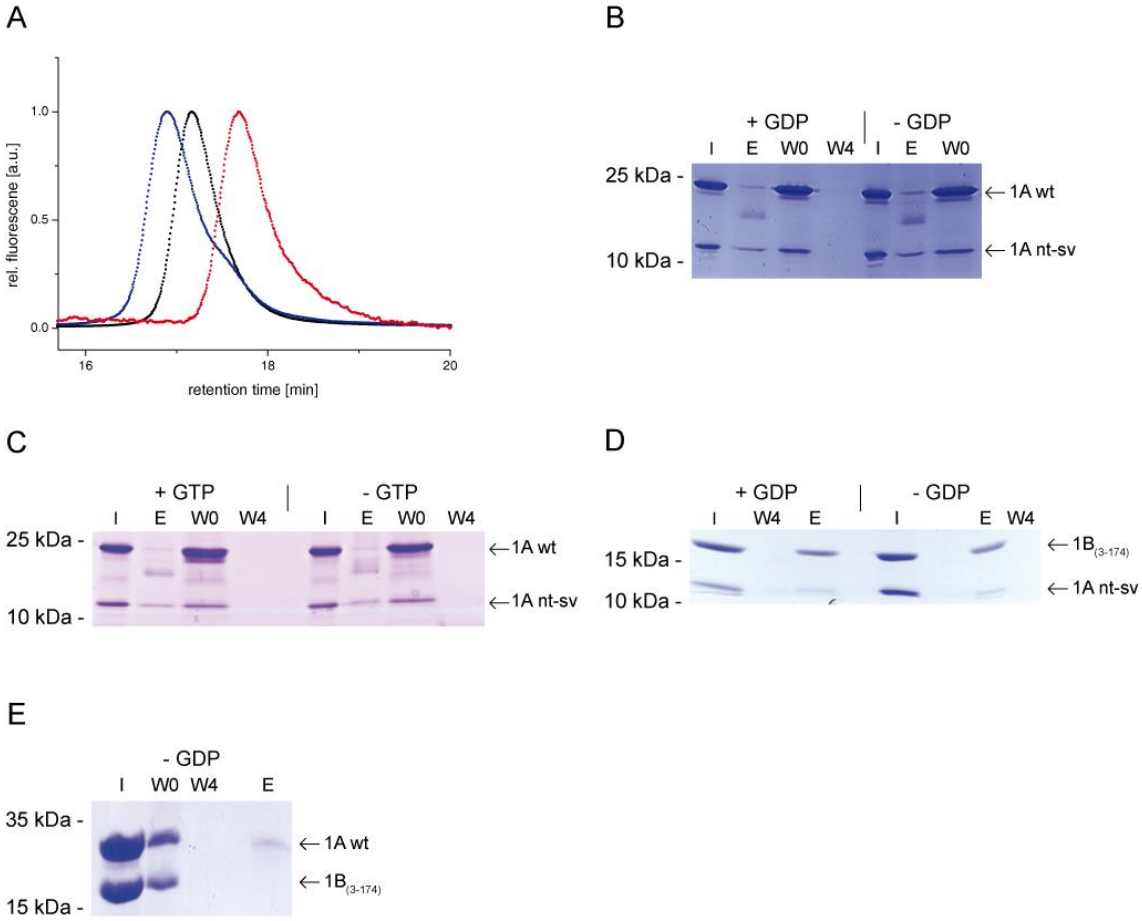

Figure 23: Nt-svRab1A interacts with other RabGTPases.
A) SEC analysis of Rab1A proteins alone (wtRab1A: black, nt-svRab1A: red) and a combination of both (blue, ratio 1/1) using a TSKG2000SW$_{XL}$ column. 2 µg of the respective protein was used. The measurements were performed at room temperature with a constant flow rate of 0.5 mL/min in PBS buffer (pH = 8.0) containing 1 mM $MgCl_2$. **B, C)** Coomassie stained 4 – 20 % SDS-gels of Co-IP studies of nt-svRab1A with its wtRab1A protein in presence and absence of GDP **(B)** or GTP **(C)**. I= Input, E= Elution, W0= Wash 0, W4= Wash 4. 20 µg of each protein was used. **D, E)** Coomassie stained 4 – 20 % SDS-gels of Co-IP studies of nt-svRab1A **(D)** or wtRab1A **(E)** with Rab1B$_{(3-174)}$. I= Input, E= Elution, W0= Wash 0, W4= Wash 4. 20 µg of each protein was utilized.

Indeed, nt-svRab1A seems to stabilize its structure by formation of hetero-oligomers with wtRab1A and other RabGTPases like Rab1B *in vivo*. As it is known that the Rab1B protein is involved in ER-Golgi trafficking (Sandoval & Simmen, 2012), this interaction hints to a general influence of nt-svRab1A on vesicular secretion.

4.5 *In vivo* function of nt-svRab1A

The characterization of nt-svRab1A *in vitro* clearly revealed that structural and functional properties of the splice isoform are impaired compared to its wild-type form. Thus, in the following the influence of these changes should be explored *in vivo*. To address the biological function of nt-svRab1A, the splice variant and wtRab1A were overexpressed in human embryonic kidney 293 cells (*HEK 293*). The cellular localization of both isoforms was investigated on one hand by creation of C-terminal fusions of GFP to the respective protein and on the other hand by western blotting. In the latter case Rab1A constructs lacking the GFP fusion were generated. In addition, experiments without transfection of the Rab1A proteins into the cells were performed under stress conditions.

4.5.1 Structural alterations do not affect membrane attachment of nt-svRab1A

In a first set of experiments the cellular behavior of the Rab1A proteins was compared byoverexpressing both isoforms as GFP fusion constructs in *HEK293* cells. Thereby the transient transfection of the cells showed cytosolic and membrane location of wtRab1A (Figure 24A). In comparison, nt-svRab1A overexpressing cells showed besides cytosolic and membrane-bound localization, additionally foci indicative for protein aggregates with incorporated nt-svRab1A (Figure 24B).

Thus, the solubility of nt-svRab1A seems to be impaired *in vivo* leading to partial aggregation of the protein.

As already mentioned above, RabGTPases share a common prenylation motif in the C-terminal region of the proteins (Pereira-Leal & Seabra, 2000; Shen & Seabra, 1996). Given that the respective sequence motif is still present in nt-svRab1A (Figure 9B) and the fluorescent microscopy images indicated potential membrane binding, western blotting was used to further study the attachment to membranes (Figure 25A, B). To do so, transiently transfected *HEK293* cells using Rab1A constructs without fusion of fluorescence marker proteins were used. The pAcGFP1N1 empty vector was utilized as a control. In the control lanes of Figure 25A no bands were detected. Consequently, the level of endogenously expressed Rab1A in *HEK293* is below the western blot detection limit. This is in good accordance to the studies of Wilhelm *et al.*, showing that the expression level of human Rab1A in *HEK293* cells is very low (Wilhelm et al, 2014).

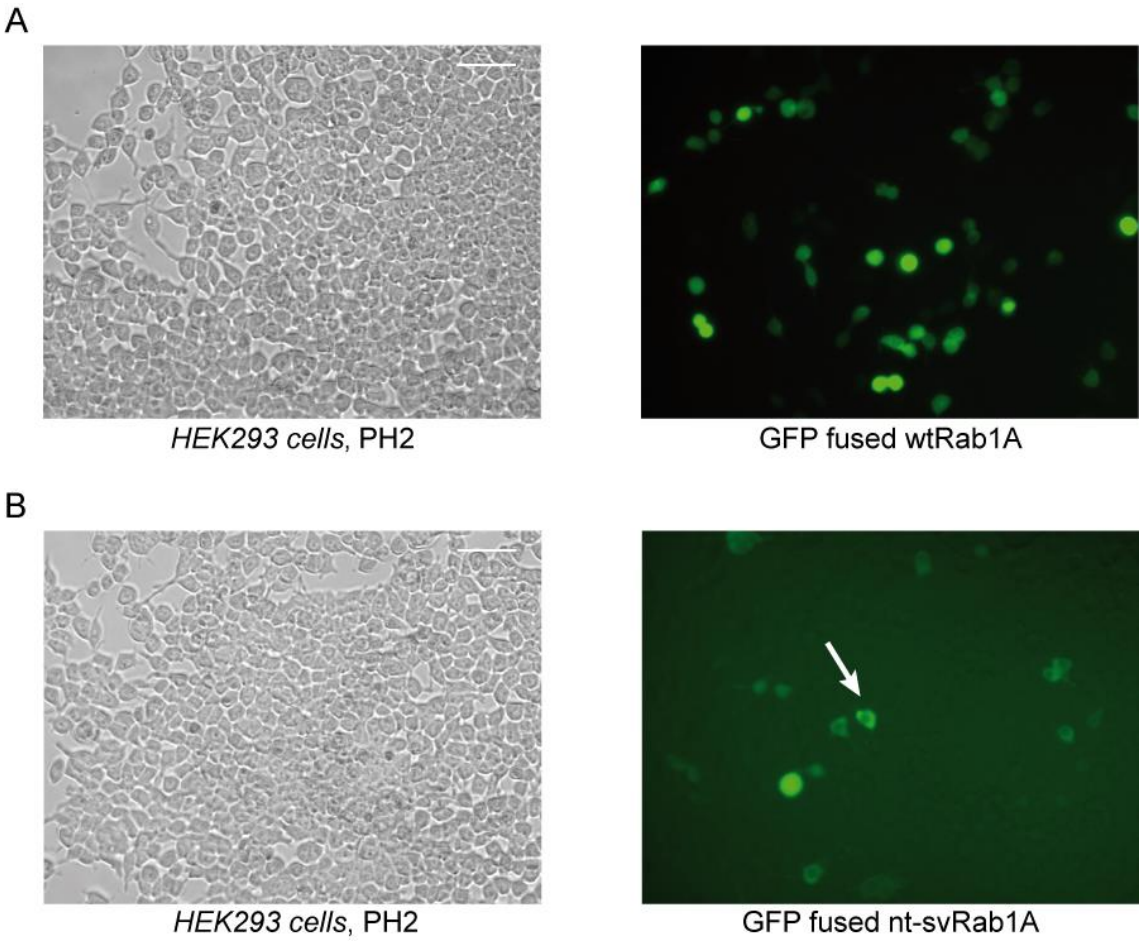

Figure 24: Over-expression studies of Rab1A proteins *in vivo*.
A/B) Light microscopy images of the over-expression of wtRab1A **(A)** and nt-svRab1A **(B)** in *HEK293* cells, scale bar: 70 µm (Foci are indicated by an arrow). Images were taken 24 h post transfection.

In agreement with fluorescent microscopy (Figure 24A) wtRab1A was identified in both the cytosolic and membrane containing protein fractions (Figure 25A). Similarly, nt-svRab1A was also present in both fractions (Figure 25B) whereby the cytosolic fraction of nt-svRab1A is smaller than that of wtRab1A.

The identification of nt-svRab1A in the membrane-bound protein fraction is surprising as posttranslational prenylation of RabGTPases typically occurs only in presence of a primary formed Rab:REP substrate complex (Rab escort protein) (Overmeyer et al, 1998), followed by presentation of the unprenylated Rab to the Rab GGTase (Kohnke et al, 2013). However, interaction of REP with nt-svRab1A is not possible due to the missing switch II region (especially its putative α2 helix) (Overmeyer et al, 1998).

This leads to the assumption that in contrast to other RabGTPases membrane attachment of nt-svRab1A is mediated by alternative mechanisms.

To investigate this in more detail, additional studies with Rab1A mutants lacking the C-terminal cysteines for prenylation were performed.

In contrast to wtRab1A, the respective nt-svRab1A mutant was still able to attach to the membrane, while in wtRab1A the depletion of the C-terminal cysteine abolished membrane binding (Figure 25).

In summary these experiments indicate that the attachment of nt-svRab1A to the membrane is still possible but independent of prenylation. Thus, nt-svRab1A membrane interaction seems to occur indirectly or via an alternative interaction mechanism.

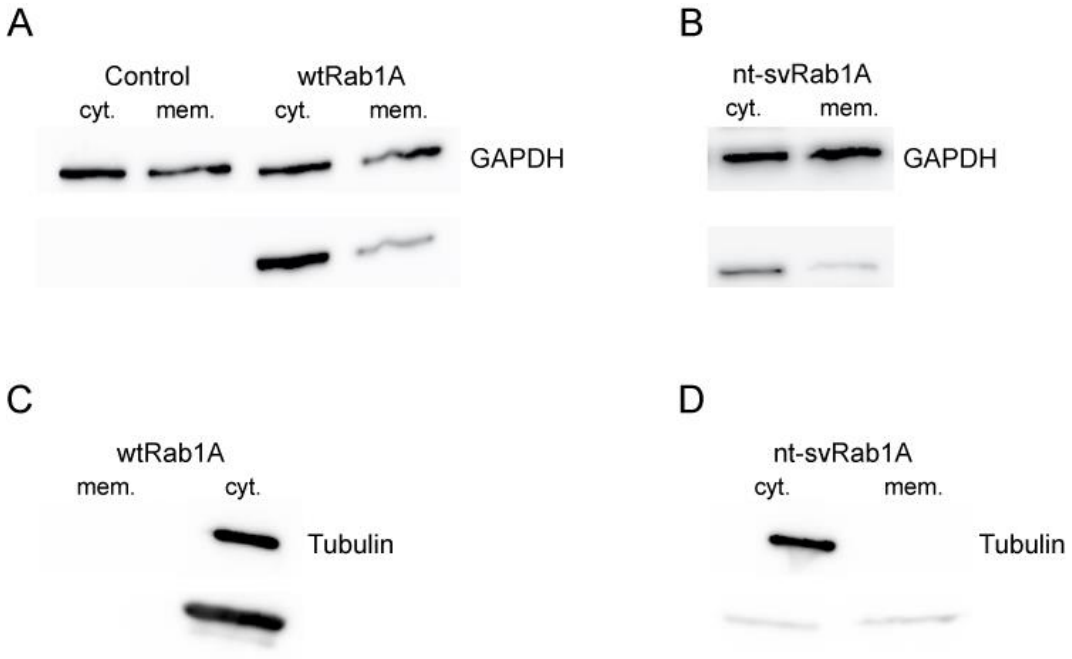

Figure 25: Nt-svRab1A distributes into a cytosolic and membrane bound fraction.
A, B) Western blots of transfected *HEK293* cells with wtRab1A protein **(A)** or nt-svRab1A protein **(B)**. Cells were lysed and then separated into the cytosolic (cyt.) and membrane containing protein fractions (mem.), as control *HEK293* cells overexpressing the pAcGFP-N1 empty vector was used. For the transfections the wtRab1A or nt-svRab1A pAcGFP-N1 construct lacking the C-terminal GFP-fusion was used. **C, D)** Westernblot of transfected *HEK293* cells with nt-svRab1A-C128A/C129A **(C)** and wtRab1A-C204A/C205A **(B)** mutant. Cells were lysed and then separated into the cytosolic (cyt.) and membrane containing protein fractions (mem.).

In chapter 4.4.5 it was possible to show, that nt-svRab1A forms hetero-dimers with wtRab1A and its close homologue Rab1B. This finding might explain the capability of nt-svRab1A of still attaching to the membrane in an indirect manner via hetero-dimer formation with its wtRab1A protein or potentially also with Rab1B and other RabGTPases.

4.5.2 Nt-svRab1A co-localizes to ER membranes

A hallmark of eukaryotic cells is their ability to segregate proteins via vesicular transport (Bock et al, 2001), essentially regulated by RabGTPases (Monetta et al, 2007; Zerial & McBride, 2001). In this context, Rab1A is mainly involved in the ER to Golgi transport (see chapter 1.4.6 (Sandoval & Simmen, 2012; Segev, 2001a)). Whether the regular localization of Rab1 GTPase in the non-trivial splice variant was affected by alternative splicing was investigated in the next paragraph. Therefore GFP fusion constructs of the respective Rab1A protein were overexpressed in *HEK293* cells, followed by localization analysis by fluorescence microscopy. For staining of the ER the ER-ID™ Red Assay Kit was used according to the manufacturer's protocol. The analysis of transiently transfected cells with either overexpressing nt-svRab1A-GFP or wtRab1A-GFP stained with an ER-specific marker demonstrated the co-localization ofboth proteins with the ER (Figure 26, (Monetta et al, 2007)). In contrast to the diffuse fluorescence pattern of the wt-Rab1A protein the fluorescent microscopy images of nt-svRab1A additionally showed foci (Figure 26B). This again indicated that protein aggregates, incorporating nt-svRab1A, are present under *in vivo* conditions.

These results explicitly demonstrated that nt-svRab1A in line with its wild type protein localizes to the ER compartment.

Thus, alternative splicing does not alter the main location of this Rab1 GTPase, regulating ER to Golgi vesicular transport.

Consequently, it seems likely that nt-svRab1A still can participate in anterograde transport.

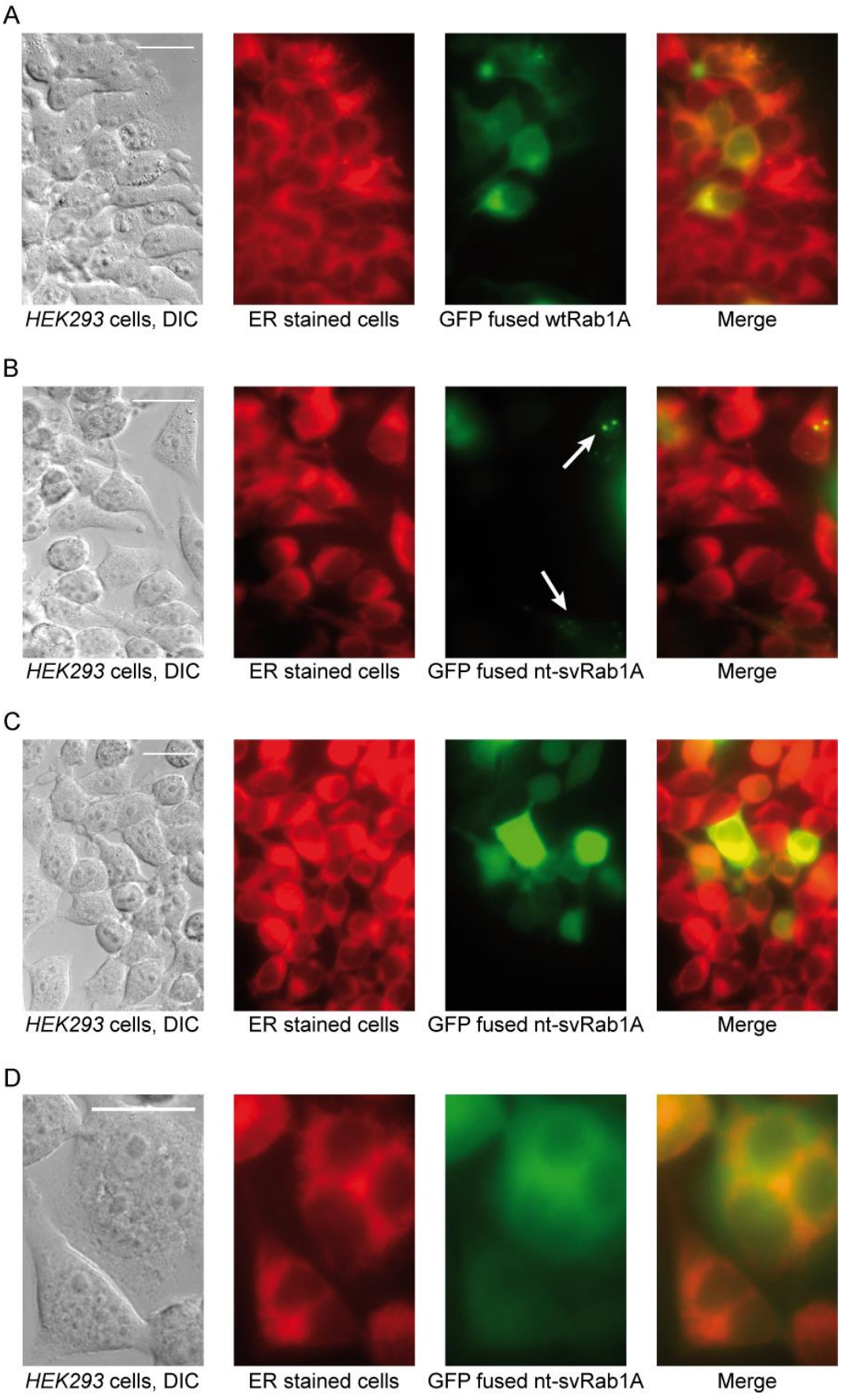

Figure 26: Nt-svRab1A co-localizes to ER membranes.
(A, B, C, D) Light microscopy images of *HEK 293* cells overexpressing wtRab1A **(A)** and nt-svRab1A **(B, C, D)**. ER was visualized by use of ER-ID™ Red Assay Kit according to the manufacturer's instructions. Scale bar: 25 µm (Foci are indicated by arrows).

4.5.3 Nt-svRab1A enhances the secretion of model proteins *in vivo*

To test the influence of nt-svRab1A on protein secretion, the efficiency of alkaline phosphatase secretion into the culture medium of *HEK293* cells (Cullen & Malim, 1992; Mukherjee et al, 2011) was monitored. Therefore, *HEK293* cells were co-transfected with a plasmid encoding secreted alkaline phosphatase or the pAcGFP-N1 empty vector or the respective Rab1A constructs. 24 h post transfection, the secreted alkaline phosphatase levels were detected by chemiluminescence. Interestingly, cells over-producing nt-svRab1A showed an 11 % higher level of secreted alkaline phosphatase than wtRab1A over-producing cells (Figure 27B). In this thesis it has been shown already, that the over-expression level of nt-svRab1A is lower compared to its wild-type form (4.5.1). Hence, to correlate the increased secretion level it was necessary to quantify the cytosolic and membrane content of both proteins. The results depicted in Figure 27A clearly point out that the over-production level of nt-svRab1A is 4 fold lower than that of wtRab1A. Accordingly this denotes that the secretion of phosphatase is indeed enhanced by ~44% in presence of nt-svRab1A.

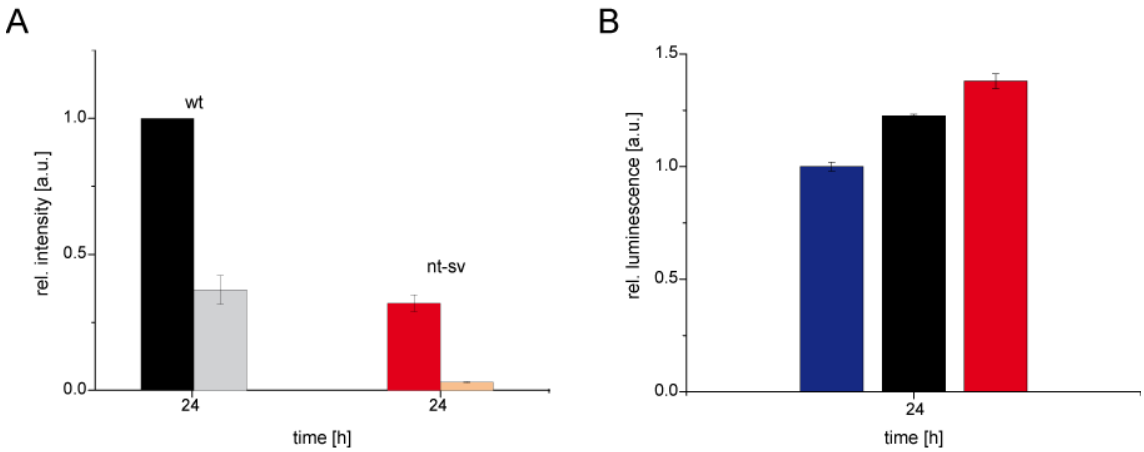

Figure 27: The presence of nt-svRab1A enhances the secretion of alkaline phosphatase.
A) Quantification of the cytosolic (cyt.) and membrane attached (mem.) content of wtRab1A (black: cyt., grey: mem.) and nt-svRab1A (red: cyt., light red: mem.) in transfected *HEK293* cells. **B)** The secretion assay was performed as described (Cullen & Malim, 1992; Mukherjee et al, 2011), using the Secreted Alkaline Phosphatase Reporter Gene Assay Kit. *HEK293* cells were co-transfected with a plasmid encoding secreted alkaline phosphatase and the pAcGFP-N1 empty vector (blue), the wtRab1A (black) or nt-svRab1A (red) constructs. The secreted alkaline phosphatase level was analyzed 24 h post transfection by chemiluminescence. The error bars indicate the standard deviation of three biologically independent experiments.

Thus, overall nt-svRab1A seems to act as a temporary activator of vesicular transport.

In a next set of experiments the cytosolic and membrane content of nt-svRab1A was analyzed over time after over-expression in *HEK293* cells. Thereby it should be examined whether a correlation between the content of nt-svRab1A protein and enhanced secretion level can be deduced. After transient transfection of the cells with nt-svRab1A, samples were taken after 20 h, 24 h and 48 h, lysed and separated into cytosolic and membrane protein containing fraction.

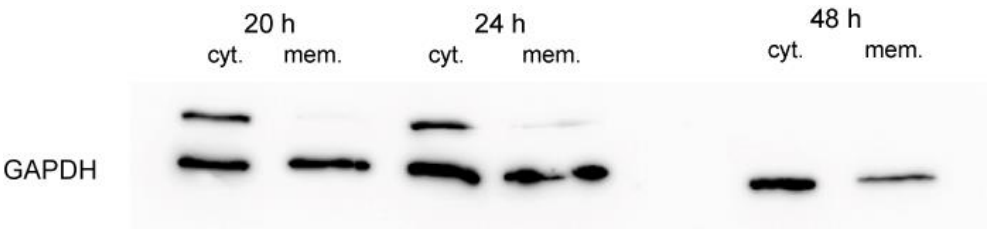

Figure 28: Time analysis of nt-svRab1A content after over-expression in *HEK293* cells.
Western blot of transfected *HEK293* cells with nt-svRab1A protein. Cells were lysed and then separated into the cytosolic (cyt.) and membrane containing protein fractions (mem.). For the transfections the nt-svRab1A GFP-fusion construct was used. Samples were taken after desired time points.

As one can clearly see no significant differences in the protein contents of nt-svRab1A present 20 h and 24 h post-transfection were observed (Figure 28). However, already 48 h post-transfection nt-svRab1A was no longer detectable. In previous studies the aggregation propensity of nt-svRab1A was described *in vivo* (4.5.1). This might be one reason for the absence of protein already after 48 h. One possibility is that the aggregated nt-svRab1A protein might get degraded by the ER associated degradation pathway.

However, as the protein levels stay almost constant from 20 h to 24 h post-transfection, the results exclude a direct correlation of the cellular nt-svRab1A content to an enhancement of vesicular transport.

Thus, a temporary overproduction of the splice variant can be ruled out as reason of the enhanced protein secretion.

4.5.4 Nt-svRab1A is not induced under ER and Golgi stress conditions

As nothing is known up to now about the conditions under which nt-svRab1A is present *in vivo* this was addressed in the following section. One assumption could be that under stress nt-svRab1A in the cell is alternatively spliced to promote vesicular transport and consequently increasing protein secretion. As the Rab1A GTPase is mainly shuttling between ER and Golgi compartments (Sandoval & Simmen, 2012), ER and Golgi stress might promote the production of nt-svRab1A.

Thapsigargin is known to be an effective inhibitor of the Ca^{2+} ion pump proteins of intracellular membranes located in sarcoplasmic reticulum and ER (Kijima et al, 1991; Lytton et al, 1991). One of the earliest and best characterized effects of Brefeldin A (BFA) is the loss of COP I coat formation, by inhibition of a subset of Golgi localized GEFs that catalyze the activation of the small GTPase Arf1 (Citterio et al, 2008; Nebenfuhr et al, 2002). Consequently, the formation of transport vesicles is blocked. In addition the assembly and maintenance of the Golgi stack and TGN is tremendously affected by BFA (Manolea et al, 2008). Thus, ER and Golgi stress conditions in MCF7 cells were mimicked by addition of Thapsigargin or BFA.

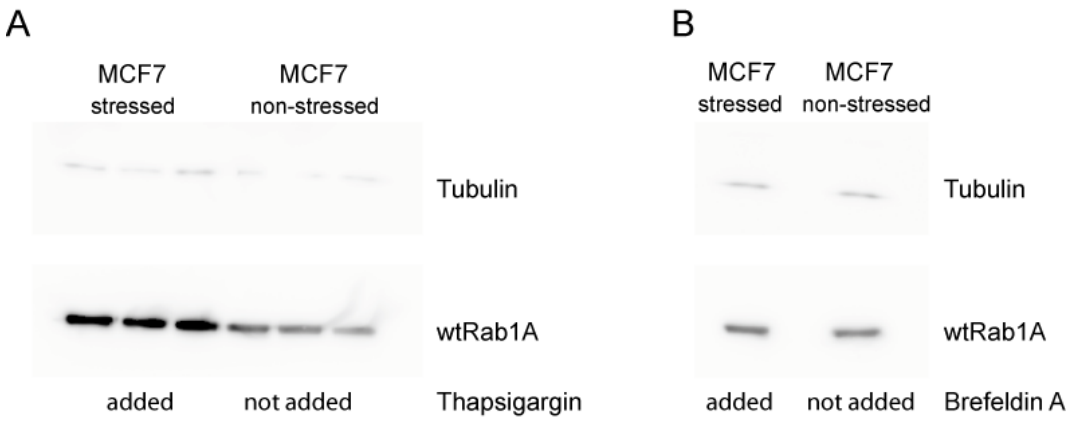

Figure 29: Analysis of nt-svRab1A expression under ER and Golgi stress conditions in MCF7 cells.
A, B) Western blots of MCF7 cells under ER **(A)** and Golgi **(B)** stress conditions. **A)** To mimic ER stress, 300 nM Thapsigargin was added to the MCF7 cells and before lysis the cells were incubated further for 3 h under standard cell culturing conditions. **B)** Golgi stress conditions were achieved by addition of 36 µM of Brefeldin A to the MCF7 cells. Prior lysis the cells were incubated further for 1 h 30 min under standard cell culturing conditions. In both cases Tubulin was used as loading control.

After incubating the cells with respective stressors, they were lysed and the endogenous levels of Rab1A proteins were detected by western blotting. The determined protein levels under stress were compared to the protein amounts under normal conditions.

As the expression level of endogenous Rab1A wild type protein in *HEK*293 cells is below the detection limit of western blotting (Wilhelm et al, 2014), MCF7 cells showing a higher expression pattern were used (Wilhelm et al, 2014).
In contrast to the wtRab1A levels present under normal conditions, higher protein levels are visible after addition of the ER stressor Thapsigargin (Figure 29A). However, it should be mentioned that no quantitative conclusion can be deduced, due to improper loading control detection.
Identification of nt-svRab1A under normal as well as under stress conditions failed.
In difference to the observations made under ER stress conditions, no changes of the wtRab1A protein levels are detectable after addition of BFA (Figure 29B).
Also nt-svRab1A could not be detected under Golgi stress conditions.

Comparative analysis of these results showed that the wtRa1A protein seems to be more sensitive to ER stress than to Golgi related stress.
Furthermore, no nt-svRab1A is induced under ER and Golgi stress conditions. So far it was not possible to ascertain under which conditions nt-svRab1A synthesis is induced *in vivo*.

5 Discussion

The results show that nt-svRab1A, which compared to wtRab1A lacks 37 % of the amino acids, represents a folded and functional protein. The comparison of both secondary structures exhibits only slight differences for nt-svRab1A, even though 76 residues are missing in the spliced isoform (Figure 14A). Thereby the identification of two significantly different but stable conformational computational models, in which major rearrangements only occur in the loop region, emphasizes these minor disparities (Figure 14C). Bioinformatics analysis of the gene structure of *rab1A* indicates that nt-svRab1A (iso-3) is highly conserved (Figure 10). Together with its expression in different tissues (Figure 11), this further argues for the importance of nt-svRab1A in the cellular context. In contrast to the wtRab1A protein and other members of the Ras superfamily, which are usually monomers (Pereira-Leal et al, 2003) the quaternary structure of nt-svRab1A is a dimer (Figure 14). One reason for explaining the oligomer formation in nt-svRab1A might be that the large exposed hydrophobic surfaces of the structural model of the monomer are buried in the predicted symmetric binding geometry of the dimer (Figure 14F). So dimerization seems to stabilize nt-svRab1A. Alternatively the observed formation of hetero-oligomers with either the $Rab1B_{(3\text{-}174)}$ GTPase (Figure 23) or the more stable wtRab1A protein (Table 4, Figure 23), might additionally increase its time of persistence in the cell. As nt-svRab1A is not as stable as wtRab1A the protein turnover for nt-svRab1A in the cell is likely to be higher. Our results on the transcriptional profiles of the two proteins, as well as the observation that nt-svRab1A protein is less stable and more aggregation prone, supports this hypothesis.
In conclusion this might be indicative of a time-restricted, regulatory, role of nt-svRab1A in the cell.

As a member of the Ras superfamily, the activity of the Rab1A protein correlates to its nucleotide bound (inactive with GDP bound and active in the GTP state) (Dong et al, 2012; Gavriljuk et al, 2013; Haas et al, 2007). Nt-svRab1A is still able to bind both nucleotides but in contrast to wtRab1A, the isoform was more efficiently stabilized by GDP (Table 4). This might imply that nt-svRab1A is predominantly present in its inactive form. Additionally, SEC analysis demonstrated that nucleotide binding has no influence on the quaternary structure of nt-svRab1A, which remained dimeric also in presence of nucleotide (Figure 18E).

Thus, assuming that the active nt-svRab1A dimer binds two GTP molecules, and the dimeric structure of the inactive GDP bound form is comparable to its active conformation, nt-svRab1A-GDP potentially could regulate itself by forming an inactive or less active nt-svRab1A-GDP:nt-svRab1A-GTP dimer. This was also hypothesized by Nan *et al.*, explaining the observation that wild-type Kras2 can suppress mutant KRas-driven lung carcinogens in mice (Nan et al, 2015).

Further, nt-svRab1A's ability to bind ADP and ATP and the underlying unspecificity for GXP nucleotides is likely due to the missing guanine base binding motif G4 (NKXD; Figure 9). G4 together with the still present G5 motif (TSA; Figure 9) is responsible for the discrimination against other nucleotides (Itzen & Goody, 2011). In general the specificity for guanine is determined by the aspartate of the NKXD motif, which for electrostatic and steric reasons would not tolerate an adenine-6 amino group (Wittinghofer & Vetter, 2011). Thus, the non-trivial splicing event leads to a loss in specificity of nt-svRab1A for GXP nucleotides.

Rab1A activation by GEFs, enhances the replacement of GDP on Rab proteins by cytosolic GTP at the donor membrane (Schoebel et al, 2011). The results show that due to the completely missing switch II region in nt-svRab1A, an interaction of nt-svRab1A with $DrrA_{(340\text{-}533)}$, a specific GEF of Rab1 (Ingmundson et al, 2007; Machner & Isberg, 2007; Schoebel et al, 2009) is not possible. It is known from binding studies that the arginine R69 in switch II (missing in nt-svRab1A) interacts strongly with a negatively charged pocket of the GEF (Schoebel et al, 2009).

Also, by Co-IP studies from HeLa lysate samples no potential GEFs, interacting with nt-svRab1A, were identified (Figure 22).

Thus, the splice event seems to alter the major regulatory role of RabGTPase itself, by prohibiting the accelerated activation of nt-svRab1A by a GEF, whereas the binding of GDP or GTP to the protein is still possible. Nevertheless, the spontaneous nucleotide exchange, leading to the auto-activation of nt-svRab1A, is feasible (Simon et al, 1996).

Consistent with this, the analysis of the GTP hydrolysis revealed that nt-svRab1A still shows intrinsic GTP hydrolysis activity (Figure 21B). However, in contrast to wtRab1A, the stimulated deactivation process of nt-svRab1A, in the presence of the Rab1 specific GAP TBC1D20 (Gavriljuk et al, 2012; Haas et al, 2007), failed (Figure 21D).

From literature it is known that the glutamine located in the switch II region (DXXGQ motif) is involved in contacting the peptide backbone of the GAP but seems to play no direct role in catalysis (Langemeyer et al, 2014; Pan et al, 2006).

An interaction of GAP with this specific glutamine (DXXGQ motif) is not possible in nt-svRab1A, due to the missing switch II region. This may be one possible explanation that TBC1D20 does not enhance GTP hydrolysis of nt-svRab1A.

Nevertheless, it cannot be fully exclude that nt-svRab1A is deactivated by a GAP that deviates from the TBC1D20 specific GTP hydrolysis mechanism. For example Rab3GAP inactivates Rab3 without containing a TBC domain (Frasa et al, 2012). In addition the active site of many small GTPases is completed by a catalytic "arginine finger" that is used by Ras-, Rho-, and RabGAPs (Gavriljuk et al, 2012). Hereby the side chain of the arginine 105 of TBC1D20 forms polar contacts with the α- and β-phosphate (Gavriljuk et al, 2012) of Rab1A which are not affected in nt-svRab1A.

At least for TBC RabGAPs *cis*-glutamine is not directly involved in GAP-catalyzed GTP hydrolysis, whereas its role in the intrinsic GTP hydrolysis reaction is of great importance (Gavriljuk et al, 2012). Additionally, it is known that the interaction of the aspartate with the magnesium ion in the DXXGQ motif (origin missing in nt-svRab1A) is critically required for tight nucleotide binding and GTP hydrolysis in most Ras –like and other G proteins (Wittinghofer & Vetter, 2011). This might explain the determined ~1000 fold lower binding affinities of nt-svRab1A to nucleotides. The interaction of the magnesium ion in nt-svRab1A is most likely only achieved by the hydroxyl group of the serine residue of the P-Loop (GXXXXGKS) and a highly conserved threonine residue of the switch I region (Bourne et al, 1991).

In this context, the observed intrinsic GTP hydrolysis of nt-svRab1A is surprising and cannot be fully explained. Nevertheless, studies on other Rab proteins showing variations in the highly conserved sequence elements, lead to altered mechanistic characteristics of the respective Rab protein (Erdman et al, 2000).

Espinosa *et al.* showed that RhoBTB3, a Rho GTPase family ATPase which is missing the NKXD motif, lost its nucleotide specificity and binds ATP in preference to GTP (Espinosa et al, 2009). Similarly, nt-svRab1A lost the specificity for GXP nucleotides and shows a ~3 fold lower apparent K_D for ATP binding (0.1 µM) compared to GTP binding ($K_{Dapp.}$ = 0.3 µM) (Figure 19 Inset: E, F).

In summary, the splice event produces a variant with significantly altered nucleotide binding and hydrolysis properties that seems to act independently of GEFs and at least TBC1D20 GAP.

Consequently, nt-svRab1A overcomes the lacking stimulation of the GTP hydrolysis by a TBC GAP system by a 4 fold higher intrinsic GTP hydrolysis rate compared to wtRab1A.

However, the intrinsic GTP hydrolysis rate of nt-svRab1A is still slow, leading to an enhanced level of active nt-svRab1A in the cell.

This activation might lead to a general influence of nt-svRab1A in vesicular trafficking.

As regulators in membrane trafficking processes Rab proteins localize to, and cycle between membranes of different cellular compartments (Gavriljuk et al, 2013). For attachment to membranes, Rabs are posttranslational modified at the C terminus by Rab geranylgeranyl-transferases II (RabGGTase) (Kohnke et al, 2013). Unlike the other prenyl-transferases, farnesyl-transferase and geranylgeranyl-transferase I, RabGGTase does not rely on a consensus sequence (Kohnke et al, 2013). This means that any cysteine- or thiol-containing fragment that can be properly presented to the active site of RabGGTase is able to undergo prenylation (Li et al, 2014). RabGGTase does not recognize its monomeric protein substrates (Rab proteins) directly (Li et al, 2014). Instead, the Rab protein must first bind to a carrier protein named Rab escort protein (REP), leading to the formation of a ternary catalytic Rab:REP:RabGGTase complex, necessary for prenylation (Li et al, 2014; Overmeyer et al, 1998). Due to the missing switch II region in nt-svRab1A, an interaction of REP with nt-svRab1A is no longer possible (Overmeyer et al, 1998). However, the results of this thesis clearly show that nt-svRab1A is still able to attach to the ER membrane and that the non-trivial splicing does not alter the localization of nt-svRab1A in the cell, compared to wtRab1A (Figure 25, Figure 26).

Contrary to wtRab1A, the respective nt-svRab1A mutant was still able to attach to the membrane, while in wtRab1A the depletion of the C-terminal cysteine abolished membrane binding (Figure 25C, D).

In summary these experiments indicate that the attachment of nt-svRab1A to the membrane is still possible but independent of prenylation. Accordingly, the interaction of nt-svRab1A with membranes seems to occur via an alternative interaction mechanism or indirectly. One assumption might be that this membrane interaction is achieved indirectly in the cell, by formation of a hetero-oligomer with its wild type protein (Figure 23A, B, C). As the Rab1B GTPase is also essential for ER to Golgi transport (Romero et al, 2013) and thus localizes to identical compartments as wtRab1A, it is absolutely likely that nt-svRab1A attaches to the membrane by interacting with Rab1B. This hypothesis can be underlined by showing already *in vitro* that nt-svRab1A hetero-dimerizes with its wtRab1A protein as well as with $Rab1B_{(3\text{-}174)}$, being a close homologue of the wild-type GTPase (Figure 23).

From literature it is known that both Rab1 proteins are involved in the anterograde transport (Haas et al, 2007). Further Rab1B takes part in the modulation of COP I and COP II recruitment (Garcia et al, 2011; Lanoix et al, 2001; Monetta et al, 2007) and also plays a role in the COP I vesicle formation, regulating the transport from Golgi to the plasma membrane, as well as in the intra-Golgi retrograde transport of Golgi enzymes (Guo & Linstedt, 2013; Lanoix et al, 1999; Lanoix et al, 2001; Monetta et al, 2007).

Thus, the interaction of nt-svRab1A with both Rab1 G proteins suggests a possibility of influencing the vesicular transport process.

In conformation to this proposal, over-expression of nt-svRab1A resulted in higher levels of alkaline phosphatase secretion (Figure 27). Further within 20 h up to 24 h post-transfection, almost constant levels of nt-svRab1A protein in the cell were detected (Figure 28). Accordingly a temporary overproduction of the splice variant can be ruled out as reason of enhanced protein secretion. While indirect methods of stimulating the vesicle-mediated transport pathway cannot be excluded, the ability of nt-svRab1A to hetero-dimerize with other RabGTPases is one potential mechanism. Such a perspective interpretation is strengthened by the recent evidence that in contrast to the existing view on Ras functioning as a monomeric GTPase, the formation of Ras-GTP dimers leads to a strong up-regulation of Mitogen-Activated Protein Kinase (MAPK), without the need of increasing the expression level of Ras (Nan et al, 2015).

There is additional evidence that the over-expression of the Rab1B leads to morphological changes in the Golgi apparatus (Romero et al, 2013), thereby blocking the whole secretion pathway. Hence, the interaction of nt-svRab1A with Rab1B might reverse such a blocking event and seems to lead to an activated vesicular transport. Additionally, whenever nt-svRab1A is generated by the splice event, its preferentially binding affinity for GDP presumably shifts the local availability of GDP and GTP to more free GTP.

Given that GTP is necessary for the activation of all G proteins, this might lead to a higher number of other activated Rab GTPases in the cell, hence accelerating Rab effector recognition, as this is only achieved in the GTP active state of the Rab GTPase (Gonzalez Jr & Scheller, 1999). As Rab effectors are involved during the different steps of vesicular transport (1.4.5) an excess of active Rab GTPases consequently leads to a stimulation of the vesicle-mediated pathway.

In addition the interaction of nt-svRab1A with wtRab1A and Rab1B seems to stabilize nt-svRab1A, similar to its self-dimerization. This would further increase the activation of the vesicle-mediated transport by decreasing the availability of wtRab1A and Rab1B.

Alternatively, it is possible that nt-svRab1A itself interferes directly with the vesicle-mediated transport pathway by an unknown mechanism. It might enhance secretion by stimulating other proteins (e.g. cytoskeleton components) involved in the vesicle-mediated transport pathway.

In general alternative splicing produces a Rab1 isoform with several unusual features that discriminates this variant from other Rab GTPases. The most prominent characteristics identified are the loss of specificity for GXP's, the lacking activation by a GEF as well as inactivation by a GAP, its determined still slow intrinsic GTPase activity, the observed membrane attachment independent from prenylation and the stabilization of its structure via dimer formation.
Nevertheless, Rab GTPases with atypical features exists, e.g. Rab24 (Erdman et al, 2000).

Overall, the results indicate a new regulatory mechanism of Rab1A and vesicular transport via a non-trivial splice isoform of Rab1A.

The non-trivial splice event yields to a structured and functional protein, which significantly adds to the functional diversity of the proteome. This is in contrast to the popular assumption that especially non-trivial splice variants are subject to nonsense-mediated mRNA decay (Jaillon et al, 2008; Lareau et al, 2007) and, thus, are non-functional. Examination of other non-trivial splice variants will help to elucidate whether alternative regulatory roles as observed for nt-svRab1A represent a general scheme of non-trivial spliced isoforms.

6 Results Part II – Different human non-trivial splice variants

In a further part of this thesis three non-trivial splice variants, representing two different non-trivial splicing categories (see 1.1), were compared. Thereby it should be elucidated whether non-trivial alternative splicing in general leads to structured proteins, thus, considerably increasing the complexity of the human proteome. Further, the functional comparison of the non-trivial splice variants, should illustrate whether these non-trivial isoforms all share an alternative regulatory role with their respective wild-type forms. In order to identify potential structural and functional alterations occurring between the diverse non-trivial categories, the splice isoforms of human cytosolic serine-hydroxyl-methyl-transferase (nt-svSHMT), human Arginase-1 (nt-svArginase) and nt-svRab1A were compared. Nt-svSHMT (Uniprot ID: P34896-3) can be assigned to the conserved α-helices category, whereas nt-svArginase-1 (Uniprot ID: P05089-3) and nt-svRab1A (Uniprot ID: P62820-3) both belong to the class in which internally conserved α/β-motifs are deleted (Figure 30).

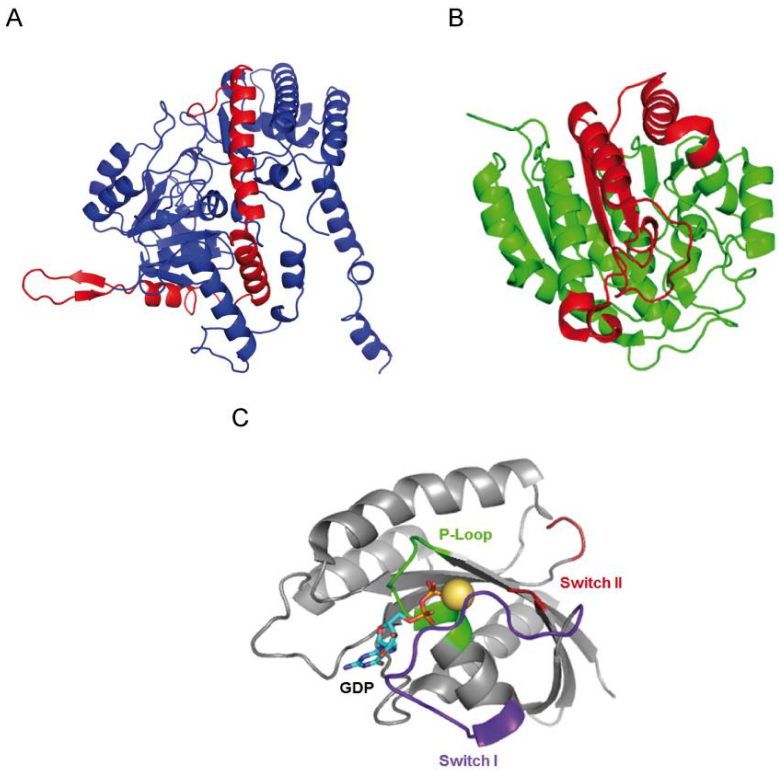

Figure 30: Structural overview of compared non-trivial splice variant.
A) Crystal structure of SHMT wild-type (PDB ID: 1BJ4, (Renwick et al, 1998)). The 79 amino acids (273 – 352), deleted in the non-trivial splice isoform are shown in red. Nt-svSHMT represents the conserved α-helices category. **B)** Crystal structure of human wild-type Arginase-1 (PDB ID: 1WVA, (Di Costanzo et al, 2005)). The highlighted red parts indicate the 85 amino acids (204 – 289) that are deleted in the respective nt-svArginase. The spliced isoform belongs to the internally α/β-motifs **C)** Crystal structure of Rab1A wild type (PDB ID: 2FOL, P-Loop: green, switch I: blue, switch II: red, nucleotide and magnesium ion are shown in ball-and-stick representation). The deleted 76 amino acids (65 – 140) in the nt-svsRab1A are marked red. The spliced isoform can be classified into the internally α/β-category.

6.1 Structural and functional characterization of nt-svSHMT

Human cytosolic SHMT is a pyridoxal-5-phosphate (PLP) dependent enzyme playing a key function in the cellular production of *5,10*-methylene-tetrahydrofolate (*5,10*-CH_2THF, major one-carbon carrier), which is necessary for many biosynthesis reactions especially for the supply of purins as basic components in nucleotide production (Liu et al, 2001b). *5,10*-CH_2THF is formed by the tetra-hydrofolate (THF) dependent conversion of serine to glycine (Agrawal et al, 2003). In this catalytic reaction, in mammals the major one-carbon units (*5,10*-CH_2THF) are generated, which are used in folate-dependent anabolic reactions (Liu et al, 2000). As both reaction products, glycine and *5,10*-CH_2THF, are involved in nucleotide biosynthesis, it is not surprising, that elevated SHMT activity has been found in human leukemic cells (Thorndike et al, 1979) and in a variety of solid tumor tissues of human an rodent origin (Snell et al, 1988). Thus, SHMT can directly be referred to cellular replication in cancer cells. Indeed, Snell *et al.* showed, that inhibition of the enzyme in cultured myeloma cells resulted in dose-dependent inhibition of cellular growth (Snell & Riches, 1989). Thus, the development of inhibitors against SHMT might represent a suitable strategy in cancer therapy. In this thesis it should be addressed whether nt-svSHMT is a potential aspirant in regulating the activity of its wild-type protein. In consequence, this might lead to a reduction of cancer cell development by nt-svSHMT.

In the following section some results, analyzing the structure and function of nt-svSHMT are presented.

In order to elucidate the role of the spliced isoform of SHMT in humans, it was investigated, if nt-svSHMT encoding mRNA is present in humans, by analyzing 21 total RNA isolates from different human tissue samples. After reverse transcription of the total RNA, the presence of wtSHMT and isoform 3 (nt-svSHMT) was detected by polymerase chain reaction using specific primers (Figure 31). In accordance with the proposed presence of nt-svSHMT in different tissues on basis of the human proteome data (Wilhelm et al, 2014), the spliced isoform is expressed in 10 out of the 21 tissues tested (Figure 31B). Interestingly, in some tissues tested both the wtSHMT and nt-svSHMT isoforms were detected, showing similar expression levels.

Besides, the mRNA levels for the wtSHMT in many tissues seemed to be under the detection limit in our experiments. Nevertheless, the presence of wtSHMT was confirmed on protein level in the human proteome study (Wilhelm et al, 2014).

This might indicate that the stability of the two SHMT protein isoforms is different, forcing the cell to produce more nt-svSHMT mRNA, to balance the protein amounts of the two isoforms.

A

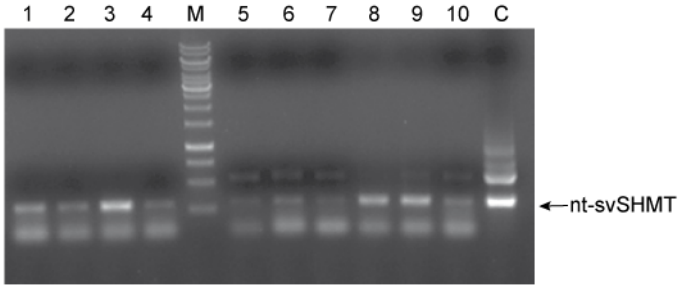

B

Tissue	Wild type		Splice Variant	
	mRNA level	protein level	mRNA level	protein level
Adrenal gland	no	yes	no	yes
Brain cerebellum	no	yes	yes	yes
Brain whole	no	yes	yes	yes
Fetal brain	no	not tested	no	not tested
Fetal liver	no	not tested	no	not tested
Liver	no	yes	no	yes
Heart	no	yes	no	yes
Kidney	no	yes	no	yes
Lung	no	yes	no	yes
Placenta	yes	yes	yes	yes
Prostate	yes	yes	yes	yes
Salivary gland	yes	yes	yes	yes
Skeletal muscle	no	no	no	no
Small intestine	no	no	no	no
Spleen	yes	yes	yes	yes
Stomach	yes	yes	yes	yes
Testis	no	yes	yes	yes
Thymus	yes	no	yes	no
Thyroid gland	no	yes	no	yes
Trachea	no	no	yes	no
Uterus	no	yes	no	no

Figure 31: Analysis of the mRNA levels of SHMT proteins in different human tissue samples.
A) Example agarose gel (1 %) of different tissues tested. As template 1.0 µg and 2.0 µg of the respective tissue RNA was used. 1.0 µg of wt or nt-svSHMT DNA was utilized as a control. The respective RNA samples were reverse transcribed into cDNA followed by polymerase chain reaction. The band at 250 base pairs indicates the presence of nt-svSHMT mRNA (marked by an arrow), whereas the identification of a band at approximately 330 base pairs shows the presence of wtSHMT mRNA. M: DNA ladder 100 bp, C: Control wtSHMT and nt-svSHMT, 1-10: Tissue samples, 1, 2: Brain cerebellum, 3, 4: Brain whole, 5, 6: Placenta, 7, 8: Salivary gland, 9, 10: Spleen. **B)** Overview of the presence of SHMT on mRNA- (this study) and protein-level (Wilhelm et al, 2014) in 21 different human tissue samples tested.

Even though nt-svSHMT is lacking 79 amino acids (17 %, amino acids 273 – 352) compared to its wild-type protein it was possible to stably purify the protein. However, in contrast to its wild-type the splice variant was much more aggregation prone, limiting its solubility to a concentration of 1 $mgmL^{-1}$. This characteristic was in line with the 7.9 °C lower thermal stability of nt-svSHMT compared to wtSHMT (Figure 32A). Interestingly, the comparison of both Far-UV-CD spectra indicated only minor differences in the secondary structure of both proteins (Figure 32B). The comparison of the secondary structural element contents of both proteins showed that major changes occurred in the α-helical regions, as well as in the antiparallel β-sheet elements (Figure 32B *Inset*). Although nt-svSHMT belongs to the non-trivial splice category in which α-helices are spliced out, the determined higher content of α-helical parts in the SHMT splice isoform is rather surprising. However, rearrangements of the structure are imaginable.

By minimizing the β-sheet content, the flexibility of the protein is enhanced, consequently increasing the possibility to close the gap of the deleted 79 amino acids by formation of further helical elements. Additionally, it can be assumed, that due to the deficiency of exon 9 in nt-svSHMT a new conformation of amino acids 75 – 85 is induced (Liu et al, 2001b). The latter residues normally stay in direct contact with the deleted region around residue 300 (missing in nt-svSHMT) and thus adopt a different conformation, thereby altering the position of the helix from residue 86 – 104 (Liu et al, 2001b).

Nevertheless, alternative splicing still led to a stable and folded protein.

In contrast to the tetrameric quaternary structure of the wt protein (Renwick et al, 1998), the structure of the nt-svSHMT was impaired. Nt-svSHMT predominantly seems to form octamers, consisting of two tetramers (Figure 32C). One possible reason for that might be that due to the altered position of the helix (residues 86 – 104) in nt-svSHMT, the interaction of these residues with the N-terminal arm of the second monomer is abolished, which normally is observed in the tight dimer structure of wtSHMT (Liu et al, 2001b). Because of these changes, modifications upon oligomerization are expected. Krishna *et al.* demonstrated that aspartate 90 is critically required in maintaining the oligomeric state of human cytosolic SHMT (Krishna Rao et al, 1999). Hence, dislocation of the helix (residues 86 – 104) in nt-svSHMT describes the impaired quaternary structure of the spliced isoform.

However, the results indicated that the nt-svSHMT stabilizes itself via the formation of higher oligomers. Still it cannot be excluded that this structural modification would lead to functional changes of nt-svSHMT.

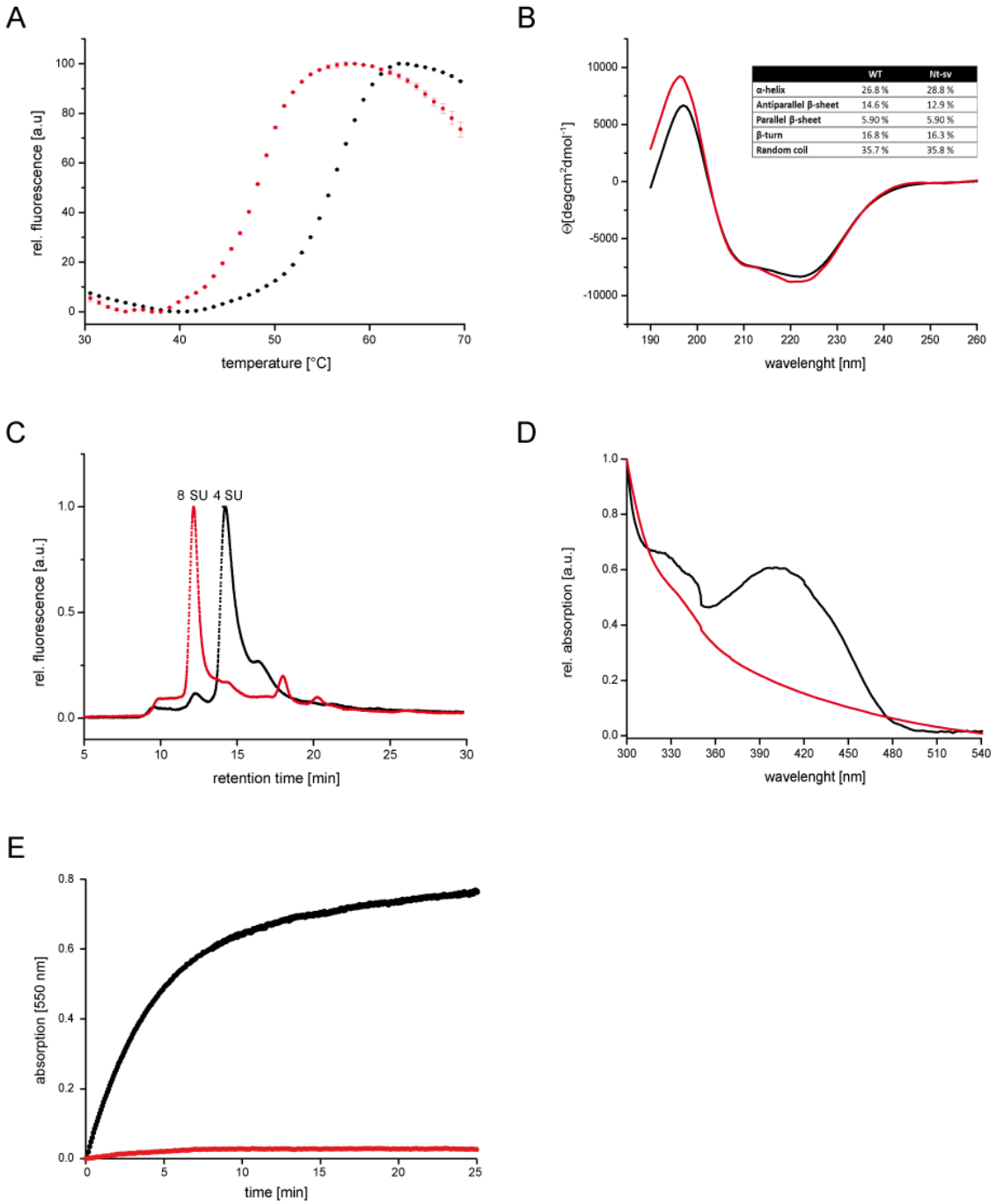

Figure 32: Nt-svSHMT is a structured and functional protein.
A) Analysis of the thermal stability of wtSHMT (black) and nt-svSHMT (red). TSA measurements were conducted in 50 mM Tris buffer (pH 7.7) with 20 mM KCl added. In total 1 µg of each protein was used. All calculated T_m values are means of at least three samples and the corresponding standard deviations are indicated. **B)** Secondary structure analysis: Far-UV CD spectroscopy of wtSHMT (black) and nt-svSHMT (red). 16 accumulations were recorded. *Inset:* Calculation of the secondary structural contents according to CDNN (Applied Photophysics). **C)** Quaternary structure analysis: SEC measurements of wtSHMT (black) and nt-svSHMT (red) using a Biosep *SEC-S3000* column operated in 50 mM Tris buffer (pH 7.7) with 20 mM KCl at 20 °C. A constant flow rate of 0.5 mL/min was applied. The calculated number of subunits for both proteins is depicted. **D)** Analysis of PLP binding to wtSHMT (black) and nt-svSHMT (red) by absorption spectroscopy. The experiments were performed in 50 mM Tris buffer (pH 7.7) containing 20 mM KCl at 20 °C. 3 µM of the respective protein was used. Buffer corrected spectra are shown. **E)** Investigations of the enzymatic activity of both SHMT proteins (wtSHMT: black, nt-svSHMT: red). Kinetic measurements were executed at 550 nm absorption over time (Stover et al, 1992). Shown are the reference corrected curves. Measurements were operated with 0.5 µM of the respective protein at 30 °C. 850 µL starting solution, consisting of 600 µL Schiff's reagent and 250 µL serine solution ($c_{Ser.}$ = 150 µM) equipped with 200 µM THF was used.

By interaction of the cofactor PLP with the protein, an absorption maxima at 410 nm is visible, due to the formation of an internal aldimine (Vazquez et al, 1991). As one can see from absorption measurements the cofactor biding to nt-svSHMT is almost completely abolished (Figure 32D). In general the cofactor covalently attaches to the lysine 257 residue (Schirch et al, 1985). As this amino acid is still present in nt-svSHMT the structural modifications might be one reason to explain this observation. Further it is known from the literature that the deletion of exon 9 opens up one side of the folate binding pocket, thereby losing the loop structure centered around proline 298 and glycine 303 (Szebenyi et al, 2000). As these loops (missing in the nt-svSHMT) are normally involved in binding THF and PLP (Szebenyi et al, 2000), the altered binding efficiency of PLP to nt-svSHMT can be explained.

The enzymatic activity of nt-svSHMT was monitored according to Stover *et al.* (Stover et al, 1992). Thereby, compared to its wild-type the nt-svSHMT showed almost no enzymatic activity (Figure 32E). This can be explained by the changed binding abilities of PLP to nt-svSHMT, which is involved as cofactor in the last step of the SHMT catalyzed reaction. Further, the structural differences most likely affected the positions of the residues asparagine 387 and arginine 402, which support in binding the quinazoline ring of THF (Szebenyi et al, 2000). Therefore, changes in THF contacts would be expected. Hence, the proposed regulatory effect of nt-svSHMT can be ruled out, as the splice isoform still exhibits the same function as wtSHMT. Consequently, nt-svSHMT can be excluded as potential inhibitor in cancer cell growth. Future studies might highlight if and how nt-svSHMT influences cellular processes. Interaction of nt-svSHMT with wtSHMT might be one possibility to regulate the activity of SHMT *in vivo*.

In summary, the non-trivial splicing event did not result in complete disruption of the structure of SHMT but seems to be a further tool of the cell to modulate its activity.

6.2 Structural and functional characterization of nt-svArginase

Human Arginase-1 is involved in a variety of metabolic processes, with the most prominent one being the catalysis of *L*-arginine to *L*-ornithine and urea in the last step of the urea cycle (Han & Viola, 2001). The metallo-enzyme Arginase-1 plays a major role in controlling cellular levels of arginine and ornithine (Bewley et al, 1999). These metabolites are required for various processes, including protein synthesis and the production of creatine, polyamines, proline and nitric oxide (Bewley et al, 1999).

In mammals the existence of three diverse Arginase isoforms were described. Thereby isoform 1 (cytosolic) and isoform 2 (mitochondrial) essentially discriminate between their metabolic functions, the subcellular localization, as well as their tissue distribution (Ilies et al, 2010). The cytosolic variant is mainly involved in the urea cycle, whereas the mitochondrial isoform participates in the regulation of the arginine homeostasis (Shi et al, 2001). Perturbations in the latter case thereby could cause diseases like asthma, cardiovascular diseases, and erectile dysfunction (Ilies et al, 2010). Also tumor growth can be promoted by variations within the standard arginine homeostasis conditions (Ilies et al, 2010).

However, up to now the physiological relevance of isoform 2 could not be solved completely. In contrary to the cytosolic variant, no degradation in the physical health was observed when the isoform was totally missing. However, it cannot be excluded that isoform 2 leads to harmful effects for humans suffering from diseases or injuries (Shi et al, 2001).

Which role the so far uncharacterized isoform 3 (nt-svArginase) plays in this whole cellular network was addressed initially in this thesis. Thereby the potential as regulator of Arginase-1 wild-type or the respective isoforms should be addressed in the future, as aberrant upregulation of either one or both Arginase isozymes leads to dysfunction of *L*-arginine homeostasis and *L*-arginine-dependent biosynthetic pathways causing several diseases (Shishova et al, 2009).

In the following paragraph some results, investigating the structure and function of nt-svArginase *in vitro* are presented.

In order to elucidate the role of the spliced isoform of Arginase in humans, it was investigated, if nt-svArginase encoding mRNA is present in humans, by analyzing 20 total RNA isolates from different human tissue samples. Nt-svArginase is present in 8 out of the 20 tissues tested (Figure 33). This is in accordance with the proposed presence of nt-svArginase in different tissues on the protein level (Wilhelm et al, 2014). In some tissues tested, both the wtArginase and nt-svArginase isoforms were detected, showing similar expression levels.

Besides, the mRNA levels for the wtArginase in many tissues seemed to be under the detection limit in our experiments. Nevertheless, the presence of wtArginase was confirmed on protein level in the human proteome study (Wilhelm et al, 2014).

This might indicate that the stability of the two Arginase protein isoforms is different forcing the cell to produce more nt-svArginase mRNA, to balance the protein amounts of the two isoforms.

A

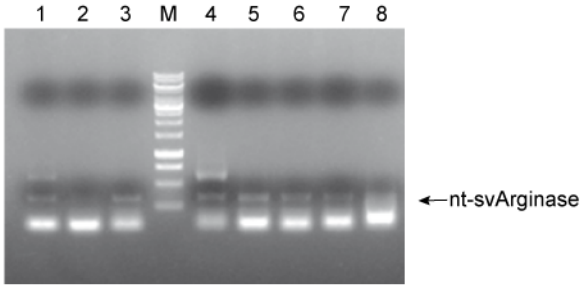

B

Tissue	Wild type		Splice Variant	
	mRNA level	protein level	mRNA level	protein level
Adrenal gland	no	yes	yes	yes
Brain cerebellum	yes	no	yes	no
Brain whole	no	no	yes	yes
Fetal brain	no	not tested	yes	not tested
Fetal liver	yes	not tested	yes	not tested
Heart	no	yes	no	yes
Kidney	no	yes	yes	yes
Lung	no	yes	no	yes
Placenta	no	no	yes	no
Prostate	no	yes	no	no
Salivary gland	no	no	yes	no
Skeletal muscle	no	no	no	no
Small intestine	no	no	no	no
Spleen	no	yes	no	yes
Stomach	no	yes	no	yes
Testis	no	yes	no	yes
Thymus	no	no	no	no
Thyroid gland	no	yes	no	yes
Trachea	no	no	no	no
Uterus	no	yes	no	yes

Figure 33: Analysis of the mRNA levels of Arginase proteins in different human tissue samples.
A) Example agarose gel (1 %) of different tissues tested. As template 1.0 µg of the respective tissue RNA was used. The respective RNA samples were reverse transcribed into cDNA followed by polymerase chain reaction. The band at 250 base pairs indicates the presence of nt-svArginase mRNA (marked by an arrow), whereas the identification of a band at approximately 350 base pairs shows the presence of wtArginase mRNA. M: DNA ladder 100 bp, 1-8: Tissue samples, 1: Brain cerebellum, 2: Brain whole, 3: Fetal brain, 4: Fetal liver, 5: Kidney, 6: Adrenal gland, 7: Placenta, 8: Salivary gland. **B)** Overview of the presence of Arginase on mRNA- (this study) and protein-level (Wilhelm et al, 2014) in 20 different human tissue samples tested.

Compared to the respective wild-type protein nt-svArginase was more instable and showed a high aggregation propensity. This is not surprising, as 27 % (85 amino acids, residues 204 – 289) of the wild-type structure, formed by α-helices and β-strands, is deleted in the spliced isoform. The thermal unfolding experiments clearly revealed differences in the unfolding behavior of both proteins (Figure 34A).

Form the literature it is known that stabilization of the quaternary structure of wtArginase is achieved mainly through intra- and intermolecular ionic interactions (Kanyo et al, 1996). Due to the presence of a 5 fold higher amount of potassium chloride in nt-svArginase sample compared to its wild-type, the slightly higher thermal stability of the isoform can be explained by the formation of more stabilizing intermolecular interactions. The addition of salt could not be avoided, to exclude precipitation of the spliced isoform. In addition, major differences between the secondary structures of both proteins were identified (Figure 34B) by Far-UV CD spectroscopy. The determination of the contents of the different secondary structural elements showed that major changes seem to occur in the α-helical regions, as well as in the antiparallel β-sheets (Figure 34B *Inset*). Due to the deletion of α-helical parts through the splicing event the strongly reduced α-helical content can be explained. Because of the spliced out β-elements in nt-svArginase also a decrease in the antiparallel β-content was expected. However the value was approximately 3 fold higher compared to wild-type.

It seems likely that non-trivial splicing might lead to structural rearrangements.

Due to the structural alterations observed for nt-svArginase it was addressed, whether the function of the protein is impaired. In a first set of experiments, the binding ability of arginine, serving as ligand in the catalyzed conversion of *L*-arginine into *L*-ornithine and urea (Di Costanzo et al, 2007), was studied. For this purpose, the thermal melting behavior of both proteins was analyzed in presence of excess *L*-arginine.

In case of ligand binding a characteristic shift in the melting transition to higher temperatures is observed. In contrast to the wt protein, no clear shifts were monitored for the splice isoform (Figure 34C). Thus, binding of arginine seems to be abolished in the splice variant. The observed strong variations in the secondary structure of the protein, very likely affected the quaternary structure of the nt-svArginase. Hence, the ligand binding ability to the catalytic center might be impossible because of sterical hindrance. Additionally, the substrate recognition in wtArginase is accomplished by amino acid residues (asparagine 130, threonine 135, serine 137, asparagine 139 and histidine 141) within two distinct N-terminal loop regions (Shishova et al, 2009). From the carboxylate side chain of the enzyme also the amino acids aspartate acid 183 and glutamic acid 186 are also involved in substrate interaction (Shishova et al, 2009). As these residues are present in nt-svArginase an altered loop structure can be expected.

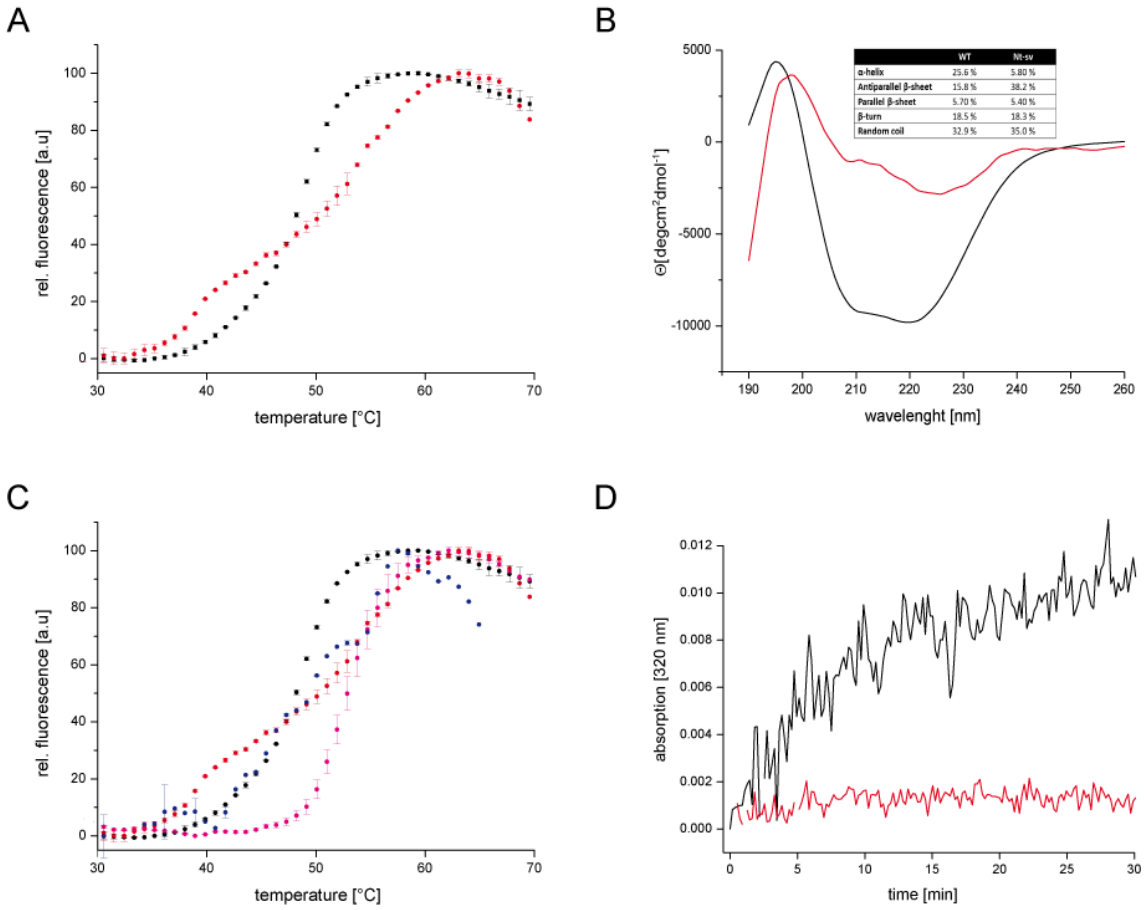

Figure 34: Nt-svArginase shows altered structural and functional characteristics.
A) Analysis of the thermal stability of wtArginase (black) and nt-svArginase (red). TSA measurements were conducted in 50 mM Tris buffer (pH 7.7) with 20 mM KCl for the wild-type and 50 mM Tris buffer (pH 9.7), containing 100 mM KCl for the non-trivial isoform. In total 1 µg of each protein was used. All calculated T_m values are means of at least three samples and the corresponding standard deviations are indicated. **B)** Secondary structure analysis: Far-UV CD spectroscopy of wtArginase (black) and nt-svArginase (red). 16 accumulations were recorded. *Inset:* Calculation of the secondary structural contents according to CDNN (Applied Photophysics). **C)** Analysis of the thermal stability in absence (wtArginase: black, nt-svArginase: red) and presence of *L*-arginine (wtArginase w *L*-Arg: magenta, nt-svArginase w *L*-Arg: blue). TSA measurements were conducted in 50 mM Tris buffer (pH 7.7) with 20 mM KCl for the wild-type and 50 mM Tris buffer (pH 9.7), containing 100 mM KCl for the non-trivial isoform. In total 1 µg of each protein was used. The ratio of protein/*L*-Arg was 1/12. All calculated T_m values are means of at least three samples and the corresponding standard deviations are indicated. **D)** Investigations of the enzymatic activity of both Arginase proteins (wtArginase: black, nt-svArginase: red). Kinetic measurements were executed at 320 nm absorption monitoring the formation of 1-nitroanilin over time (Baggio et al, 1999). Shown are the reference corrected curves. Measurements were operated with 15 µM of the respective protein at 20 °C. 1 mL starting solution consisting of 40 µL enzyme solution and 960 µL of NGB (0.1 µM) was used.

From this, it can be assumed that the enzymatic function of the protein is changed compared to wtArginase. For investigations on the enzymatic activity of nt-svArginase, 1-nitro-3-guanidiniumbenzene was used as a substrate (Baggio et al, 1999; Baggio et al, 1997). The catalytic reaction to nitroanilin and urea was monitored in absorption at 372 nm, indicating the formation of nitroanilin (Baggio et al, 1999). As expected nt-svArginase was completely inactive, whereas for the wt protein a characteristic enzymatic curve could be shown (Figure 34D).

In general Arginase catalyzed reactions proceed via metal activated hydrolysis (Baggio et al, 1997), in which a metal-bridging water molecule or hydroxide ion initiates the nucleophilic attack of the substrate guanidine carbon atom (Bewley et al, 1999). Thereby the positioning of the substrate for the nucleophilic attack is achieved by the amino acid glutamic acid 277 (Cama et al, 2003), which is missing in nt-svArginase. Furthermore, wtArginase is only completely active if each monomeric subunit consists of two symmetrically bridged manganese-ions (Christianson & Cox, 1999; Scolnick et al, 1997; Stone et al, 2010), in which one manganese-ion (Mn^{2+}_{B}) is stabilized by acid aspartic acid 232 and aspartic acid 234 (Cama et al, 2003; Kanyo et al, 1996), which is spliced out in nt-svArginase. These facts in addition to the prior discussed variations in substrate recognition and feasible changes in the catalytic center induced by structural modifications might verify the results obtained.

Weather lack in activity consequently results in a non-functional variant, not contributing to the protein diversity, needs to be further investigated by *in vivo* studies. In opposition, a regulatory role due to its inactivity might be also one possibility. Thus, a potential imbalance of the Arginase homeostasis, caused by malfunction of isoform 2, might be regulated by the presence of nt-svArginase. Whether this is attained in direct or indirect manner needs to be revised in the future.

In summary the results suggest that the non-trivial splicing event leads to a tremendous or even complete change in structure and function of nt-svArginase.

6.3 Comparison of these human non-trivial splice variants

In this section the collected results of the human non-trivial splice variants of SHMT, Arginase and Rab1A were compared. The view of these experiments was to clarify, whether general structural and functional features for all non-trivial splice variants can be retrieved and/or alterations which can be deduced from the non-trivial splice variant category can be correlated.

Basically all non-trivial splice isoforms exhibited very low expression yields and similar aggregation propensities compared to their corresponding wild type proteins. In some cases the addition of high salt concentrations to the storage buffer was mandatory to exclude precipitation (nt-svArginase). Given that the spliced proteins were even more aggregation prone during concentration, it was not possible to exceed concentrations over 50 µM. In addition long term storage of the non-trivial splice variants failed due to precipitation under various conditions.

The presence of stabilizing agents in the storage buffer also had no positive influence on enhancing their half-life. Consequently, the isoforms always needed to be freshly purified prior their use in experiments. The instability of the non-trivial variants and too low concentrations reduced the methods spectra that could be applied. For example high resolution methods for structural characterization, like NMR or X-ray crystallography, were not applicable.

Nevertheless, even though 20 % up to 40 % of the native structure is deleted in the respective non-trivial isoforms it was feasible to isolate stable and folded protein for the non-trivial variants. Thus, proteins in general seem to be more robust and tolerant against structural deletions, insertions and replacements (Birzele et al, 2008a).

The results of this thesis explicitly disproved the assumption that alternative transcripts are prone to NMD (Lareau & Brenner, 2015) or protein degradation immediately after their translation.

In fact non-trivial alternative splicing seems to contribute not only to the human proteome diversity (as illustrated by the achieved results for the non-trivial splice isoforms of human Arginase-1, cytosolic SHMT and Rab1A), but also has regulatory implication on cellular functions (as described for nt-svRab1A).

It is known from literature that on mRNA level approximately 74 % of the multi-exon genes are alternatively spliced (Kriventseva et al, 2003).

Though, it cannot be excluded that some of the many potential non-trivial spliced proteins are artifacts, which finally will not fold into stable proteins.

The comparison of the three different secondary structures showed that only minor changes were detected for the SHMT (Figure 32B) and Rab1A isoform (Figure 14A). Strong structural alterations were observed for nt-svArginase (Figure 34B). One might expect that the strongest modifications of the conformation occur to non-trivial splice variants with the highest structural deletion rate compared to their native protein. In nt-svSHMT ~ 20 % are spliced out, nt-svRab1A misses ~ 40 % of the wild-type structure and in nt-svArginase ~ 30 % are deleted. But as only minimal secondary structural variations appeared between the two extremes (nt-svRab1A and nt-svSHMT) such an easy correlation could not be verified.

Further, no conclusion about secondary structural alterations can be drawn from the affiliation of the distinct spliced protein to a certain non-trivial splice category (e.g. α-conserved motif, α/β internally conserved regions).

A common feature of these variants is their aggregation propensity, which is in line with the observed lower thermal stability compared to their wild-type proteins (Figure 18A, B, Figure 32A, Figure 34A). By analyzing the respective contents of secondary structural elements of all three isoforms it was not surprising that more prominent changes were detected in α-helical regions or β-secondary structured parts, than in random coil elements. Nt-svRab1A showed a 1.5 fold elevated β-turn content compared to its wild-type protein. In case of nt-svArginase approximately 2 times more β-sheets were present than in the native form. Also in the splice variant of SHMT the α-helical ratio was slightly increased. Thus, the alternative splicing mechanism seems to promote rearrangements of the non-trivial protein structure.

In addition it is intriguing that the non-trivial variants show a higher oligomeric quaternary structure than the respective wild-type proteins. Hence the less stable monomeric fold appears to be stabilized through oligomerization. This is underlined by the determined quaternary structures for nt-svSHMT (Figure 32C) and nt-svRab1A (Figure 14D), in which both proteins formed higher oligomers.

Besides the intramolecular contacts, oligomerization leads to the formation of additional intermolecular interfaces. Thereby the structures of the spliced isoforms are further stabilized by the additional contacts. Most likely the binding geometry results in a compact protein-protein interface, which buries potential hydrophobic surface areas that are solvent exposed in the corresponding monomer. This was verified for nt-svRab1A (Figure 14F) and need to be further addressed in the future for other non-trivial splice variants.

As presented for nt-svRab1A, hetero-oligomerization (Figure 23) also suggests being an alternative method, in which the non-trivial splice variants stabilize their structure in indirect manner by interaction with other proteins. Thereby it seems that the spliced isoforms interact either with their corresponding wild-types or with close homologues (Figure 23).

In summary the structural investigations seem to support the view that alternative splicing preferentially results in slight rearrangements and a basically conservation and adaption of the wild-type structure and not in the formation of completely new and independent domain folds or a new protein structure for the non-trivial isoforms.

The structural changes for all three characterized non-trivial splice variants (nt-svSHMT, nt-svArginase, nt-svRab1A), resulted in tremendously altered functions, compared to their respective wild-type proteins.
For Rab1A the most prominent characteristics identified were the loss of specificity for GXP's (Figure 19), the lacking activation by a GEF (Figure 20) as well as an inactivation by a GAP (Figure 21D) and its determined still slow intrinsic GTPase activity (Figure 21B). Thus, the non-trivial splicing event altered the major regulatory tool of Rab GTPases itself by completely changing its activation and inactivation mechanism. However, by co-localization experiments (Figure 26) it was possible to show, that the main reaction site of Rab1 GTPases, regulating ER to Golgi transport, was not affected in nt-svRab1A. This was also underlined by the observed membrane attachment (Figure 25B). However, the attachment itself in contrast to the wild-type was no longer dependent on prenylation (Figure 25D). Further, the results clearly elucidated that in contrast to wtRab1A, nt-svRab1A temporary activated the vesicular transport (Figure 27).
Overall, the findings indicated that nt-svRab1A is involved in regulating Rab1A and the vesicular transport in an up to now unknown new mechanism.

As binding of the substrate *L*-Arginine was due to the structural modifications completely abolished in the nt-svArginase (Figure 34C), it no longer showed enzymatic activity (Figure 34D). In future experiments it has to be analyzed if this splice variant behaves similar to nt-svRab1A in terms of interacting with its wild-type protein or other Arginase isoforms a regulatory influence would be possible. It is also imaginable that nt-svArginase even represents an isoform with a completely novel function.

In case of the isoform of SHMT, alternative splicing did also lead to severe functional changes. Due to the changed ability of co-factor binding, nt-svSHMT showed almost no enzymatic activity (Figure 32E). A regulatory influence can also not be excluded for this protein but needs to be addressed in detail in future experiments.

Overall the comparison elucidated that both members of the internally conserved α/β-category (nt-svArginase, nt-svRab1A) exhibit novel functional characteristics. Thus, alternative splicing indeed increased the functional diversity of the proteome.
Further the results for the nt-svSHMT, belonging to the α-conserved category, highlighted the potential of non-trivial splicing as regulatory tool, for reducing wild-type functionality.

In summary it might be assumed that members of the same non-trivial splice category show similar changes in functionality, as verified for nt-svArginase and nt-svRab1A. Therefore, analog to the spliced isoform of SHMT other members of the α-conserved category should also reveal reduced functionality. Representatives of other categories could even display more functional alterations up to the generation of completely inactive non-functional proteins. This could be hypothesized for members of the large scale event category (50 % structure deletion to wild-type), in which first trials in expressing the Histone deacetylase 8 (Uniprot ID: Q9BY41) failed totally. This of course has to be verified with a statistically chosen collective of protein members.
Further studies elucidating the exact conditions under which these isoforms are present *in vivo* will contribute to the general understanding of the non-trivial alternative splicing mechanism.

Overall, the results of this thesis show that alternative splicing executes a more prominent role in protein structure evolution and creation of functional diversity than previously expected.

7 Abbreviations

Abbreviations:	***Full name:***
A	Absorbance
a.u.	Arbitrary unit
Amp	Ampicillin sodium salt
APS	Ammonium persulfate
Arf	ADP –ribosylation factor
BFA	Brefeldin A
bp	Base pair
BS	Branch site
c [$molL^{-1}$]	Protein concentration
c [ms^{-1}]	Speed of light
C. elegans	*Caenorhabditis elegans*
CATCHR	Complexes associated with tethering
CD	Circular dichroism Spectroscopy
5,10-CH_2THF	*5,10*-methylene-tetrahydrofolate
Co-IP	Co-Immunoprecipitation
COP I	Coat protein complex I
COP II	Coat protein complex II
CV	Column volume
d [cm]	Path length
Da	Dalton
dDENN	Downstream DENN
ddH2O	Double distilled water
DENN	Differntially expressed in normal and neoplastic cells
DMEM	Dulbecco's Modified Eagle Medium
dNTPs	Desoxynucleotide triphosphates
DrrA	Defect in Rab recruitment A
DTT	1,4-Dithiothreit
E. coli	*Escheria coli*
EDTA	Ethylenediaminetetraacetic acid,
EE	Early Endosome
EEA1	Early Endosome antigen-1
ER	Endoplasmic reticulum
ERES	ER exit sites
ESE	Exonic splicing enhancer
ESS	Exonic splicing silencer
EtOH	Ethanol
eq.	equivalent(s)
FCS	Fetal Calf Serum
FTase	Farnesyltransferase
GAP	GTPase activating protein
GBF1	Golgi-specific brefeldin A resistant factor 1
GDF	GDI displacement factor
GDP	Guanosine 5'-diphosphate sodium salt

GEF	Guanine nucleotide exchange factor
GGTase	Rab geranylgeranyltransferase
GNBP	Guanine nucleotide binding protein
GTD	Globular tail domain
GTP	Guanosine 5’-triphosphate sodium salt hydrate
h	Hour
h [Js]	Plank constant
HEK293	Human embryonic kidney 293 cells
HEPES	2-[4-(2-hydroxyethyl)piperazin-1yl]
hnRNP	Heterologous nuclear RNP
HOMO	Highest occupied molecular orbital
HPLC	Analytical Size Exclusion Chromatography
HPLC	High Performance Liquid Chromatography
I	Emitted radiation intensity
I_0	Inclined radiation intensity
IC	Intermediate compartment
IEC	Ion Exchange Chromatography
IMAC	Immobilized Metal Ion Chromatography
$I_{\parallel}$	Parallel fluorescence intensity
IPTG	Isopropyl-β-*D*-thiogalactopyranosid
$I_{\perp}$	Perpendicular fluorescence intensity
ISE	Intronic splicing enhancer
ISS	Intronic splicing silencer
kB	Kilo base
LCP	Left circular polarized
LCV	Legionella-containing vacuole
LE	Late Endosome
LUMO	Lowest unoccupied molecular orbital
M	Molar
MANT-ADP	2’-(or-3’)-O-(*N*-Methylanthraniloyl) Adenosine 5’–diphosphate disodium salt
MANT-ATP	2’-(or-3’)-O-(*N*-Methylanthraniloyl) Adenosine 5’–triphosphate trisodium salt
MANT-GDP	2’-(or-3’)-O-(*N*-Methylanthraniloyl) Guanosine 5’–diphosphate disodium salt
MANT-GTP	2’-(or-3’)-O-(*N*-Methylanthraniloyl) Guanosine 5’–triphosphate trisodium salt
min	Minute
MRW	Mean molecular weight of the amino acid
MS	Mass spectrometry
MTC	Multisubunit tethering complex
MW [gmol-1]	Molecular weight
MWCO [kDa]	Molecular weight cutoff
N_{aa}	Number of amino acid residues
nt-sv	Non-trivial splice variant

ON	Overnight
p.a.	Pro analysi (highest purity grade)
PBS	Phosphate buffered saline
PBS-T	Phosphate buffered saline containing 0.1 % Tween 20
PCR	Polymerase Chain Reaction
pI	Isoelectric point
PM	Plasma membrane
PPT	Polypyrimidine tract
PRA-1	Prenylated Rab acceptor
r	Anisotropy
R [$Jmol^{-1}K^{-1}$]	Gas constant
r_0	Intrinsic anisotropy of the molecule
Rab	Ras-related in brain
Rabex-5	Rabaptin-5-associated exchange factor for Rab5
RabGDI	Rab GDP dissociation inhibitor
Ran	Ras –like nuclear
Ras	Ras sarcoma
RCC1	Regulator of chromosome condensation
RCP	Right circular polarized
REP	Rab escort protein
RFI	Relative fluorescence intensity
Rho	Ras homologous
rpm	Rounds per minute
RT	Room temperature
SDS-PAGE	Sodium dodecyl sulfate Polyacrylamide Electrophoresis
sec	Second
SEC	Size Exclusion Chromatography
SF1	Splice factor
SHMT	Serinehydroxymethyltransferase
SNARE	Soluble *N*-ethylmaleimide-sensitve factor
snRNA	Small nuclear ribonucleic acid
snRNP	Small nuclear ribonucleic protein
SR	Serine-arginine protein family
SRP	Signal-recognition particle
ss	Splice site
T [K]	Temperature
TBC	Tre2-Bub2-Cdc-16
TEMED	*N,N,N',N'*-Tetramethyl-ethane-1,2-diamine
tER	Transitional ER
TGN	*trans*-Golgi network
THF	Tetra-hydrofolate
TIP	Tail interacting protein
TRAPP	Transport protein particle
TRIS	Tris-(hydroxymethyl)aminomethane
Trs	TRAPP subunit
TSA	Thermal Shift Assay

U2AF	U2 auxiliary factor
uDENN	Upstream DENN
UV-VIS	Ultraviolet-Visible Absorption Spectroscopy
VAMP	Vesicle associated membrane protein
V_m [m^3mol^{-1}]	Molar volume of the fluorophore
VPS	Vascuolar protein sorting
(v/v)	Percent by volume
VTC	Vesicular tubular cluster
WT	Wild-type
(w/v)	Weight per volume
Ypt	Yeast protein transport
ΔE [J]	Energy difference
ε [$M^{-1}cm^{-1}$]	Molar extinction coefficient
η [$kgs^{-1}m^{-1}$]	Viscosity of the solvent
θ [mdeg]	Measured ellipticity at wavelength λ
θ [ns]	Rotational correlation time
θ_{MRW} [$degcm^2dmol^{-1}$]	Mean residue ellipticity at wavelength λ
λ [nm]	Wavelength
ν [Hz]	Frequency

8 References

Agrawal S, Kumar A, Srivastava V, Mishra BN (2003) Cloning, expression, activity and folding studies of serine hydroxymethyltransferase: a target enzyme for cancer chemotherapy. *J. Mol. Microbiol. Biotechnol.* **6:** 67-75

Aitzetmüller K, Asshauer J, Brown P, Colin H, Crispin T, Crombeen J, Daldrup T, Engelhardt H, Guiochon G, Halasz I (2012) *Practice of High Performance Liquid Chromatography: Applications, Equipment and Quantitative Analysis*: Springer Science & Business Media.

Aivazian D, Serrano RL, Pfeffer S (2006) TIP47 is a key effector for Rab9 localization. *J. Cell Biol.* **173:** 917-926

Ali BR, Wasmeier C, Lamoreux L, Strom M, Seabra MC (2004) Multiple regions contribute to membrane targeting of Rab GTPases. *J. Cell Sci.* **117:** 6401-6412

Allan BB, Balch WE (1999) Protein sorting by directed maturation of Golgi compartments. *Science (New York, NY)* **285:** 63-66

Archibald JM (2015) Endosymbiosis and Eukaryotic Cell Evolution. *Curr. Biol.* **25:** R911-921

Ast G (2004) How did alternative splicing evolve? *Nat. Rev. Genet.* **5:** 773-782

Atkins PW, de Paula J. (2006) Physikalische Chemie, 4. vollständig überarbeitete Auflage. Wiley-VCH, Weinheim.

Baggio R, Cox JD, Harper SL, Speicher DW, Christianson DW (1999) A new chromophoric assay for arginase activity. *Anal. Biochem.* **276:** 251-253

Baggio R, Elbaum D, Kanyo ZF, Carroll PJ, Cavalli RC, Ash DE, Christianson DW (1997) Inhibition of Mn2+ 2-arginase by borate leads to the design of a transition state analogue inhibitor, 2 (S)-amino-6-boronohexanoic acid. *J. Am. Chem. Soc.* **119:** 8107-8108

Bainton DF (1981) The discovery of lysosomes. *J. Cell Biol.* **91:** 66s-76s

Barlowe CK, Miller EA (2013) Secretory protein biogenesis and traffic in the early secretory pathway. *Genetics* **193:** 383-410

Barr F, Lambright DG (2010) Rab GEFs and GAPs. *Curr. Opin. Cell Biol.* **22:** 461-470

Barrowman J, Bhandari D, Reinisch K, Ferro-Novick S (2010) TRAPP complexes in membrane traffic: convergence through a common Rab. *Nat. Rev. Mol. Cell Biol.* **11:** 759-763

Bennett MK, Scheller RH (1993) The molecular machinery for secretion is conserved from yeast to neurons. *Proc. Natl. Acad. Sci.USA* **90:** 2559-2563

Bepperling A, Alte F, Kriehuber T, Braun N, Weinkauf S, Groll M, Haslbeck M, Buchner J (2012) Alternative bacterial two-component small heat shock protein systems. *Proc. Natl. Acad. Sci.USA* **109:** 20407-20412

Berget SM (1995) Exon recognition in vertebrate splicing. *J. Biol. Chem.* **270:** 2411-2414

Berndt N, Sebti SM (2011) Measurement of protein farnesylation and geranylgeranylation in vitro, in cultured cells and in biopsies, and the effects of prenyl transferase inhibitors. *Nat. Protoc.* **6:** 1775-1791

Bewley MC, Jeffrey PD, Patchett ML, Kanyo ZF, Baker EN (1999) Crystal structures of Bacillus caldovelox arginase in complex with substrate and inhibitors reveal new insights into activation, inhibition and catalysis in the arginase superfamily. *Structure (London, England : 1993)* **7:** 435-448

Bhuin T, Roy JK (2014) Rab proteins: the key regulators of intracellular vesicle transport. *Exp. Cell Res.* **328:** 1-19

Birnboim HC, Doly J (1979) A rapid alkaline extraction procedure for screening recombinant plasmid DNA. *Nucleic Acids Res.* **7:** 1513-1523

Birzele F, Csaba G, Zimmer R (2008a) Alternative splicing and protein structure evolution. *Nucleic Acids Res.* **36:** 550-558

Birzele F, Kuffner R, Meier F, Oefinger F, Potthast C, Zimmer R (2008b) ProSAS: a database for analyzing alternative splicing in the context of protein structures. *Nucleic Acids Res.* **36:** D63-68

Black DL (2003) MECHANISMS OF ALTERNATIVE PRE-MESSENGER RNA SPLICING. *Annu. Rev. Biochem.* **72:** 291-336

Bock JB, Matern HT, Peden AA, Scheller RH (2001) A genomic perspective on membrane compartment organization. *Nature* **409:** 839-841

Böhm G, Muhr R, Jaenicke R (1992) Quantitative analysis of protein far UV circular dichroism spectra by neural networks. *Protein Eng.* **5:** 191-195

Bourne HR, Sanders DA, McCormick F (1991) The GTPase superfamily: conserved structure and molecular mechanism. *Nature* **349:** 117-127

Braakman I, Bulleid NJ (2011) Protein folding and modification in the mammalian endoplasmic reticulum. *Annu. Rev. Biochem.* **80:** 71-99

Bradford MM (1976) A rapid and sensitive method for the quantitation of microgram quantities of protein utilizing the principle of protein-dye binding. *Anal. Biochem.* **72:** 248-254

Braunschweig U, Gueroussov S, Plocik AM, Graveley BR, Blencowe BJ (2013) Dynamic integration of splicing within gene regulatory pathways. *Cell* **152:** 1252-1269

Brocker C, Engelbrecht-Vandre S, Ungermann C (2010) Multisubunit tethering complexes and their role in membrane fusion. *Curr. Biol.* **20:** R943-952

Cai H, Reinisch K, Ferro-Novick S (2007) Coats, tethers, Rabs, and SNAREs work together to mediate the intracellular destination of a transport vesicle. *Dev. Cell* **12:** 671-682

Cama E, Emig FA, Ash DE, Christianson DW (2003) Structural and functional importance of first-shell metal ligands in the binuclear manganese cluster of arginase I. *Biochemistry* **42:** 7748-7758

Carney DS, Davies BA, Horazdovsky BF (2006) Vps9 domain-containing proteins: activators of Rab5 GTPases from yeast to neurons. *Trends Cell Biol.* **16:** 27-35

Cartegni L, Chew SL, Krainer AR (2002) Listening to silence and understanding nonsense: exonic mutations that affect splicing. *Nat. Rev. Genet.* **3:** 285-298

Chattopadhyay A, Raghuraman H (2004) Application of fluorescence spectroscopy to membrane protein structure and dynamics. *Curr. Science* **87:** 175-180

Chen M, Manley JL (2009) Mechanisms of alternative splicing regulation: insights from molecular and genomics approaches. *Nat. Rev. Mol. Cell Biol.* **10:** 741-754

Cheng W, Yin K, Lu D, Li B, Zhu D, Chen Y, Zhang H, Xu S, Chai J, Gu L (2012) Structural Insights into a Unique Legionella pneumophila Effector LidA Recognizing Both GDP and GTP Bound Rab1 in Their Active State. *PLoS Pathog.* **8:** e1002528

Christianson DW, Cox JD (1999) Catalysis by metal-activated hydroxide in zinc and manganese metalloenzymes. *Annu. Rev. Biochem.* **68:** 33-57

Chua CE, Tang BL (2015) Role of Rab GTPases and their interacting proteins in mediating metabolic signalling and regulation. *Cell. Mol. Life Sci.: CMLS* **72:** 2289-2304

Citterio C, Vichi A, Pacheco-Rodriguez G, Aponte AM, Moss J, Vaughan M (2008) Unfolded protein response and cell death after depletion of brefeldin A-inhibited guanine nucleotide-exchange protein GBF1. *Proc. Natl. Acad. Sci. USA* **105:** 2877-2882

Colicelli J (2004) Human RAS superfamily proteins and related GTPases. *Science's STKE: signal transduction knowledge environment* **2004:** Re13

Creighton TE, Chasman DI (1997) *Protein structure: a practical approach*, Vol. 26: IRL press Oxford.

Csaba G, Birzele F, Zimmer R (2008) Protein structure alignment considering phenotypic plasticity. *Bioinformatics* **24:** i98-104

Cullen BR, Malim MH (1992) Secreted placental alkaline phosphatase as a eukaryotic reporter gene. In *Methods Enzymol.*, Ray W (ed), Vol. Volume 216, pp 362-368. Academic Press

Cunningham F, Amode MR, Barrell D, Beal K, Billis K, Brent S, Carvalho-Silva D, Clapham P, Coates G, Fitzgerald S, Gil L, Giron CG, Gordon L, Hourlier T, Hunt SE, Janacek SH, Johnson N, Juettemann T, Kahari AK, Keenan S, Martin FJ, Maurel T, McLaren W, Murphy DN, Nag R, Overduin B, Parker A, Patricio M, Perry E, Pignatelli M, Riat HS, Sheppard D, Taylor K, Thormann A, Vullo A, Wilder SP, Zadissa A, Aken BL, Birney E, Harrow J, Kinsella R, Muffato M, Ruffier M, Searle SM, Spudich G, Trevanion SJ, Yates A, Zerbino DR, Flicek P (2015) Ensembl 2015. *Nucleic Acids Res.* **43:** D662-669

Di Costanzo L, Pique ME, Christianson DW (2007) Crystal structure of human arginase I complexed with thiosemicarbazide reveals an unusual thiocarbonyl mu-sulfide ligand in the binuclear manganese cluster. *J. Am. Chem. Soc.* **129:** 6388-6389

Di Costanzo L, Sabio G, Mora A, Rodriguez PC, Ochoa AC, Centeno F, Christianson DW (2005) Crystal structure of human arginase I at 1.29-A resolution and exploration of inhibition in the immune response. *Proc. Natl. Acad. Sci. USA* **102:** 13058-13063

Dong N, Zhu Y, Lu Q, Hu L, Zheng Y, Shao F (2012) Structurally Distinct Bacterial TBC-like GAPs Link Arf GTPase to Rab1 Inactivation to Counteract Host Defenses. *Cell* **150:** 1029-1041

Erdman RA, Shellenberger KE, Overmeyer JH, Maltese WA (2000) Rab24 is an atypical member of the Rab GTPase family. Deficient GTPase activity, GDP dissociation inhibitor interaction, and prenylation of Rab24 expressed in cultured cells. *J. Biol. Chem.* **275:** 3848-3856

Espinosa EJ, Calero M, Sridevi K, Pfeffer SR (2009) RhoBTB3: a Rho GTPase-family ATPase required for endosome to Golgi transport. *Cell* **137:** 938-948

Eswaran J, Horvath A, Godbole S, Reddy SD, Mudvari P, Ohshiro K, Cyanam D, Nair S, Fuqua SA, Polyak K, Florea LD, Kumar R (2013) RNA sequencing of cancer reveals novel splicing alterations. *Sci. Rep.* **3:** 1689

Etienne-Manneville S, Hall A (2002) Rho GTPases in cell biology. *Nature* **420:** 629-635

Fairbanks G, Steck TL, Wallach DFH (1971) Electrophoretic analysis of the major polypeptides of the human erythrocyte membrane. *Biochemistry* **10:** 2606-2617

Farnsworth CC, Seabra MC, Ericsson LH, Gelb MH, Glomset JA (1994) Rab geranylgeranyl transferase catalyzes the geranylgeranylation of adjacent cysteines in the small GTPases Rab1A, Rab3A, and Rab5A. *Proc. Natl. Acad. Sci. USA* **91:** 11963-11967

Fischer von Mollard G, Stahl B, Li C, Sudhof TC, Jahn R (1994) Rab proteins in regulated exocytosis. *Trends Biochem. Sci.* **19:** 164-168

Fling SP, Gregerson DS (1986) Peptide and protein molecular weight determination by electrophoresis using a high-molarity tris buffer system without urea. *Anal. Biochem.* **155:** 83-88

Frasa MA, Koessmeier KT, Ahmadian MR, Braga VM (2012) Illuminating the functional and structural repertoire of human TBC/RABGAPs. *Nat. Rev. Mol. Cell Biol.* **13:** 67-73

Garcia IA, Martinez HE, Alvarez C (2011) Rab1b regulates COPI and COPII dynamics in mammalian cells. *Cell Logist.* **1:** 159-163

Gavriljuk K, Gazdag EM, Itzen A, Kotting C, Goody RS, Gerwert K (2012) Catalytic mechanism of a mammalian Rab.RabGAP complex in atomic detail. *Proc. Natl. Acad. Sci. USA* **109:** 21348-21353

Gavriljuk K, Itzen A, Goody RS, Gerwert K, Kötting C (2013) Membrane extraction of Rab proteins by GDP dissociation inhibitor characterized using attenuated total reflection infrared spectroscopy. *Proc. Natl. Acad. Sci. USA* **110:** 13380-13385

Ghomashchi F, Zhang X, Liu L, Gelb MH (1995) Binding of prenylated and polybasic peptides to membranes: affinities and intervesicle exchange. *Biochemistry* **34:** 11910-11918

Goldberg J (1998) Structural basis for activation of ARF GTPase: mechanisms of guanine nucleotide exchange and GTP-myristoyl switching. *Cell* **95:** 237-248

Gonzalez Jr L, Scheller RH (1999) Regulation of Membrane Trafficking: Structural Insights from a Rab/Effector Complex. *Cell* **96:** 755-758

Goody PR, Heller K, Oesterlin LK, Müller MP, Itzen A, Goody RS (2012) Reversible phosphocholination of Rab proteins by Legionella pneumophila effector proteins. *EMBO J.* **31:** 1774-1784

Goody RS, Hofmann-Goody W (2002) Exchange factors, effectors, GAPs and motor proteins: common thermodynamic and kinetic principles for different functions. *Eur. Biophys. J.: EBJ* **31:** 268-274

Goody RS, Itzen A (2013) Modulation of small GTPases by Legionella. *Curr. Top. Microbiol. Immunol.* **376:** 117-133

Gopal R, Park JS, Seo CH, Park Y (2012) Applications of circular dichroism for structural analysis of gelatin and antimicrobial peptides. *Int. J. Mol. Sci.* **13:** 3229-3244

Göttle M, Dove S, Steindel P, Shen Y, Tang W-J, Geduhn J, König B, Seifert R (2007) Molecular Analysis of the Interaction of Bordetella pertussis Adenylyl Cyclase with Fluorescent Nucleotides. *Mol. Pharmacol.* **72:** 526-535

Guo Y, Linstedt AD (2013) Binding of the vesicle docking protein p115 to the GTPase Rab1b regulates membrane recruitment of the COPI vesicle coat. *Cell. Logist.* **3:** e27687

Haas AK, Yoshimura S, Stephens DJ, Preisinger C, Fuchs E, Barr FA (2007) Analysis of GTPase-activating proteins: Rab1 and Rab43 are key Rabs required to maintain a functional Golgi complex in human cells. *J. Cell Sci.* **120:** 2997-3010

Haas J, Park E-C, Seed B (1996) Codon usage limitation in the expression of HIV-1 envelope glycoprotein. *Curr. Biol.* **6:** 315-324

Hall A (1990) The cellular functions of small GTP-binding proteins. *Science (New York, NY)* **249:** 635-640

Hall A, Self AJ (1986) The effect of Mg2+ on the guanine nucleotide exchange rate of p21N-ras. *J. Biol. Chem.* **261:** 10963-10965

Han S, Viola RE (2001) A spectrophotometric assay of arginase. *Anal. Biochem.* **295:** 117-119

Hong W (2005) SNAREs and traffic. *Biochim. Biophys. Acta* **1744:** 493-517

Hoskins AA, Moore MJ (2012) The spliceosome: a flexible, reversible macromolecular machine. *Trends Biochem. Sci.* **37:** 179-188

Hutagalung AH, Novick PJ (2011) Role of Rab GTPases in membrane traffic and cell physiology. *Physiol. Rev.* **91:** 119-149

Ilies M, Di Costanzo L, North ML, Scott JA, Christianson DW (2010) 2-aminoimidazole amino acids as inhibitors of the binuclear manganese metalloenzyme human arginase I. *J. Med. Chem.* **53:** 4266-4276

Ingmundson A, Delprato A, Lambright DG, Roy CR (2007) Legionella pneumophila proteins that regulate Rab1 membrane cycling. *Nature* **450:** 365-369

Itzen A, Goody RS (2011) GTPases involved in vesicular trafficking: structures and mechanisms. *Sem. Cell Dev. Biol.* **22:** 48-56

Jahn R, Scheller RH (2006) SNAREs--engines for membrane fusion. *Nat. Rev. Mol. Cell Biol.* **7:** 631-643

Jaillon O, Bouhouche K, Gout JF, Aury JM, Noel B, Saudemont B, Nowacki M, Serrano V, Porcel BM, Segurens B, Le Mouel A, Lepere G, Schachter V, Betermier M, Cohen J, Wincker P, Sperling L, Duret L, Meyer E (2008) Translational control of intron splicing in eukaryotes. *Nature* **451:** 359-362

John J, Rensland H, Schlichting I, Vetter I, Borasio GD, Goody RS, Wittinghofer A (1993) Kinetic and structural analysis of the Mg(2+)-binding site of the guanine nucleotide-binding protein p21H-ras. *J. Biol. Chem.* **268:** 923-929

Johnson WC (1990) Protein secondary structure and circular dichroism: A practical guide. *Proteins: Struct., Funct., Bioinf.* **7:** 205-214

Jordens I, Marsman M, Kuijl C, Neefjes J (2005) Rab proteins, connecting transport and vesicle fusion. *Traffic (Copenhagen, Denmark)* **6:** 1070-1077

Kalin S, Hirschmann DT, Buser DP, Spiess M (2015) Rabaptin5 is recruited to endosomes by Rab4 and Rabex5 to regulate endosome maturation. *J. Cell Sci.* **128:** 4126-4137

Kanyo ZF, Scolnick LR, Ash DE, Christianson DW (1996) Structure of a unique binuclear manganese cluster in arginase. *Nature* **383:** 554-557

Kaufmann KW, Lemmon GH, Deluca SL, Sheehan JH, Meiler J (2010) Practically useful: what the Rosetta protein modeling suite can do for you. *Biochemistry* **49:** 2987-2998

Kelly SM, Jess TJ, Price NC (2005) How to study proteins by circular dichroism. *Biochim. Biophys. Acta* **1751:** 119-139

Keren H, Lev-Maor G, Ast G (2010) Alternative splicing and evolution: diversification, exon definition and function. *Nat. Rev. Genet.* **11:** 345-355

Kijima Y, Ogunbunmi E, Fleischer S (1991) Drug action of thapsigargin on the Ca2+ pump protein of sarcoplasmic reticulum. *J. Biol. Chem.* **266:** 22912-22918

Kim E, Goren A, Ast G (2008) Alternative splicing: current perspectives. *BioEssays: news and reviews in molecular, cellular and developmental biology* **30:** 38-47

Kim E, Magen A, Ast G (2007) Different levels of alternative splicing among eukaryotes. *Nucleic Acids Res.* **35:** 125-131

Kim M-S, Pinto SM, Getnet D, Nirujogi RS, Manda SS, Chaerkady R, Madugundu AK, Kelkar DS, Isserlin R, Jain S, Thomas JK, Muthusamy B, Leal-Rojas P, Kumar P, Sahasrabuddhe NA, Balakrishnan L, Advani J, George B, Renuse S, Selvan LDN, Patil AH, Nanjappa V, Radhakrishnan A, Prasad S, Subbannayya T, Raju R, Kumar M, Sreenivasamurthy SK, Marimuthu A, Sathe GJ, Chavan S, Datta KK, Subbannayya Y, Sahu A, Yelamanchi SD, Jayaram S, Rajagopalan P, Sharma J, Murthy KR, Syed N, Goel R, Khan AA, Ahmad S, Dey G, Mudgal K, Chatterjee A, Huang T-C, Zhong J, Wu X, Shaw PG, Freed D, Zahari MS, Mukherjee KK, Shankar S, Mahadevan A, Lam H, Mitchell CJ, Shankar SK, Satishchandra P, Schroeder JT, Sirdeshmukh R, Maitra A, Leach SD, Drake CG, Halushka MK, Prasad TSK, Hruban RH, Kerr CL, Bader GD, Iacobuzio-Donahue CA, Gowda H, Pandey A (2014) A draft map of the human proteome. *Nature* **509:** 575-581

Klebe C, Prinz H, Wittinghofer A, Goody RS (1995) The kinetic mechanism of Ran-nucleotide exchange catalyzed by RCC1. *Biochemistry* **34:** 12543-12552

Kohnke M, Delon C, Hastie ML, Nguyen UT, Wu YW, Waldmann H, Goody RS, Gorman JJ, Alexandrov K (2013) Rab GTPase prenylation hierarchy and its potential role in choroideremia disease. *PloS one* **8:** e81758

Kraulis PJ, Domaille PJ, Campbell-Burk SL, Van Aken T, Laue ED (1994) Solution structure and dynamics of ras p21.GDP determined by heteronuclear three- and four-dimensional NMR spectroscopy. *Biochemistry* **33:** 3515-3531

Krawczak M, Reiss J, Cooper DN (1992) The mutational spectrum of single base-pair substitutions in mRNA splice junctions of human genes: causes and consequences. *J. Hum. Genet.* **90:** 41-54

Krishna Rao JV, Jagath JR, Sharma B, Appaji Rao N, Savithri HS (1999) Asp-89: a critical residue in maintaining the oligomeric structure of sheep liver cytosolic serine hydroxymethyltransferase. *Biochem. J.* **343 Pt 1:** 257-263

Kriventseva EV, Koch I, Apweiler R, Vingron M, Bork P, Gelfand MS, Sunyaev S (2003) Increase of functional diversity by alternative splicing. *Trends Genet.* **19:** 124-128

Lachance V, Angers S, Parent JL (2014) New insights in the regulation of Rab GTPases by G protein-coupled receptors. *Small GTPases* **5:** 1-5

Lacowicz JR (2006) *Protein fluorescence*, Vol. 6: Springer Science & Business Media.

Laemmli UK (1970) Cleavage of Structural Proteins during the Assembly of the Head of Bacteriophage T4. *Nature* **227:** 680-685

Langemeyer L, Nunes Bastos R, Cai Y, Itzen A, Reinisch KM, Barr FA (2014) Diversity and plasticity in Rab GTPase nucleotide release mechanism has consequences for Rab activation and inactivation. *Elife* **3:** e01623

Lanoix J, Ouwendijk J, Lin CC, Stark A, Love HD, Ostermann J, Nilsson T (1999) GTP hydrolysis by arf-1 mediates sorting and concentration of Golgi resident enzymes into functional COP I vesicles. *EMBO J.* **18:** 4935-4948

Lanoix J, Ouwendijk J, Stark A, Szafer E, Cassel D, Dejgaard K, Weiss M, Nilsson T (2001) Sorting of Golgi resident proteins into different subpopulations of COPI vesicles: a role for ArfGAP1. *J. Cell Biol.* **155:** 1199-1212

Lareau LF, Brenner SE (2015) Regulation of splicing factors by alternative splicing and NMD is conserved between kingdoms yet evolutionarily flexible. *Mol. Biol. Evol.*

Lareau LF, Inada M, Green RE, Wengrod JC, Brenner SE (2007) Unproductive splicing of SR genes associated with highly conserved and ultraconserved DNA elements. *Nature* **446:** 926-929

Lazar T, Gotte M, Gallwitz D (1997) Vesicular transport: how many Ypt/Rab-GTPases make a eukaryotic cell? *Trends Biochem. Sci.* **22:** 468-472

Leaver-Fay A, Tyka M, Lewis SM, Lange OF, Thompson J, Jacak R, Kaufman K, Renfrew PD, Smith CA, Sheffler W, Davis IW, Cooper S, Treuille A, Mandell DJ, Richter F, Ban YE, Fleishman SJ, Corn JE, Kim DE, Lyskov S, Berrondo M, Mentzer S, Popovic Z, Havranek JJ, Karanicolas J, Das R, Meiler J, Kortemme T, Gray JJ, Kuhlman B, Baker D, Bradley P (2011) ROSETTA3: an object-oriented software suite for the simulation and design of macromolecules. *Methods Enzymol.* **487:** 545-574

Leipe DD, Wolf YI, Koonin EV, Aravind L (2002) Classification and evolution of P-loop GTPases and related ATPases. *J. Mol. Biol.* **317:** 41-72

Li F, Yi L, Zhao L, Itzen A, Goody RS, Wu Y-W (2014) The role of the hypervariable C-terminal domain in Rab GTPases membrane targeting. *Proc. Natl. Acad. Sci. USA* **111:** 2572-2577

Lipatova Z, Tokarev AA, Jin Y, Mulholland J, Weisman LS, Segev N (2008) Direct interaction between a myosin V motor and the Rab GTPases Ypt31/32 is required for polarized secretion. *Mol. Biol. Cell* **19:** 4177-4187

Liu H-X, Cartegni L, Zhang MQ, Krainer AR (2001a) A mechanism for exon skipping caused by nonsense or missense mutations in BRCA1 and other genes. *Nat. Genet.* **27:** 55-58

Liu X, Reig B, Nasrallah IM, Stover PJ (2000) Human cytoplasmic serine hydroxymethyltransferase is an mRNA binding protein. *Biochemistry* **39:** 11523-11531

Liu X, Szebenyi DM, Anguera MC, Thiel DJ, Stover PJ (2001b) Lack of catalytic activity of a murine mRNA cytoplasmic serine hydroxymethyltransferase splice variant: evidence against alternative splicing as a regulatory mechanism. *Biochemistry* **40:** 4932-4939

Lo M-C, Aulabaugh A, Jin G, Cowling R, Bard J, Malamas M, Ellestad G (2004) Evaluation of fluorescence-based thermal shift assays for hit identification in drug discovery. *Anal. Biochem.* **332:** 153-159

Loirand G, Sauzeau V, Pacaud P (2013) Small G proteins in the cardiovascular system: physiological and pathological aspects. *Physiol. Rev.* **93:** 1659-1720

Lord C, Ferro-Novick S, Miller EA (2013) The highly conserved COPII coat complex sorts cargo from the endoplasmic reticulum and targets it to the golgi. *Cold Spring Harb. Perspect. Biol.* **5**

Lytton J, Westlin M, Hanley MR (1991) Thapsigargin inhibits the sarcoplasmic or endoplasmic reticulum Ca-ATPase family of calcium pumps. *J. Biol. Chem.* **266:** 17067-17071

Machner MP, Isberg RR (2006) Targeting of Host Rab GTPase Function by the Intravacuolar Pathogen Legionella pneumophila. *Dev. Cell* **11:** 47-56

Machner MP, Isberg RR (2007) A bifunctional bacterial protein links GDI displacement to Rab1 activation. *Science (New York, NY)* **318:** 974-977

Mancias JD, Goldberg J (2005) Exiting the endoplasmic reticulum. *Traffic (Copenhagen, Denmark)* **6:** 278-285

Mandell DJ, Coutsias EA, Kortemme T (2009) Sub-angstrom accuracy in protein loop reconstruction by robotics-inspired conformational sampling. *Nat. Methods* **6:** 551-552

Manolea F, Claude A, Chun J, Rosas J, Melancon P (2008) Distinct functions for Arf guanine nucleotide exchange factors at the Golgi complex: GBF1 and BIGs are required for assembly and maintenance of the Golgi stack and trans-Golgi network, respectively. *Mol. Biol. Cell* **19:** 523-535

Marat AL, Dokainish H, McPherson PS (2011) DENN domain proteins: regulators of Rab GTPases. *J. Biol. Chem.* **286:** 13791-13800

Masters C, Crane D (1996) Recent developments in peroxisome biology. *Endeavour* **20:** 68-73

Mellman I, Warren G (2000) The road taken: past and future foundations of membrane traffic. *Cell* **100:** 99-112

Memon AR (2004) The role of ADP-ribosylation factor and SAR1 in vesicular trafficking in plants. *Biochim. Biophys. Acta* **1664:** 9-30

Mihai Gazdag E, Streller A, Haneburger I, Hilbi H, Vetter IR, Goody RS, Itzen A (2013) Mechanism of Rab1b deactivation by the Legionella pneumophila GAP LepB. *EMBO Rep.* **14:** 199-205

Monetta P, Slavin I, Romero N, Alvarez C (2007) Rab1b interacts with GBF1 and modulates both ARF1 dynamics and COPI association. *Mol. Biol. Cell* **18:** 2400-2410

Mukherjee S, Liu X, Arasaki K, McDonough J, Galan JE, Roy CR (2011) Modulation of Rab GTPase function by a protein phosphocholine transferase. *Nature* **477:** 103-106

Murthy SNP, Lorand L (2000) Nucleotide binding by the erythrocyte transglutaminase/Gh protein, probed with fluorescent analogs of GTP and GDP. *Proc. Natl. Acad. Sci. USA* **97:** 7744-7747

Nan X, Tamguney TM, Collisson EA, Lin LJ, Pitt C, Galeas J, Lewis S, Gray JW, McCormick F, Chu S (2015) Ras-GTP dimers activate the Mitogen-Activated Protein Kinase (MAPK) pathway. *Proc. Natl. Acad. Sci. USA* **112:** 7996-8001

Nebenfuhr A, Ritzenthaler C, Robinson DG (2002) Brefeldin A: deciphering an enigmatic inhibitor of secretion. *Plant Physiol.* **130:** 1102-1108

Nielsen E, Severin F, Backer JM, Hyman AA, Zerial M (1999) Rab5 regulates motility of early endosomes on microtubules. *Nat. Cell Biol.* **1:** 376-382

Niesen FH, Berglund H, Vedadi M (2007) The use of differential scanning fluorimetry to detect ligand interactions that promote protein stability. *Nat. Protoc.* **2:** 2212-2221

Nieto Moreno N, Giono LE, Cambindo Botto AE, Munoz MJ, Kornblihtt AR (2015) Chromatin, DNA structure and alternative splicing. *FEBS Lett.* **589:** 3370-3378

Nilsen TW, Graveley BR (2010) Expansion of the eukaryotic proteome by alternative splicing. *Nature* **463:** 457-463

Novick P, Zerial M (1997) The diversity of Rab proteins in vesicle transport. *Curr. Opin.Cell Biol.* **9:** 496-504

Nowak DE, Tian B, Brasier AR (2005) Two-step cross-linking method for identification of NF-kappaB gene network by chromatin immunoprecipitation. *BioTechniques* **39:** 715-725

Oesterlin LK, Goody RS, Itzen A (2012) Posttranslational modifications of Rab proteins cause effective displacement of GDP dissociation inhibitor. *Proc. Natl. Acad. Sci. USA* **109:** 5621-5626

Overmeyer JH, Wilson AL, Erdman RA, Maltese WA (1998) The putative "switch 2" domain of the Ras-related GTPase, Rab1B, plays an essential role in the interaction with Rab escort protein. *Mol. Biol. Cell* **9:** 223-235

Paduch M, Jelen F, Otlewski J (2001) Structure of small G proteins and their regulators. *Acta Biochim. Pol.* **48:** 829-850

Pan X, Eathiraj S, Munson M, Lambright DG (2006) TBC-domain GAPs for Rab GTPases accelerate GTP hydrolysis by a dual-finger mechanism. *Nature* **442:** 303-306

Papanikou E, Glick BS (2014) Golgi compartmentation and identity. *Curr. Opin. Cell Biol.* **29:** 74-81

Park HH (2013) Structural basis of membrane trafficking by Rab family small G protein. *Int. J. of Mol. Sci.* **14:** 8912-8923

Pereira-Leal JB, Hume AN, Seabra MC (2001) Prenylation of Rab GTPases: molecular mechanisms and involvement in genetic disease. *FEBS Lett.* **498:** 197-200

Pereira-Leal JB, Seabra MC (2000) The mammalian Rab family of small GTPases: definition of family and subfamily sequence motifs suggests a mechanism for functional specificity in the Ras superfamily. *J. Mol. Biol.* **301:** 1077-1087

Pereira-Leal JB, Seabra MC (2001) Evolution of the Rab family of small GTP-binding proteins. *J. Mol. Biol.* **313:** 889-901

Pereira-Leal JB, Strom M, Godfrey RF, Seabra MC (2003) Structural determinants of Rab and Rab Escort Protein interaction: Rab family motifs define a conserved binding surface. *Biochem. Biophys. Res. Commun.* **301:** 92-97

Pfeffer S, Aivazian D (2004) Targeting Rab GTPases to distinct membrane compartments. *Nat. Rev. Mol. Cell Biol.* **5:** 886-896

Pisareva VP, Hellen CUT, Pestova TV (2007) Kinetic Analysis of the Interaction of Guanine Nucleotides with Eukaryotic Translation Initiation Factor eIF5B†. *Biochemistry* **46:** 2622-2629

Pisareva VP, Pisarev AV, Hellen CUT, Rodnina MV, Pestova TV (2006) Kinetic analysis of interaction of eukaryotic release factor 3 with guanine nucleotides. *J. Biol. Chem.*

Porath J, Carlsson JAN, Olsson I, Belfrage G (1975) Metal chelate affinity chromatography, a new approach to protein fractionation. *Nature* **258:** 598-599

Pryer NK, Wuestehube LJ, Schekman R (1992) Vesicle-mediated protein sorting. *Annu. Rev. Biochem.* **61:** 471-516

Qu L-B, Chen X-L, Yang R, Wang L, Zeng H-J (2007) Investigation of the Interaction between Isoflavonoids and Bovine Serum Albumin by Fluorescence Spectroscopy. *Chin. J. Chem.* **25:** 1151-1155

Raj B, Blencowe BJ (2015) Alternative Splicing in the Mammalian Nervous System: Recent Insights into Mechanisms and Functional Roles. *Neuron* **87:** 14-27

Rak A, Fedorov R, Alexandrov K, Albert S, Goody RS, Gallwitz D, Scheidig AJ (2000) Crystal structure of the GAP domain of Gyp1p: first insights into interaction with Ypt/Rab proteins. *EMBO J.* **19:** 5105-5113

Rak A, Pylypenko O, Niculae A, Goody RS, Alexandrov K (2003) Crystallization and preliminary X-ray diffraction analysis of monoprenylated Rab7 GTPase in complex with Rab escort protein 1. *J. Struct. Biol.* **141:** 93-95

Renault L, Guibert B, Cherfils J (2003) Structural snapshots of the mechanism and inhibition of a guanine nucleotide exchange factor. *Nature* **426:** 525-530

Renault L, Kuhlmann J, Henkel A, Wittinghofer A (2001) Structural Basis for Guanine Nucleotide Exchange on Ran by the Regulator of Chromosome Condensation (RCC1). *Cell* **105:** 245-255

Renwick SB, Snell K, Baumann U (1998) The crystal structure of human cytosolic serine hydroxymethyltransferase: a target for cancer chemotherapy. *Structure (London, England : 1993)* **6:** 1105-1116

Repasky GA, Chenette EJ, Der CJ (2004) Renewing the conspiracy theory debate: does Raf function alone to mediate Ras oncogenesis? *Trends Cell Biol.* **14:** 639-647

Rimmer CA (2011) Lloyd R. Snyder, Joseph J. Kirkland, John W. Dolan: Introduction to modern liquid chromatography. *Anal. Bioanal. Chem.* **399:** 1809-1810

Romero N, Dumur CI, Martinez H, Garcia IA, Monetta P, Slavin I, Sampieri L, Koritschoner N, Mironov AA, De Matteis MA, Alvarez C (2013) Rab1b overexpression modifies Golgi size and gene expression in HeLa cells and modulates the thyrotrophin response in thyroid cells in culture. *Mol. Biol. Cell* **24:** 617-632

Rothman JE, Wieland FT (1996) Protein sorting by transport vesicles. *Science (New York, NY)* **272:** 227-234

Sandoval CO, Simmen T (2012) Rab proteins of the endoplasmic reticulum: functions and interactors. *Biochem. Soc. Trans.* **40:** 1426-1432

Saraste M, Sibbald PR, Wittinghofer A (1990) The P-loop--a common motif in ATP- and GTP-binding proteins. *Trends Biochem. Sci.* **15:** 430-434

Sasaki T, Kikuchi A, Araki S, Hata Y, Isomura M, Kuroda S, Takai Y (1990) Purification and characterization from bovine brain cytosol of a protein that inhibits the dissociation of GDP from and the subsequent binding of GTP to smg p25A, a ras p21-like GTP-binding protein. *J. Biol. Chem.* **265:** 2333-2337

Schagger H, von Jagow G (1987) Tricine-sodium dodecyl sulfate-polyacrylamide gel electrophoresis for the separation of proteins in the range from 1 to 100 kDa. *Anal. Biochem.* **166:** 368-379

Schirch V, Hopkins S, Villar E, Angelaccio S (1985) Serine hydroxymethyltransferase from Escherichia coli: purification and properties. *J. Bacteriol.* **163:** 1-7

Schlichting I, Almo SC, Rapp G, Wilson K, Petratos K, Lentfer A, Wittinghofer A, Kabsch W, Pai EF, Petsko GA, et al. (1990) Time-resolved X-ray crystallographic study of the conformational change in Ha-Ras p21 protein on GTP hydrolysis. *Nature* **345:** 309-315

Schoebel S, Cichy AL, Goody RS, Itzen A (2011) Protein LidA from Legionella is a Rab GTPase supereffector. *Proc. Natl. Acad. Sci. USA* **108:** 17945-17950

Schoebel S, Oesterlin LK, Blankenfeldt W, Goody RS, Itzen A (2009) RabGDI Displacement by DrrA from Legionella Is a Consequence of Its Guanine Nucleotide Exchange Activity. *Mol. Cell* **36:** 1060-1072

Schöppner P, Csaba G, Braun T, Daake M, Richter B, Lange OF, Zacharias M, Zimmer R, Haslbeck M Regulatory implications of non-trivial splicing: Isoform 3 of Rab1A shows enhanced basal activity and is not controlled by accessory proteins. *J. Mol. Biol.*

Schreiber K, Csaba G, Haslbeck M, Zimmer R (2015) Alternative Splicing in Next Generation Sequencing Data of Saccharomyces cerevisiae. *PloS one* **10:** e0140487

Schwerk C, Schulze-Osthoff K (2005) Regulation of Apoptosis by Alternative Pre-mRNA Splicing. *Mol. Cell* **19:** 1-13

Scolnick LR, Kanyo ZF, Cavalli RC, Ash DE, Christianson DW (1997) Altering the binuclear manganese cluster of arginase diminishes thermostability and catalytic function. *Biochemistry* **36:** 10558-10565

Segev N (2001a) Ypt and Rab GTPases: insight into functions through novel interactions. *Curr. Opin. Cell Biol.* **13:** 500-511

Segev N (2001b) Ypt/rab gtpases: regulators of protein trafficking. *Science's STKE: signal transduction knowledge environment* **2001:** re11

Shen F, Seabra MC (1996) Mechanism of Digeranylgeranylation of Rab Proteins: Formation of a complex between monogeranylgeranyl-Rab and Rab Escort protein *J. Biol. Chem.* **271:** 3692-3698

Shi O, Morris SM, Jr., Zoghbi H, Porter CW, O'Brien WE (2001) Generation of a mouse model for arginase II deficiency by targeted disruption of the arginase II gene. *Mol. Cell. Biol.* **21:** 811-813

Shishova EY, Di Costanzo L, Emig FA, Ash DE, Christianson DW (2009) Probing the specificity determinants of amino acid recognition by arginase. *Biochemistry* **48:** 121-131

Simon I, Zerial M, Goody RS (1996) Kinetics of Interaction of Rab5 and Rab7 with Nucleotides and Magnesium Ions. *J. Biol. Chem.* **271:** 20470-20478

Sivars U, Aivazian D, Pfeffer S (2005) Purification and properties of Yip3/PRA1 as a Rab GDI displacement factor. *Methods Enzymol.* **403:** 348-356

Skoog DA, Leary JJ (2013) *Instrumentelle Analytik: Grundlagen-Geräte-Anwendungen*: Springer-Verlag.

Snell K, Natsumeda Y, Eble JN, Glover JL, Weber G (1988) Enzymic imbalance in serine metabolism in human colon carcinoma and rat sarcoma. *Br. J. Cancer* **57:** 87-90

Snell K, Riches D (1989) Effects of a triazine antifolate (NSC 127755) on serine hydroxymethyltransferase in myeloma cells in culture. *Cancer Lett.* **44:** 217-220

Sprang SR, Coleman DE (1998) Invasion of the nucleotide snatchers: structural insights into the mechanism of G protein GEFs. *Cell* **95:** 155-158

Stenmark H, Olkkonen VM (2001) The Rab GTPase family. *Genome Biol.* **2:** reviews 1-7

Stone EM, Chantranupong L, Georgiou G (2010) The second-shell metal ligands of human arginase affect coordination of the nucleophile and substrate. *Biochemistry* **49:** 10582-10588

Stover P, Zamora M, Shostak K, Gautam-Basak M, Schirch V (1992) Escherichia coli serine hydroxymethyltransferase. The role of histidine 228 in determining reaction specificity. *J. Biol. Chem.* **267:** 17679-17687

Subramani S (1998) Components involved in peroxisome import, biogenesis, proliferation, turnover, and movement. *Physiol. Rev.* **78:** 171-188

Suh HY, Lee DW, Lee KH, Ku B, Choi SJ, Woo JS, Kim YG, Oh BH (2009) Structural insights into the dual nucleotide exchange and GDI displacement activity of SidM/DrrA. *EMBO J.* **29:** 496-504

Szebenyi DM, Liu X, Kriksunov IA, Stover PJ, Thiel DJ (2000) Structure of a murine cytoplasmic serine hydroxymethyltransferase quinonoid ternary complex: evidence for asymmetric obligate dimers. *Biochemistry* **39:** 13313-13323

Thoma NH, Iakovenko A, Goody RS, Alexandrov K (2001) Phosphoisoprenoids modulate association of Rab geranylgeranyltransferase with REP-1. *J. Biol. Chem.* **276:** 48637-48643

Thorndike J, Pelliniemi TT, Beck WS (1979) Serine hydroxymethyltransferase activity and serine incorporation in leukocytes. *Cancer Res.* **39:** 3435-3440

Tress ML, Martelli PL, Frankish A, Reeves GA, Wesselink JJ, Yeats C, Olason PI, Albrecht M, Hegyi H, Giorgetti A, Raimondo D, Lagarde J, Laskowski RA, Lopez G, Sadowski MI, Watson JD, Fariselli P, Rossi I, Nagy A, Kai W, Storling Z, Orsini M, Assenov Y, Blankenburg H, Huthmacher C, Ramirez F, Schlicker A, Denoeud F, Jones P, Kerrien S, Orchard S, Antonarakis SE, Reymond A, Birney E, Brunak S, Casadio R, Guigo R, Harrow J, Hermjakob H, Jones DT, Lengauer T, Orengo CA, Patthy L, Thornton JM, Tramontano A, Valencia A (2007) The implications of alternative splicing in the ENCODE protein complement. *Proc. Natl. Acad. Sci. USA* **104:** 5495-5500

Tsao D, Dokholyan NV (2010) Macromolecular crowding induces polypeptide compaction and decreases folding cooperativity. *PCCP.* **12:** 3491-3500

Valencia A, Chardin P, Wittinghofer A, Sander C (1991) The ras protein family: evolutionary tree and role of conserved amino acids. *Biochemistry* **30:** 4637-4648

Vazquez MA, Munoz F, Donoso J, Garcia Blanco F (1991) Spectroscopic study of the Schiff bases of dodecylamine with pyridoxal 5'-phosphate and 5'-deoxypyridoxal. A model for the Schiff bases of pyridoxal 5'-phosphate in biological systems. *Biochem. J.* **279 (Pt 3):** 759-767

Vellai T, Vida G (1999) The origin of eukaryotes: the difference between prokaryotic and eukaryotic cells. *Proc. Biol. Sci. / Roy. Soc.* **266:** 1571-1577

Vetter IR, Wittinghofer A (2001) The guanine nucleotide-binding switch in three dimensions. *Science (New York, NY)* **294:** 1299-1304

Vitale G, Rybin V, Christoforidis S, Thornqvist P, McCaffrey M, Stenmark H, Zerial M (1998) Distinct Rab-binding domains mediate the interaction of Rabaptin-5 with GTP-bound Rab4 and Rab5. *EMBO J.* **17:** 1941-1951

Wahl MC, Will CL, Lührmann R (2009) The Spliceosome: Design Principles of a Dynamic RNP Machine. *Cell* **136:** 701-718

Wang ET, Sandberg R, Luo S, Khrebtukova I, Zhang L, Mayr C, Kingsmore SF, Schroth GP, Burge CB (2008) Alternative isoform regulation in human tissue transcriptomes. *Nature* **456:** 470-476

Watson P, Stephens DJ (2005) ER-to-Golgi transport: form and formation of vesicular and tubular carriers. *Biochim. Biophys. Acta* **1744:** 304-315

Weis K (2003) Regulating access to the genome: nucleocytoplasmic transport throughout the cell cycle. *Cell* **112:** 441-451

Wennerberg K, Rossman KL, Der CJ (2005) The Ras superfamily at a glance. *J .Cell Sci.* **118:** 843-846

Wiegandt D, Vieweg S, Hofmann F, Koch D, Li F, Wu YW, Itzen A (2015) Locking GTPases covalently in their functional states. *Nat. Commun.* **6:** 7773

Wijdeven RH, Jongsma ML, Neefjes J, Berlin I (2015) ER contact sites direct late endosome transport. *BioEssays: news and reviews in molecular, cellular and developmental biology* **37:** 1298-1302

Wilhelm M, Schlegl J, Hahne H, Gholami AM, Lieberenz M, Savitski MM, Ziegler E, Butzmann L, Gessulat S, Marx H, Mathieson T, Lemeer S, Schnatbaum K, Reimer U, Wenschuh H, Mollenhauer M, Slotta-Huspenina J, Boese J-H, Bantscheff M, Gerstmair A, Faerber F, Kuster B (2014) Mass-spectrometry-based draft of the human proteome. *Nature* **509:** 582-587

Wittinghofer A, Vetter IR (2011) Structure-function relationships of the G domain, a canonical switch motif. *Annu. Rev. Biochem.* **80:** 943-971

Wong JJ, Au AY, Ritchie W, Rasko JE (2015) Intron retention in mRNA: No longer nonsense: Known and putative roles of intron retention in normal and disease biology. *BioEssays: news and reviews in molecular, cellular and developmental biology*

Wu Y-W, Tan K-T, Waldmann H, Goody RS, Alexandrov K (2007) Interaction analysis of prenylated Rab GTPase with Rab escort protein and GDP dissociation inhibitor explains the need for both regulators. *Proc. Natl. Acad. Sci. USA* **104:** 12294-12299

Wu YW, Oesterlin LK, Tan KT, Waldmann H, Alexandrov K, Goody RS (2010) Membrane targeting mechanism of Rab GTPases elucidated by semisynthetic protein probes. *Nat. Chem. Biol.* **6:** 534-540

Xu H, Freitas MA (2009) MassMatrix: a database search program for rapid characterization of proteins and peptides from tandem mass spectrometry data. *Proteomics* **9:** 1548-1555

Yoshimura S, Gerondopoulos A, Linford A, Rigden DJ, Barr FA (2010) Family-wide characterization of the DENN domain Rab GDP-GTP exchange factors. *J. Cell Biol.* **191:** 367-381

Yura K, Shionyu M, Hagino K, Hijikata A, Hirashima Y, Nakahara T, Eguchi T, Shinoda K, Yamaguchi A, Takahashi K, Itoh T, Imanishi T, Gojobori T, Go M (2006) Alternative splicing in human transcriptome: functional and structural influence on proteins. *Gene* **380:** 63-71

Zacharias M (2003) Protein-protein docking with a reduced protein model accounting for side-chain flexibility. *Protein Sci.* **12:** 1271-1282

Zerial M, McBride H (2001) Rab proteins as membrane organizers. *Nat. Rev. Mol. Cell Biol.* **2:** 107-117

Zhu Y, Hu L, Zhou Y, Yao Q, Liu L, Shao F (2010) Structural mechanism of host Rab1 activation by the bifunctional Legionella type IV effector SidM/DrrA. *Proc. Natl. Acad. Sci. USA* **107:** 4699-4704

9 Appendix

Appendix 1: Mass spectrometry results of Co-IPs of wtRab1A and nt-svRab1A in HeLa lysate samples.

Accession	ΣCoverage	Σ# Unique Peptides	Σ# Peptides	Σ# PSMs	Score wtRab1A	Score nt-svRab1A
P62820	85,85	16	24	342	127,33	107,08
P07437	61,04	7	19	91	34,84	34,07
E7ETK2	89,92	7	18	365	33,84	298,21
P11142	35,6	16	20	36	32,27	20,22
P68371	58,65	5	17	53	28,70	27,03
P14618	40,49	16	16	30	26,28	8,60
P38646	34,76	18	18	30	23,77	17,35
P60709	53,6	15	15	39	19,78	8,68
P08107	23,87	9	12	24	19,67	9,58
P68363	58,09	15	21	56	14,16	25,04
P04075	23,63	6	6	11	10,53	13,07
P04792	46,34	7	7	41	9,61	45,74
P00338	26,2	8	9	14	8,45	11,57
P68104	18,4	5	5	20	7,51	17,03
G3V1A4	22,82	2	2	8	6,16	7,77
P06733	17,97	5	5	8	5,81	2,24
Q14247-3	15,2	4	4	5	5,26	2,22
P07237	7,09	3	3	5	4,20	2,33
P49327	7,33	13	13	42	43,93	0,00
P10809	43,63	16	16	20	29,40	0,00
P11021	32,57	13	15	19	29,22	0,00
P08238	17,68	5	10	15	24,31	0,00
P07900	15,03	4	9	11	21,33	0,00
Q92841	15,09	3	8	13	21,10	0,00
P00505	30,93	9	9	10	19,35	0,00
Q01813	22,96	11	13	14	18,83	0,00
Q13501	33,64	9	9	12	17,36	0,00
P26639	17,15	9	9	11	15,57	0,00
Q16822	12,5	6	6	7	14,39	0,00
P10909-4	23,8	7	7	9	14,35	0,00
O00571-2	10,53	4	5	7	14,34	0,00
P27824	14,7	7	7	8	14,28	0,00
B4DLW8	14,21	2	7	9	12,91	0,00
P17858	12,18	4	7	8	12,81	0,00
B4DEM7	17,58	8	8	8	12,15	0,00
P05388	24,61	5	5	6	11,88	0,00
P08237	10,9	5	7	7	11,75	0,00
A8MUB1	31,64	4	10	12	11,53	0,00
Q01105-3	20	4	4	4	10,70	0,00
P67809	17,28	4	4	6	10,58	0,00
Q08380	7,86	4	4	5	10,05	0,00

Accession	ΣCoverage	Σ# Unique Peptides	Σ# Peptides	Σ# PSMs	Score wtRab1A	Score nt-svRab1A
Q01105-3	20	4	4	4	10,70	0,00
P67809	17,28	4	4	6	10,58	0,00
Q08380	7,86	4	4	5	10,05	0,00
P06748-2	20,38	3	3	3	8,97	0,00
P26038	13,34	3	5	6	8,94	0,00
P35250-2	27,81	6	6	7	8,93	0,00
H0YA55	12,56	7	7	12	8,90	0,00
C9J9K3	17,05	3	3	3	8,50	0,00
B4DPJ8	10,2	4	4	4	8,09	0,00
Q9Y3F4	18,29	4	4	5	8,02	0,00
B4DUR8	11	5	5	5	7,97	0,00
P11940-2	8,41	4	4	4	7,94	0,00
P36578	11,01	3	3	4	7,94	0,00
P05198	12,7	3	3	3	7,69	0,00
P06493	21,55	5	5	8	7,01	0,00
P51553	12,98	2	2	2	6,88	0,00
P19338	7,75	4	4	7	6,53	0,00
P29401	15,57	7	7	8	6,49	0,00
E9PQZ1	14,71	3	3	3	6,17	0,00
P62913-2	16,95	3	3	3	5,94	0,00
E7EQR4	7,58	2	4	5	5,68	0,00
P23921	3,16	2	2	2	4,81	0,00
P31025	12,5	2	2	2	4,79	0,00
Q5T3N1	17,16	2	2	2	4,74	0,00
J3QR09	13,47	2	2	2	4,71	0,00
Q06210-2	4,26	2	2	2	4,65	0,00
Q9UBS4	7,54	2	2	2	4,65	0,00
M0R3B2	21,49	3	3	3	4,59	0,00
Q06830	12,06	2	2	2	4,28	0,00
P0C0L4-2	1,59	2	2	3	4,23	0,00
P52292	9,45	3	3	3	4,21	0,00
P08195-2	7,56	3	3	3	4,18	0,00
Q99832-3	7,21	2	2	3	4,16	0,00
F8VZJ2	19,85	2	2	2	4,05	0,00
O95817	9,91	5	5	5	4,05	0,00
K7EPT6	5,12	2	2	2	4,04	0,00
P17987	6,83	2	2	3	3,97	0,00
Q5T6W5	13,79	3	3	3	3,94	0,00
K7EME0	13,45	2	2	2	3,93	0,00
P46777	7,41	2	2	2	3,87	0,00
Q9Y3Z3-3	11,33	6	6	7	3,86	0,00
B7Z6M1	4,44	2	2	2	3,73	0,00
H7C144	8,77	3	3	3	3,73	0,00
P13010	10,66	4	4	4	3,71	0,00

Accession	ΣCoverage	Σ# Unique Peptides	Σ# Peptides	Σ# PSMs	Score wtRab1A	Score nt-svRab1A
P13010	10,66	4	4	4	3,71	0,00
H0YIP0	10,05	2	2	3	3,46	0,00
B7Z2E6	29,6	2	2	2	3,38	0,00
P14625	3,99	2	2	2	3,22	0,00
P55072	4,22	3	3	3	2,63	0,00
F5H4D6	10,56	2	2	3	2,41	0,00
P12273	18,49	2	2	2	2,36	0,00
P62258-2	16,31	2	2	2	2,27	0,00
Q9Y6G9	5,54	2	2	2	2,25	0,00
P10398	4,95	2	2	2	2,18	0,00
B1AHC8	16,2	6	6	7	2,17	0,00
B4DQ14	5,71	2	2	2	2,16	0,00
P40938-2	13,11	3	3	3	1,96	0,00
C9JXZ7	23,58	2	2	2	1,88	0,00
H0Y8Y3	16,88	3	3	3	1,87	0,00
J3KTJ8	9,28	2	2	2	1,85	0,00
O95831-6	9,7	2	2	2	1,67	0,00
O95573	4,58	2	2	3	1,61	0,00
E9PLD0	44,97	3	11	104	0,00	178,58
Q15286-2	11,18	1	2	23	0,00	35,21
Q14574-2	2,98	2	2	3	0,00	8,87
P05089-3	22,46	5	5	6	0,00	8,75
P60174-1	12,85	2	2	3	0,00	8,37
P08727	11	2	5	6	0,00	7,51
P07737	32,86	3	3	3	0,00	7,27
P31944	11,98	2	2	3	0,00	5,92
E7EM57	18,13	4	4	4	0,00	3,88
B7Z2F4	11,83	3	3	4	0,00	2,40
F8VV32	19,23	2	2	2	0,00	2,02
F5H7X1	22,35	2	2	3	0,00	1,76

10 Publications

Parts of this thesis are reprinted from Regulatory implications of non-trivial splicing: Isoform 3 of Rab1A shows enhanced basal activity and is not controlled by accessory proteins, doi: 10.1016/j.jmb2016.02.028, © (2016), with permission from Elsevier.

10.1 Published

Schöppner, P., Csaba, G., Braun, T., Daake, M., Richter, B., Lange, O. F., Zacharias, M., Zimmer, R., Haslbeck, M. (2016). Regulatory implications of non-trivial splicing: Isoform 3 of Rab1A shows enhanced basal activity and is not controlled by accessory proteins. Journal of Molecular Biology (doi: 10.1016/j.jmb2016.02.028)

10.2 In preparation

Altenbuchner, P.T. [¥], Werz, P. D. L. [¥], **Schöppner, P. [¥]**, Adams, F., Schwarzenböck, C., Kronast, A. Pöthig, A., Jandl, C., Haslbeck M., and Rieger B. Next Generation of Multi-Responsive Nanocarriers for the Targeted Drug Delivery to Cancer Cells (JACS Int. Ed.)

11 Danksagung

An erster Stelle möchte ich mich bei meinem Doktorvater, Johannes Buchner, bedanken, der mir ermöglicht hat, meine Arbeit an seinem Lehrstuhl anzufertigen und die vielfältigen wissenschaftlichen Mittel zu nutzen.
Besonders bedanken möchte ich mich bei Martin Haslbeck, der durch seine fachlichen Diskussionen, Ideen und Anregungen erheblich zum Fortgang der Doktorarbeit beigetragen hat. Vielen Dank, für die wissenschaftliche Freiheit die du mir zur Verwirklichung der Doktorarbeit entgegen gebracht hast.
Ein spezieller Dank gilt Aymelt Itzen, der erheblichen Anteil an dem erfolgreichen Ausgang des nt-svRab1A Projektes hatte. Kathi, Adam, Evelyn, Rudi und Ronny danke ich für die sehr gute Zusammenarbeit. Danke, dass ihr immer ein offenes Ohr für die Problemchen hattet, die während der Arbeit an der Rab Spleißvariante so aufgetreten sind.
Des Weiteren möchte ich mich bei meinen Kollaboratoren, Ralf Zimmer, Oliver Lange und Martin Zacharias für die gute Zusammenarbeit bedanken.
Bettina Richter danke ich für die großartige Unterstützung und Hilfsbereitschaft während der gesamten Doktorarbeit. Du hast mir die vielen stressigen Situationen dadurch erheblich erleichtert.
Herzlich danken möchte ich meiner langjährigen Laborkollegin Ritti, ohne dich hätte ich die Zeit am Lehrstuhl nicht überlebt. Die Zusammenarbeit mit dir war immer mit einer Menge Spaß verbunden, unsere gegenseitige Motivation legendär. Ich werde unsere amüsante Zeit am Lehrstuhl nie vergessen.
Katrin, Marina, Sandy, Christine, Chrissy, Pri und Katha, danke ich für die tatkräftige Unterstützung, die tolle Zusammenarbeit, unsere tiefgründigen Gespräche, die etlichen Kaffeepausen und eure aufbauenden Worte in allen Lebenslagen. Ihr seid die besten Kolleginnen, die man sich nur wünschen kann.
Gordi, dir dank ich für deinen seltenen Humor, der mich öfters hat Tränen lachen lassen.
Von Herzen danke ich meinen langjährigen Studienfreunden Richard, Peter, Michi und Mark, denn ohne eure Unterstützung hätte ich nicht bis zum Ende durchgehalten. Das Studium mit euch wird mir sicher immer in Erinnerung bleiben.
Bene, dir dank ich dafür, dass du dich am Ende doch für unseren Lehrstuhl entschieden hast und ich dich dadurch kennenlernen durfte. Danke für die tolle Zeit und für die wunderschönen Erlebnisse. Ohne dich hätte ich am Ende fast durchgedreht.
Tausend Dank an den gesamten Buuucheeeer Lehrstuhl, nur durch euch wurde die Zeit am Lehrstuhl zu einer wirklich unvergesslich schönen Zeit.
Der größte Dank gilt meinen Eltern, die mich stets uneingeschränkt und bedingungslos unterstützt haben. Danke, dass ihr mir immer den Rücken freigehalten habt und mich in den schwierigsten Situationen immer wieder aufs Neue motiviert habt. Vielen Dank, ohne euch wäre das alles nicht möglich gewesen.

12 Eidesstattliche Erklärung

Hiermit erkläre ich an Eides statt, dass ich die vorliegende Arbeit selbständig verfasst und keine anderen als die angegebenen Quellen und Hilfsmittel verwendet habe. Die aus fremden Quellen übernommenen Gedanken sind als solche kenntlich gemacht. Diese Arbeit hat in gleicher oder ähnlicher Form noch keiner Prüfungsbehörde vorgelegen. Teile dieser Arbeit wurden in einem wissenschaftlichen Journal veröffentlich.

München, ……...

Patricia Schöppner